공학박사학위논문

Hybrid Evolutionary Computation Algorithm Based on Gene Expression Programming and Particle Swarm Optimization for Prediction of Mechanical Rock Excavation Performance

암석의 기계굴착 성능 예측을 위한

유전자발현프로그래밍과 입자군집최적화에 기초한

혼합형 진화 계산 알고리즘

2022 년 8 월

서울대학교 대학원

에너지시스템공학부

Shahabedin Hojjati

Hybrid Evolutionary Computation Algorithm Based on Gene Expression Programming and Particle Swarm Optimization for Prediction of Mechanical Rock Excavation Performance

암석의 기계굴착 성능 예측을 위한
유전자발현프로그래밍과 입자군집최적화에 기초한
혼합형 진화 계산 알고리즘

지도교수 전 석 원

이 논문을 공학박사 학위논문으로 제출함
2022년 6월

서울대학교 대학원
에너지시스템공학부
Shahabedin Hojjati

Shahabedin Hojjati의 박사 학위논문을 인준함
2022년 7월

위 원 장 송 재 준
부위원장 전 석 원
위 원 Deniz Tumac
위 원 류 동 우
위 원 민 기 복

ABSTRACT

Hybrid Evolutionary Computation Algorithm Based on Gene Expression Programming and Particle Swarm Optimization for Prediction of Mechanical Rock Excavation Performance

Shahabedin Hojjati

Department of Energy Systems Engineering

The Graduate School

Seoul National University

With the advances in mechanical excavation technology, increasing number of underground spaces are built using mechanical excavation rather than the conventional drilling and blasting method.

In the field of mechanical rock excavation, there are a fair number of deterministic solutions for the relations between different variables. However, in many cases, establishing such a relation is extremely difficult. As a result, many researchers try to explain those relations using regression analysis. Due to the complex and non-linear nature of rock cutting phenomenon, it is not easy to reasonably determine the form of the non-linear functions that fit to the statistical data as it is required by the conventional non-linear function fitting techniques. As a result, a combination of Gene Expression Programming (*GEP*) and Particle

Swarm Optimization (*PSO*) was used for data analysis in this study in order to solve problems in the field of mechanical excavation. *GEP* and *PSO* are evolutionary computation techniques and the *GEP-PSO* algorithm is capable of automatically finding the form and constants of a non-linear function that fits on a data set. The algorithm was used in order to develop a performance prediction model for impact hammer, a prediction model for specific energy required by point attack picks, and models for prediction of cutting, normal, and side force acting on a point attack pick. In all cases, the results generated using the *GEP-PSO* algorithm produced significantly high prediction accuracy in comparison to those generated by multiple linear regression. When possible, comparisons were made between the results generated by the *GEP*-PSO algorithm and the prediction models developed by other researchers to show the advantages of the models developed over the course of the present study. In addition to high level of accuracy, the models developed using *GEP-PSO* algorithm could overcome shortcomings of the existing prediction models to a fair extent. The developed models are more advantageous as they provide more reliability/accuracy while requiring few easy-to-obtain input parameters, and/or they include the significant input parameters that have been neglected by the existing prediction models.

***Keywords*: Artificial Intelligence, Prediction Model, Impact Hammer, Point Attack Pick, Specific Energy, Cutter Force**

Student ID: 2017-34695

TABLE OF CONTENTS

LIST OF FIGURES

LIST OF TABLES

1. INTRODUCTION

The increase in global population and urbanization rate has increased the use of underground spaces. Since 1950, the world population has tripled (Ritchie, 2019). Meanwhile, as Figure 1-1 shows, the share of the world population living in urban area has increased from 29.61% in 1950 to 56.61% in 2021 and is predicted to increase to 68.36% in 2050. In addition to the increase in traditional need for roads, railways, metro, and utility tunnels, a growing number of urban life aspects are put underground in order to make the surface available for other purposes (Anagnostou and Ehrbar, 2013). Hong Kong, with a high population density of which a 100% is living in urban areas, may be a representative example of this trend (Wallace and Ng, 2016). Figure 1-2 shows population growth and tunnel development in Hong Kong.

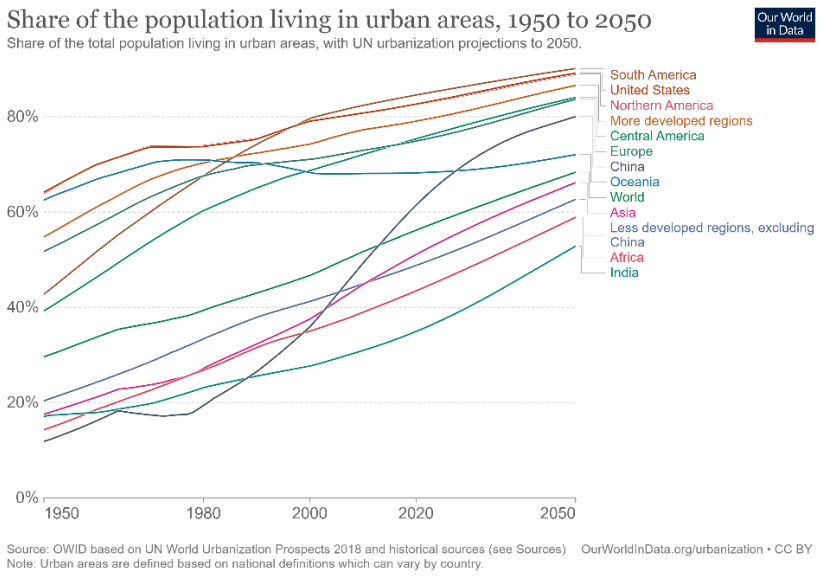

Figure 1-1: Share of the population living in urban areas and its projection

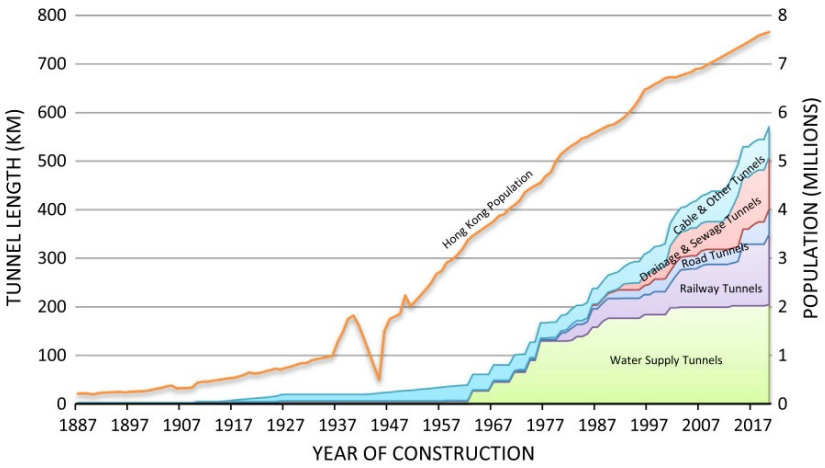

Figure 1-2: Population growth and tunnel development in Hong Kong (adapted from Pang (2015))

There are two main methods of excavation, namely, drilling and blasting and mechanical excavation. The latter is a younger method that has started to develop since 1950s. With the advances in mechanical excavation technology, increasing number of underground spaces are built using mechanical excavation rather than the conventional drilling and blasting (Bilgin et al., 2013). Figure 1-3 is generated using the results of a survey conducted on Scopus.com. The figure shows the share of mechanical excavation, compared to that of drilling and blasting, in the publications in "Tunnelling and Underground Space Technology", "Rock Mechanics and Rock Engineering", and "International Journal of Rock Mechanics and Mining Sciences" on the subject of "excavation" between the years 1996 and 2021.

Ozdemir (1998, 1992, 1990) summarized the basic advantages of mechanical excavations over drilling and blasting as:

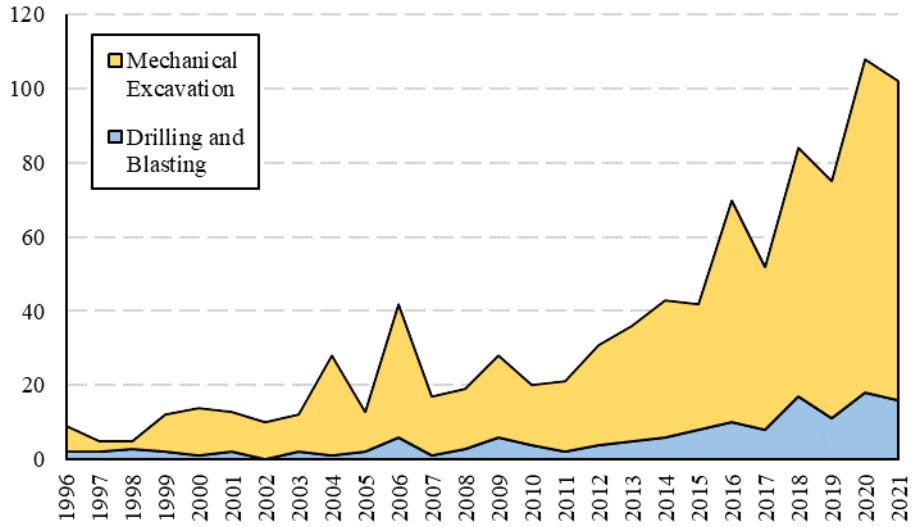

Figure 1-3: Number of publications in "Tunnelling and Underground Space Technology", “Rock Mechanics and Rock Engineering”, and “International Journal of Rock Mechanics and Mining Sciences” on the subjects of “Mechanical Excavation” and “Drilling and Blasting”

- Safer and more environment-friendly operation (no explosive handling—forbidden in urban areas, no blast vibrations in urban areas, no noxious gases, no dust, better workmanship, lesser accidents)
- Minimum ground disturbance (lesser overbreak, lesser scaling-support-ventilation requirement, minimized support maintenance, superior ground control in jointed/broken rocks)
- Uniform muck size (easy muck/excavated material haulage, no secondary breakage of large rock chunks, lower crushing and mineral processing costs)

- Selective mining/excavation capability (minimum ore dilution/minimum mixing with gang, increased ore recovery, separate excavation of rock layers in different strengths making excavation easier)
- Continuous operation (not periodic, conducive to automation, excavation—loading—ground supporting simultaneously)
- Higher production/excavation rates in favorable ground conditions (higher economical benefits/saving money, earlier mining of high-grade ore, earlier job completion)

It is very common in engineering to investigate the relation between two or more variables. In some cases, that relation is "deterministic", which means that the target variable can be perfectly predicted based on the predictor variable(s). For instance, the relation between displacement of an object and its velocity is a form of deterministic relation. However, there are numerous instances, where the relation between variables is too complicated to be explained in a deterministic manner. The impact of a father's height on his son's height may be an example of that kind of dependence. In such cases, regression analysis is used to approach the problem in a non-deterministic way (Montgomery and Runger, 2018).

In the field of mechanical rock excavation, there are a fair number of deterministic solutions for the relations between different variables. However, in many cases, as rock is a discontinuous, inhomogeneous, anisotropic, and non-elastic material, and due to the complex nature of the process of rock cutting, it is extremely difficult to establish such a deterministic relation. As a result, many researchers try to explain those relations using regression analysis. With some occasional exceptions, the

relations in nature are intrinsically non-linear (Nisbet et al., 2018; Zielesny, 2016). When dealing with curve fitting problems, three scenarios may occur (Zielesny, 2016):

1. The structure of the mathematical equation that describes the curve (model function) is either theoretically, or empirically known, but the parameters of the equation are unknown. For instance, it is known that the curve may be described using an exponential function of the form $f(x)=ae^{x}+b$, and the parameters "a" and "b" are to be determined.
2. The structure of the model function is unknown, but may be postulated.
3. The structure of the model function is unknown and there is no reasonable way to make an educated guess about it.

In the first two scenarios, the problem may be reduced to an optimization problem with the goal of finding the parameters in the model function structure such that the error of estimate is minimized. In case the model function is linear with one or more arguments, the optimization problem at hand may be solved analytically. Please note that, here, the linear model function does not necessarily show a linear relation between the argument (x) and the function value (y). It should only be linear in constants. For instance, $f(x)=ae^{x}+b$ is a linear model function with one argument (x) while $f(x)=ax^{b}+c$ is a non-linear model function with one argument (x). In the case of non-linear model functions, analytical solution is not applicable. In such cases, iterative optimization techniques have to be used (Zielesny, 2016).

In the third scenario, where the structure of the model function is completely unknown, machine learning techniques can be used (Zielesny, 2016).

Machine learning is a subcategory of artificial intelligence that studies computer programs that are capable of improving their performance by learning from experience (Russell and Norvig, 2020). According to Mitchell (1997):

> "A computer program is said to learn from experience *E* with respect to some class of tasks *T* and performance measure *P*, if its performance at tasks in *T*, as measured by *P*, improves with experience *E*."

For instance, a computer program that is designed to play Chess (task *T*) learns to increase its chance of winning (performance measure *P*) by checking the consequences of different moves in different chess board settings (experience *E*).

Machine learning algorithms may be divided into three vast branches, namely supervised learning, unsupervised learning, and reinforcement learning. In supervised learning, the goal is to map the values of inputs to the values of outputs in the data. In other words, given a set of (x, y) data, the machine learns how to map x values to y values. In unsupervised learning, the goal is to learn how to detect patterns in a set of input data. This category of machine learning is most commonly used for clustering, i.e. recognition of different clusters in input data. A computer vision system that learns how to cluster similar input images into a category that may be called "dog", "horse", "chair", etc. is an example of unsupervised machine learning. In reinforcement learning,

the machine learns by rewards and punishments. For instance, for a system designed to play chess, at the end of the game, the machine is told whether it has won or lost. The task of judging which step(s) during the game contributed more to the win/loss is left to the machine (Russell and Norvig, 2020).

Based on the above explanations, it may be concluded that a supervised machine learning method should be used for regression when the structure of the model function is completely unknown. Artificial Neural Networks (*ANN*) and Symbolic Regression Methods (*SRMs*) are two branches of machine learning methods that are capable of performing that task (Diveev and Shmalko, 2021; Mitchell, 1997). However, it should be noted that an *ANN* is a mathematical architecture rather than an equation. In other words, it merely is a replacement for the unknown function that fits to a certain curve and does not reveal any information about the function or its properties (Diveev and Shmalko, 2021). This characteristic of *ANN*s does not assist the process of understanding the mathematical relation between a parameter of interest and the parameters that govern it. In contrast to *ANN*, *SRM*s are methods of machine learning that are designed for generating mathematical equations and investigating the space of those equations with the objective of finding the function that fits best on the given data (Diveev and Shmalko, 2021).

Genetic Programming (*GP*), Gene Expression Programming (*GEP*), Grammatical Evolution, Analytic Programming, and Parse Matrix Evolution are instances of *SRM*s (Diveev and Shmalko, 2021; Ferreira, 2006). Among them, *GEP* was selected as a data analysis tool in this

study. In brief, *GEP* is an "evolutionary computation technique/evolutionary algorithm" that stochastically evolves a randomly generated population of "encoded individuals/computer programs/candidate solutions" through generations with the objective of improving their "fitness/prediction accuracy". Chapter 4 explains the reasons behind making this choice in addition to a comprehensive explanation of *GEP*.

The candidate solutions generated by *GEP* may contain numerical constants. The basic *GEP* algorithm can only adjust those constants randomly. In such a situation, use of a more supervised optimization algorithm may be helpful. Therefore, Particle Swarm Optimization (*PSO*) was used in order to further optimize the numerical constants in the solutions generated by *GEP*. In *PSO*, a swarm of "particles/potential solutions" conduct a guided search through the solutions space in order to find the optimum solutions/constants. More detailed explanations about *PSO* are provided in Chapter 4.

The present study addressed three problems in the field of mechanical excavation with the aid of *GEP* and *PSO* algorithms:

- Development of a performance prediction model for impact hammer
- Development of a prediction model for specific energy required by point attack picks
- Development of models for prediction of cutting, normal, and side force acting on a point attack pick

Chapter 2, “Literature Review”, provides a review of literature that led to identification of those problems as well as explanations about the knowledge gaps that were filled in by the present research.

Chapter 3, “Statistical Data”, describes the statistical data that were used in order to tackle the selected problems. Chapter 5, “Results and Discussion” presents the results of data analysis and the relevant discussions. Finally, the conclusions of this study in relation to the selected problems are brought in Chapter 6, “Conclusions”.

2. LITERATURE REVIEW

This chapter offers a review of literature that led to selection of the subjects studied during the course of this research in addition to explanations about the identified knowledge gaps that were filled in by the present work.

2.1 Impact hammer performance prediction

Mechanical excavation, and drilling and blasting, are the two main methods of excavation in the field of tunneling. In order to choose between these two excavation methods, their feasibility, installation problems, ability to handle adverse geological conditions, total cost, and advance rate should be considered by the decision maker (Terezopoulos, 1987). Even when choosing between different mechanical excavators, it is important to know their respective advance rates. Thus, determining the advance rate of the excavator is an important factor from the starting point of a project (Terezopoulos, 1987).

According to Copur et al. (2012), impact hammers may be used for excavation in highly fractured ground with a uniaxial compressive strength (*UCS*) of less than 100 *MPa*. When the ground is suitable for the use of impact hammers, when excavating short tunnels (i.e., cross-cuts), metro stations, or in an urban area where the use of explosives is prohibited by regulations, the lower capital cost can make an impact hammer a more appropriate choice compared to a tunnel boring machine (*TBM*) and roadheader. Their operational flexibility is another advantage that makes impact hammers an indispensable part of the mining industry. Their flexibility allows the operator to either follow the pattern of

irregular ore bodies or take advantage of foliations and beddings in favor of faster excavation (Tuncdemir, 2008).

2.1.1 Existing performance prediction models

A few empirical models have previously been developed for predicting the instantaneous breaking rate (*IBR*) of an impact hammer. Bilgin et al. (1996) proposed a model (Eqs. 2.1 and 2.2) that statistically related the *IBR* of the impact hammer to its input power (*P*, *Hp*), *UCS* (*MPa*), and rock quality designation (*RQD*, %) in a moderately good relationship with an R^2 value of 0.63:

$$IBR=4.24\times P\times(RMCI)^{(-0.567)} \tag{2.1}$$

$$RMCI=UCS\times\left(\frac{RQD}{100}\right)^{(2/3)} \tag{2.2}$$

where *RMCI* is the rock mass cuttability index in *MPa*.

The relationship between the *IBR* of the impact hammer (m^3/h) and the N-type Schmidt hammer rebound value (*SHRV*) (as determined using the method suggested by Poole and Farmer (1980)) was investigated by Bilgin et al. (2002). For *RQD* values of 25–49%, they found a strong correlation (Eq. 2.3).

$$IBR=(-1.05\times SHRV)+70.1,\ R^2=0.83 \tag{2.3}$$

Aksoy (2009) proposed a model for predicting the *IBR* based on the machine power (*P*), block punch index (*BPI*), and geological strength index (*GSI*). The model proposed by Aksoy (2009) is valid for *RQD* values of less than 20% (or *GSI* < 35). Kucuk et al.(2011) used an adaptive neuro-fuzzy inference system (*ANFIS*) to establish a model for predicting the *IBR* of an impact hammer. They incorporated the *BPI*, *GSI*, and *P* in their model. The model is applicable to rocks with a *GSI* value of less than 35 (*RQD* < 20%). Aksoy et al. (2011) studied the relationship between the *IBR* and the *P*, *GSI*, and *BPI*. They suggested two new prediction models for excavations in slopes and tunnels and one for both. Iphar (2012) demonstrated the efficiency of an artificial neural network (*ANN*) and *ANFIS* for predicting the performance of impact hammers. He constructed his models based on the *SHRV* and *RQD* values derived from a database with twenty-one samples that were previously generated by Bilgin et al. (2002). After an intensive study on forty-four different projects, Aksoy et al. (2013) developed a new parameter called the rock structure index (*RSI*). They found a relationship between the *RSI*, output *P*, and *IBR* of an impact hammer, with a relatively strong R^2 value of 0.70. Tumac and Hojjati (2016) investigated the effects of the *UCS*, *RQD*, Brazilian tensile strength (*BTS*), density, *SHRV*, shore scleroscope hardness (*SSH*), and Cerchar abrasivity index on the performance of an impact hammer used to excavate a metro tunnel. They concluded that the *UCS* and *RQD* are the two most important rock properties and can be used to describe the performance of an impact hammer (Eq. 2.4):

$$IBR=(0.763\times RQD_T)+(0.649\times UCS_T)-6.183 \quad (2.4)$$

where *IBR* is the instantaneous breaking rate of the hammer in m^3/h, and UCS_T and RQD_T are defined as follows:

$$UCS_T=45.944\times UCS^{-0.279} \quad (2.5)$$

$$RQD_T=69.322-(14.79\times \ln(RQD)) \quad (2.6)$$

Eq. 2.4 is applicable for rocks with *UCS* values of 8.9–195.6 *MPa* and *RQD* values of 10–60%.

For more details regarding the existing impact hammer performance prediction models, please refer to Tumac and Hojjati (2016).

2.1.2 Performance prediction model

The present study investigated the performance of impact hammers in two tunneling projects in Istanbul. A relatively large number of data points were collected and used to investigate the effects of the properties of the excavated rock and machine power on the performances of the impact hammers. Based on the previous studies, *RQD*, *UCS*, and *SHRV* were selected as the representative intact rock/rock mass properties as they have been more frequently reported to have an effect on *IBR*. For machine related parameters, only *P* was included as it is the only machine related parameter that has been used by previous researches. A hybrid evolutionary function fitting algorithm, which combined *GEP* and particle swarm optimization, was used to establish the statistical model. Finally, the performance of the model was numerically tested against a model developed using multiple linear regression (*MLR*) analysis and

those developed by Bilgin et al. (1996) (Eqs. 2.1 and 2.2), Bilgin et al. (2002) (Eq. 2.3), and Tumac and Hojjati (2016) (Eq. 2.24). In comparison to the existing impact hammer performance prediction models, the statistical model suggested in the present study, either is applicable to a wider range of rocks, was developed based on a significantly higher number of data points, requires a small number of more easily obtainable and more commonly used input parameters, or reaches a notably higher accuracy level.

2.2 Specific energy prediction

As mentioned in the previous section, determining the advance rate of mechanical excavators is an important factor in choosing the excavation method from the early phase of feasibility study (Copur et al., 2017; Rostami, 2011; Yetkin et al., 2016). For many types of excavation systems, such as *TBM*, roadheader, impact hammer, chain saw, surface miner, etc., advance rate prediction models exist (Bilgin et al., 1996; Comakli, 2019; Copur et al., 2011; Entacher et al., 2014; Khademi Hamidi et al., 2010; Ozfirat et al., 2017; Rostami, 2011; Tumac and Hojjati, 2016). However, estimating advance rate based on specific energy (*SE*) is considered to be a more generic and popular approach as it is not limited to a certain type of mechanical excavation system (Acaroglu et al., 2008; Balci et al., 2004; Bilgin et al., 2006, 2005; Comakli et al., 2014; Copur et al., 2001; Rostami, 2011; Rostami et al., 1994; Tiryaki and Dikmen, 2006; Tumac et al., 2007; Wang et al., 2018; Yilmaz et al., 2015). Eqs. 2.7, 2.8, and 2.9 show the formulation for this approach (Rostami, 2011).

In Eq. 2.7, *ICR* is the instantaneous cutting rate (m^3/h), *P* is the output power of the machine (*kWh*/*hour*), η is the machine's efficiency (in percent), and *SE* is the specific energy (kWh/m^3) (Pomeroy, 1963; Roxborough, 1973).

$$ICR=\frac{P\times\eta}{SE} \tag{2.7}$$

By dividing the *ICR*, calculated using Eq.2.7, by cross sectional area of excavation (*A* in m^2), the rate of penetration (*ROP*) may be estimated:

$$ROP=\frac{ICR}{A} \tag{2.8}$$

Finally, the daily advance rate (*DAR*) is determined using the following equation:

$$DAR=ROP\times MUT\times N_s\times H \tag{2.9}$$

where *MUT* is Machine Utilization Time and is defined as the net excavation time excluding the delays due to muck removal, support installation, etc., N_s is the number of shifts per day, and *H* is the number of working hours per shift.

2.2.1 Parameters with a significant impact on specific energy

As it was clarified, assessment of *SE* for different types of rock along the alignment of an excavation work is of crucial importance for estimating the advance rate of the excavation system. Full-scale linear rock cutting (*FSLC*) experiment is the most effective and widely used method for determining *SE* (Abu Bakar et al., 2014; Abu Bakar and Gertsch, 2013; Balci et al., 2004; Balci, 2009; Balci and Bilgin, 2007; Bilgin et al., 2005, 2006, 2013; Chang et al., 2006; Cho et al., 2013; Copur et al., 2001, 2003; Copur, 2010; Copur et al., 2011, 2016, 2017; Dogruoz et al., 2016; Dogruoz and Bolukbasi, 2014; Gertsch et al., 2007; Ma et al., 2015; Pan et al., 2018; Xue et al., 2018). According to Bilgin et al. (2006), at *FSLC* experiment, the drag (or cutting), normal, and side forces acting on an unscaled cutter (disk cutter, point attack pick, etc.) are recorded while a linear cut, with a fixed depth of penetration, is being made on a large block of rock cemented in a stiff frame. At the end of each cut, the volume of the rock excavated by the cutter is carefully measured. Then, depending on the desired experiment plan, the same cutting process will be repeated using different values for spacing between the adjacent cuts and/or different values of depth of cut in order to find the optimum ratio of cut spacing to depth of cut at which the *SE* is minimized (Bilgin et al., 2013). For each individual pair of "depth of cut and cut spacing" values, the *SE* is determined using the following equation (Pomeroy, 1963; Roxborough, 1973):

$$SE=\frac{FC}{Q} \tag{2.10}$$

where *FC* is the cutting force (*kN*), *Q* is the yield which is defined as the volume of rock cut in unit length of cutting (m^3/km), and *SE* is the specific energy (MJ/m^3).

As the size of the cutter is the same as that of a real one, the results of this increasingly popular test bear minimum amount of uncertainty and can potentially cover anomalous aspects of rock behavior that are rather inexplicable by its physical and mechanical properties (Bilgin et al., 2013). The outcomes of the *FSLC* may be used to either predict the performance of the mechanical excavators or enhance it through choosing the optimum ratio of cut spacing to depth of cut (*s*/*d*) for an excavation work (Bilgin et al., 2013). The relation between the *SE* and *s*/*d* is commonly presented in form of the well-known graph shown in Figure 2-1. According to Bilgin et al. (2013), either of a too tight or a too wide cut spacing results in an inefficient rock cutting. With a constant depth of cut (*d*), smaller values of spacing (*s*) result in higher *SE* as the fragmentation process shifts from chipping towards grinding/overcrushing (Figure 2-1-*A*). While the ratio of *s* to *d* increases, the required *SE* for fragmentation decreases to an optimum point, where tool wear is also optimum (Figure 2-1-*B*). For *s*/*d* values larger than the optimum value, the required *SE* increases again due to insufficient chip formation (Figure 2-1-*C*). The significant effect of cut spacing, depth of cut, and *s*/*d* on *SE* required by point attack picks is experimentally verified by Copur et al. (2001), Copur et al. (2003), Yao et al. (2011), Copur et al. (2017), Jeong (2017), Wang et al. (2017), and Park et al. (2018).

In addition to cut spacing and depth of cut, rock properties and some

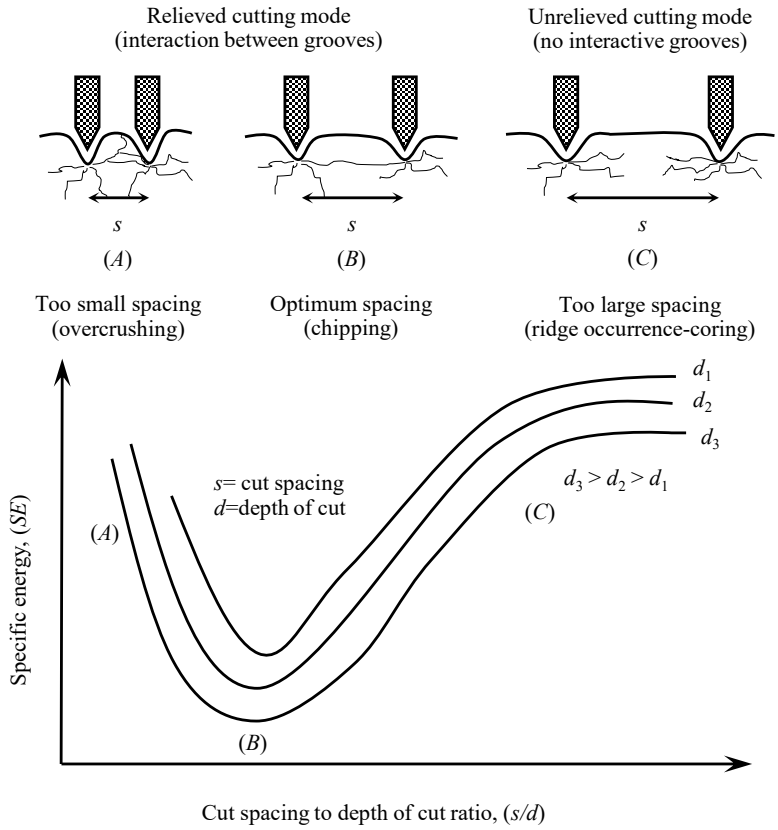

Figure 2-1: Effect of cut spacing (s), depth of cut (d), and their ratio (s/d) on specific energy and cutting efficiency (adapted from Bilgin et al. (2014)).

other geometrical features of the cutting system also affect *SE*. Copur et al. (2001) studied applicability of mechanical miners to production in Turkish mines. They used *SE*, determined by conducting a set of *FSLC* tests on eleven different rock types using point attack picks, to predict production rate (Eq.2.7). As a conclusion of their study, Copur et al. (2001) showed that optimum *SE* may be expressed as a function of *UCS* and *BTS*. Balci et al. (2004) investigated the relationship between rock properties and optimum *SE*. They used a collection of 23 different rock

types to determine the optimum *SE* values adopting the same approach as Copur et al. (2001). Balci et al. (2004) reported a moderately strong statistical relationship between the optimum *SE* and each of *UCS*, *BTS*, static and dynamic elasticity moduli, *SHRV*, and product of *UCS* and *BTS*. This conclusion, except for the relation between *SE* and product of *UCS* and *BTS*, was verified by another study conducted by Bilgin et al. (2006). Tumac et al. (2007) reported a relationship between *SE* and *SSH*. Yilmaz et al. (2015) found a statistical relation between a parameter called hybrid dynamic hardness, which is a function of rock surface hardness, and *SE* values published by Tumac et al. (2007) and Tumac (2014). Wang et al. (2018) investigated the effect of different factors on *SE* and reconfirmed the significant effect of *UCS* and *BTS* on *SE*. The research conducted by Park et al. (2018) also showed the effect of *UCS* on *SE*.

Reportedly, in addition to rock properties, cut spacing, and depth of cut, there are certain cutter related parameters that have an effect on *SE*. For point attack picks for instance, attack angle (θ_{attack}), skew angle (θ_{skew}), and tip angle (θ_{tip}) may have a considerable effect on *SE*. See Figure 2-2 for the definition of those angles.

Jeong (2017), Jeong et al. (2020), and Park et al. (2018) investigated the effect of attack and θ_{skew} on *SE* required by point attack picks using a relatively large set of lab-scale linear cutting tests. They concluded that changes in those angles can lead to significant changes in *SE*. Figure 2-3 shows representative cases from those studies.

Roepke and Voltz (1983) conducted a series of cutting tests on coal using point attack picks with 60° and 90° tip angles. As Figure 2-3 shows, for all values of depth of cut that they used during their tests, the cutter

with 60° tip angle consumed significantly less energy compared to the one with 90° tip angle.

The main disadvantage of *FSLC* experiment is that collecting the samples used in this test is usually time consuming, costly, and sometimes, impossible (Balci et al., 2004; Cho et al., 2013; Copur et al., 2017; Dursun and Kemal, 2016; Entacher et al., 2014; Kang et al., 2016; Yasar et al., 2015; N. Gunes Yilmaz et al., 2015). In addition, the full-scale linear cutting machine is an equipment that is usually not easily accessible (Balci et al., 2004; Wang et al., 2018; Yasar et al., 2015). In order to deal with this disadvantage, many researchers have suggested statistical prediction models that relate optimum *SE* values determined using relieved full-scale cutting test and different cutter types (i.e. point attack picks, disk, chisel, etc.) to properties of rock, excavation system,

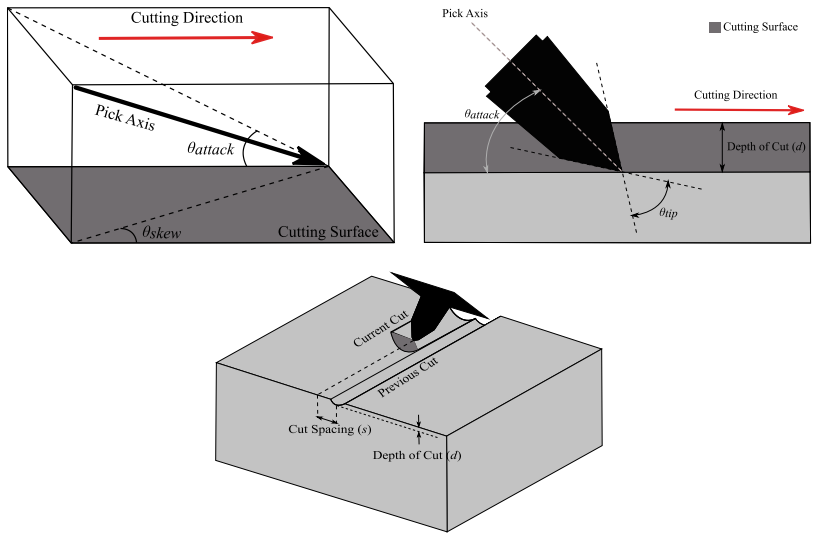

Figure 2-2: Definitions for Tip angle (θ_{tip}), Attack angle (θ_{attack}), Skew angle (θ_{skew}), Depth of Cut (d), and Cut Spacing (s) (Jeong, 2017))

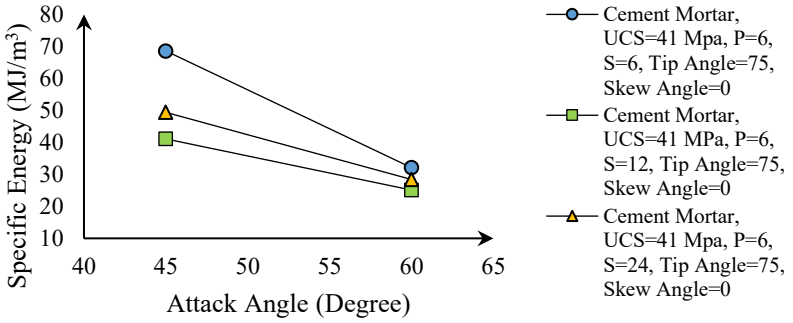

(*a*)

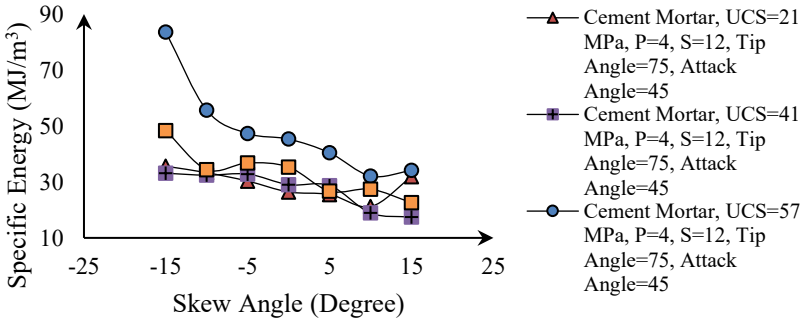

(*b*)

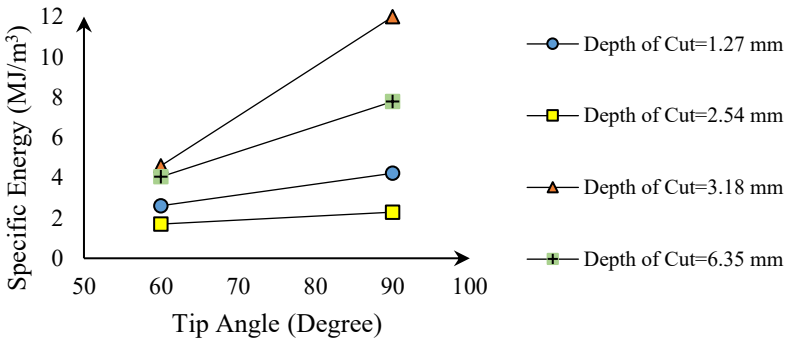

(*c*)

Figure 2-3: The relationship between specific energy and attack angle, skew angle, and tip angle according to the data published by Park et al. (2018) (plots (*a*) and (*b*)) and Roepke and Voltz (1983) (plot (*c*))

or the outputs of other rock cutting tests such as small-scale linear cutting. Considering the models developed for point attack picks, usually due to the limited number of *FSLC* tests, those models fail to include all of the cutting parameters that significantly contribute to the value of *SE* (θ_{tip}, θ_{attack}, θ_{skew}, penetration depth, cutter spacing, and cut spacing to depth of cut ratio) (Balci et al., 2004; Bilgin et al., 2006; Copur et al., 2001, 2003, 2017; Tumac et al., 2007; Wang et al., 2018; N. Gunes Yilmaz et al., 2015). Although a small number of input parameters is regarded as an advantage for a prediction model, in this case, it limits the applicability of those models for roughly determining optimized cutting parameters at early stages of a project when *FSLC* test is not reasonably economic to be conducted yet. In addition, in the later stages of the project, a model that effectively describes the relation between *SE* and cutting parameters may be very useful for decreasing the number of the *FSLC* experiments that are required to find the optimum *SE* value.

2.2.2 Specific energy prediction model

The second objective of this study is to statistically predict *SE* required by point attack picks in relieved cutting mode such that it includes representative rock properties, i.e. *UCS* or *BTS*, in addition to the cutting parameters that have a significant effect on *SE*, i.e. penetration depth (d) and cut spacing (s), ratio of cut spacing to depth of cut (s/d), θ_{tip}, θ_{attack}, θ_{skew}. See Figure 2-1and Figure 2-2 for definitions of the cutting parameters.

2.3 Forces acting on a point attack pick

Point attack picks are widely used in rock excavation machines such as roadheaders, shearers, trenchers, surface miners, or continuous miners.

As Figure 2-4 shows, there are three orthogonal forces acting on a pick while it is cutting. Cutting force is the force acting opposite to the direction of cutting action, normal force is the force acting in the direction of the normal to the cutting surface, and side force is the force acting in a direction normal to cutting and normal force. Those forces are of interest for designers as they can be used to assess the required torque and thrust for the machine as well as the stability of the cutters and vibration of the drum (Park et al., 2018). Full-scale linear cutting (*FSLC*) test is the most dependable method for estimating the forces acting on cutters (point attack, disk, etc.) and the SE required by them. However, as mentioned in the previous section, the *FSLC* machine is not so common around the world. Even when the test equipment is available, obtaining the large samples required by *FSLC* test is a difficult task (Balci et al., 2004; Cho et al., 2013; Dursun and Kemal, 2016; Entacher et al., 2014; Kang et al., 2016; Yasar et al., 2015; Yilmaz et al., 2015). Therefore, it appeals to the designers to have some tools for estimating those forces at least in the preliminary stages of a project.

2.3.1 Existing force prediction models

The most famous theoretical models for estimation of maximum cutting force acting on point attack picks in unrelieved cutting mode are those suggested by Evans (1984) (Eq. 2.11), Göktan (1990) (Eq. 2.12), and Roxborough and Liu (1995) (Eq. 2.13) (Bilgin et al., 2013). However, as those models are developed for unrelieved cutting mode, they usually fail to reasonably predict forces acting on cutters in relieved mode (Bilgin, 1977; Bilgin et al., 2006).

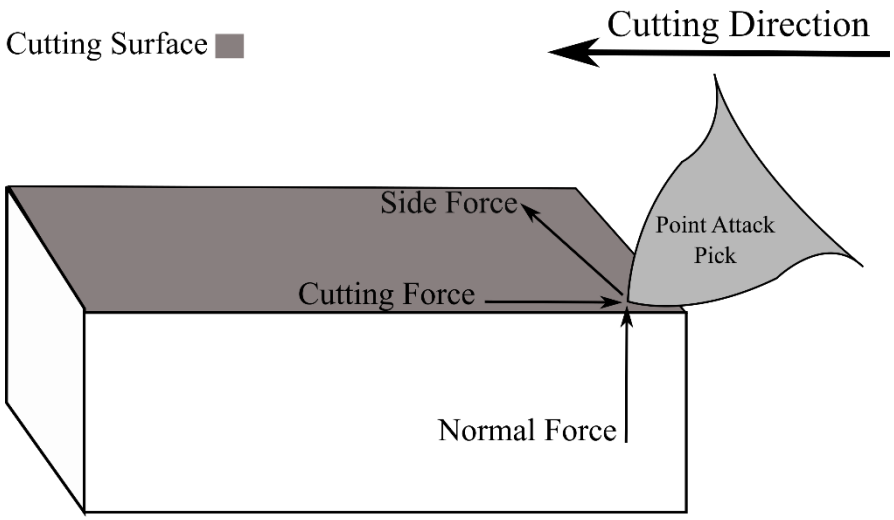

Figure 2-4: Orthogonal forces acting on a conical pick

$$F_{CP}=\frac{16\pi d^2 {\sigma_t}^2}{\cos^2\left(\frac{\theta_{tip}}{2}\right)\sigma_c} \tag{2.11}$$

$$F_{CP}=\frac{4\pi\sigma_t d^2 \sin^2({}^{\theta_{tip}}/_{2}+\theta_{friction})}{\cos({}^{\theta_{tip}}/_{2}+\theta_{friction})} \tag{2.12}$$

$$F_{CP}=\frac{16\pi\sigma_c d^2 {\sigma_t}^2}{\left[2\sigma_t+\left(\sigma_c\cos({}^{\theta_{tip}}/_{2})\right)\left(\frac{1+\tan(\theta_{friction})}{\tan(\theta_{friction}/2)}\right)\right]^2} \tag{2.13}$$

where F_{CP} is the peak cutting force, d is the depth of penetration, σ_t is the tensile strength of rock, σ_c is the uniaxial compressive strength of rock, θ_{tip} is the cutter's tip angle, and $\theta_{friction}$ is the friction angle between cutter and rock.

To address that issue, researchers tried to develop empirical/semi-empirical models that can predict cutting or normal force in relieved cutting mode (Bilgin et al., 2006; Goktan and Gunes, 2005; Tiryaki et al., 2010; Wang et al., 2017a; Yasar, 2020).

Based on the results of 14 *FSLC* tests conducted by Tuncdemir (2002) and Kel (2003), Goktan and Gunes (2005) developed a semi-empirical model for prediction of peak cutting force (Eq. 2.14). According to their conclusion, mean cutting force may be predicted by dividing the predicted peak cutting force to three (Eq. 2.15).

$$F_{CP}=\frac{12\pi\sigma_t d^2\sin^2\left[1/2\left(\theta_{tip}/2+\theta_{attack}\right)+\theta_{friction}\right]}{\cos\left[1/2\left(\theta_{tip}/2+\theta_{attack}\right)+\theta_{friction}\right]},\ R^2=0.83 \qquad (2.14)$$

$$F_{CM}=\frac{4\pi\sigma_t d^2\sin^2\left[1/2\left(\theta_{tip}/2+\theta_{attack}\right)+\theta_{friction}\right]}{\cos\left[1/2\left(\theta_{tip}/2+\theta_{attack}\right)+\theta_{friction}\right]},\ R^2=0.97 \qquad (2.15)$$

where F_{CP} is the peak cutting force in *kN*, F_{CM} is the mean cutting force in *kN*, σ_t is the Brazilian tensile strength in *MPa*, d is the depth of cut in *mm*, θ_{tip} is the cutter's tip angle in *degree*, θ_{attack} is the attack angle of the pick in *degree*, and $\theta_{friction}$ is the friction angle between cutter and rock in *degree* (is set equal to 10° by Goktan and Gunes (2005)).

Bilgin et al. (2006) suggested a group of equations for prediction of mean cutting and mean normal force using simple regression. Among their suggested equations, those that use *UCS*, *BTS*, and *SHRV* as predictors, are more accurate in terms of R^2 (Eq. 2.16 - Eq. 2.21).

$$F_{CM}/d = 2.347\sigma_c^{0.785},\ R^2 = 0.808 \quad (2.16)$$

$$F_{CM}/d = 16.794\sigma_t^{0.721},\ R^2 = 0.754 \quad (2.17)$$

$$F_{CM}/d = 3.292e^{0.058SH},\ R^2 = 0.716 \quad (2.18)$$

$$F_{NM}/d = 0.752\sigma_c^{1.051},\ R^2 = 0.817 \quad (2.19)$$

$$F_{NM}/d = 10.687\sigma_t^{0.947},\ R^2 = 0.735 \quad (2.20)$$

$$F_{NM}/d = 1.141e^{0.079SHRV},\ R^2 = 0.744 \quad (2.21)$$

where F_{CM} is the mean cutting force in *kgf*, F_{NM} is the mean normal force in *kgf*, d is the depth of cut in *mm*, σ_c is the uniaxial compressive strength in *MPa*, σ_t is the Brazilian tensile strength in *MPa*, and *SHRV* is *N*-24 type Schmidt hammer rebound value (average of the top 10 out of 20 values, which are the results of impacts separated by at least one plunger diameter).

Tiryaki et al. (2010) used the 26 data points generated by Balci and Bilgin (2007) in order to develop models for prediction of mean cutting force. They analyzed the data using *MLR*, multiple non-linear regression (*MNLR*), regression trees, and *ANN*. Eq. 2.22 and Eq. 2.23 show the *MLR* and *MNLR* model developed by Tiryaki et al. (2010), respectively.

$$F_{CM} = -19.3 + 0.36d + 0.04\sigma_c + 0.03E_{dyn},\ R^2 = 0.89 \quad (2.22)$$

$$F_{CM} = 0.01d^{1.08}\sigma_c^{0.32}E_{dyn}^{0.29}SHRV^{0.52},\ R^2 = 0.95 \quad (2.23)$$

where F_{CM} is in *kN*, d is the depth of cut in *mm*, σ_c is the uniaxial compressive strength in *MPa*, E_{dyn} is the dynamic elasticity modulus in *GPa*, and *SHRV* is the hardness determined using *N*24 Schmidt hammer.

Wang et al. (2017) proposed empirical models for prediction of cutting force in relieved cutting mode (Eq. 2.28 – Eq. 2.29) and normal force in unrelieved and relieved cutting mode (Eq. 2.26 – Eq. 2.27 and Eq. 2.30 – Eq. 2.31) based on empirical models developed for prediction of cutting force in unrelieved cutting mode (Eq. 2.24 – Eq. 2.25).

$$F_{CPU}=\frac{(1.0999\sigma_c+15.7017\sigma_t)\sin^2\left(\left(\theta_{tip}/2+\theta_{attack}\right)/2+\theta_{friction}/3\right)}{\cos\left(\left(\theta_{tip}/2+\theta_{attack}\right)/2+\theta_{friction}/3\right)}d^2+4562,\ R^2=0.82 \tag{2.24}$$

$$F_{CMU}=\frac{(0.3955\sigma_c+5.6468\sigma_t)\sin^2\left(\left(\theta_{tip}/2+\theta_{attack}\right)/2+\theta_{friction}/3\right)}{\cos\left(\left(\theta_{tip}/2+\theta_{attack}\right)/2+\theta_{friction}/3\right)}d^2+1581,\ R^2=0.85 \tag{2.25}$$

$$F_{NPU}=\begin{cases}0.336F_{CPU}\sigma_c{}^{0.234},\ R^2=0.67\\ 0.56\mathrm{F}_{CPU}e^{0.234\sigma_t},\ R^2=0.70\end{cases} \tag{2.26}$$

$$F_{NMU}=\begin{cases}0.313F_{CMU}\sigma_c{}^{0.285},\ R^2=0.67\\ 0.585\mathrm{F}_{CMU}e^{0.092\sigma_t},\ R^2=0.71\end{cases} \tag{2.27}$$

$$F_{CPR}=0.779F_{CPU},\ R^2=0.73 \tag{2.28}$$

$$F_{CMR}=0.779F_{CMU},\ R^2=0.70 \tag{2.29}$$

$$F_{NPR}=\begin{cases}0.316F_{CPR}\sigma_c{}^{0.224},\ R^2=0.69\\ 0.524F_{CPR}e^{0.069\sigma_t},\ R^2=0.65\end{cases} \tag{2.30}$$

$$F_{NMR}=\begin{cases}0.311F_{CMR}\sigma_c{}^{0.268},\ R^2=0.70\\ 0.561F_{CMR}e^{0.085\sigma_t},\ R^2=0.71\end{cases} \tag{2.31}$$

where F_{CPU} is the peak cutting force in unrelieved cutting mode in *kN*, F_{CMU} is the mean cutting force in unrelieved cutting mode in *kN*,

F_{NPU} is the peak normal force in unrelieved cutting mode in *kN*, F_{NMU} is the mean normal force in unrelieved cutting mode in *kN*, F_{CPR} is the peak cutting force in relieved cutting mode in *kN*, F_{CMR} is the mean cutting force in relieved cutting mode in *kN*, F_{NPR} is the peak normal force in relieved cutting mode in *kN*, F_{NMR} is the mean normal force in relieved cutting mode in *kN*, σ_c is the uniaxial compressive strength in *MPa*, σ_t is the Brazilian tensile strength in *MPa*, θ_{tip} is the cutter's tip angle in *degree*, θ_{attack} is the attack angle of the pick in *degree*, and $\theta_{friction}$ is the friction angle between cutter and rock in *degree*.

Yasar (2020) proposed a model for prediction of cutting force in relieved cutting mode (Eq. 2.32). He concluded that the cutting force in relieved cutting mode is equal to the calculated cutting force for unrelieved cutting mode multiplied by 0.72. He also suggested that the maximum cutting force in each cutting mode is equal to 2.45 times the mean cutting force in the same cutting mode.

$$FC=kk_r\varepsilon d\sigma_c \frac{\sin\frac{1}{2}(\frac{\pi}{2}-\alpha)}{1-\sin\frac{1}{2}(\frac{\pi}{2}-\alpha)} e^{-0.054\beta} \tag{2.32}$$

k=1 for mean cutting force and k=2.45 for maximum cutting force

k_r=1 for unrelieved cutting and k_r=0.72 for relieved cutting

ε=6.36 for σ_c/σ_t <10 and ε=7.24 for σ_c/σ_t >10

$\alpha=\frac{\pi}{2}-(\theta_{attack}+\frac{\theta_{tip}}{2})$=rake angle and β=back clearance angle=$\theta_{attack}-\frac{\theta_{tip}}{2}$

where *FC* is cutting force in *N*, σ_c is the uniaxial compressive strength in *MPa*, σ_t is the Brazilian tensile strength in *MPa*, θ_{tip} is the

cutter's tip angle in *degree*, and θ_{attack} is the attack angle of the pick in *degree*.

2.3.2 Parameters with a significant impact on forces

According to the previously published prediction models, *UCS*, *BTS*, depth of penetration, cutter's tip angle, attack angle of the cutter, and friction angle between cutter and rock may have a significant effect on normal and cutting force acting on a conical pick in relieved cutting mode. However, none of them reflects the effect of cut spacing (*s*).

Park et al. (2018) showed that "*s*" has a significant effect on peak cutting force, mean cutting force, peak normal force, and mean normal force. Effect of "*s*" on mean and peak side force was previously shown by Jeong (2017) (Figure 2-5). In addition to "*s*", the models previously developed by other researchers do not consider the effect of θ_{skew} on cutting and normal force. The significant effect of θ_{skew} on cutting, normal, and side force were previously shown by Park et al. (2018) and Jeong et al. (2020).

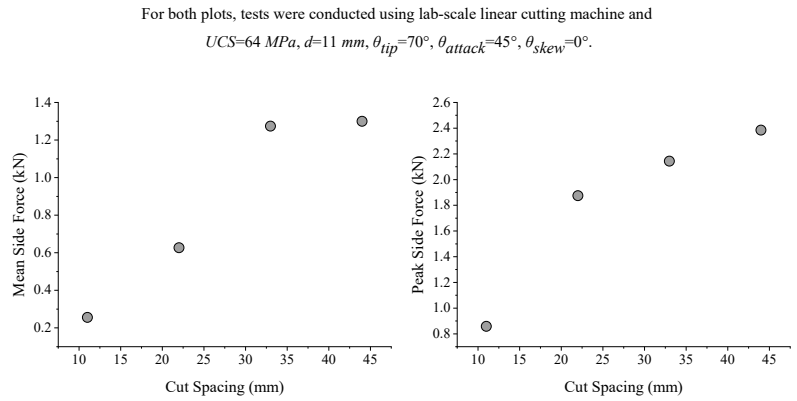

Figure 2-5: Representative cases showing effect of cut spacing on mean and peak side force according to Jeong (2017)

It should be added that, to the extent of authors' knowledge, there are currently no prediction models for either peak or mean side force acting on a point attack pick.

2.3.3 Forces prediction models

As the third objective of this study, an effort was made in order to find empirical prediction models for average and maximum values of forces (cutting, normal, and side) acting on a point attack pick such that they can accommodate representative rock properties such as *UCS* or *BTS* as well as all of the previously mentioned important machine-related parameters, i.e., d, s, θ_{tip}, θ_{attack}, and θ_{skew}.

3. STATISTICAL DATA

In order to solve the problems identified during the survey of literature, statistical data were collected. The following sections provide a description of the data used to tackle each of the problems defined in the previous chapter.

3.1 Impact hammer performance

The database used in this study was a combination of the data collected during the construction of two metro tunnels in Istanbul, namely Levent-Hisarustu tunnel and Uskudar-Cekmekoy tunnel.

3.1.1 Levent-Hisarustu tunnel

Located in European side of Istanbul, the 3,104 m long underground mini-metro tunnel connects Levent station in Yenikapi-Haciosman metro line to Hisarustu in Asiyan neighborhood. The studied area is located in Trakya Formation of the Carboniferous age. Fine- to coarse-grained strongly fractured mudstone, laminated and fractured siltstone, shale, sandstone, and conglomerate are the constituents of the Trakya formation. In addition, presence of diabase and andesite dykes was evident through driving the tunnel. According to Bilgin et al. (2002), *RQD* values of the formation vary between 0% to 75%. According to Tuncdemir (2008), in Trakya Formation, uniaxial compressive strength (*UCS*), elasticity modulus, dry specific gravity, and porosity range from 22.1 to 59.2 *MPa*, 6.63 *GPa* to 18.5 *GPa*, 2.49 to 2.75 g/cm^3, and 2.9 to 34.71% in turn.

The single tracked tunnel has a 34.72 m^2 cross section and was excavated in two sequences based on New Austrian Tunneling Method

(*NATM*). The upper bench, with cross sectional area of 27.3 m^2, was excavated 25-30 m ahead of the 7.42 m^2 lower bench. To excavate the tunnel, a *JCB* excavator matched with an *MTB 120* hydraulic hammer was used. Table 3-1 shows the technical features of the hydraulic hammer.

Sixty zones of site investigations were defined along the tunnel alignment. *RQD* was chosen to be the representative of the rock mass properties. *RQD* values were carefully recorded for the defined zones as the excavation was progressing. As suggested by Ulusay and Hudson (2007), volumetric joint count (J_v) was used for determination of *RQD*.

Table 3-1: The technical features of the hydraulic hammer used to construct Levent-Hisarustu metro line.

Specifications	Values
Operating weight (kg)	1200
Impact energy (J)	1880
Operating pressure (bar)	135
Maximum pressure for safety (bar)	175 – 185
Oil flow (l/min)	70 – 130
Back pressure (bar)	10
Hammer diameter (*mm*)	110
Accumulator pressure (bar)	40
Blow frequency (bpm)	400/700
Machine's input power (*Hp*)	30

In addition, for each individual zone, machine performance was recorded. Sandstone with *UCS* values varying from 68.6 to 145 *MPa* and *RQD* of 40% to 60% was the dominant rock (60%) encountered along the tunnel alignment. Siltstone with *UCS* of 45.8 to 123.3 *MPa* and *RQD* values of 38%-44% occurred in 20% of the tunnel alignment. The remaining 20% was equally divided between diabase (158.7 $MPa \leq UCS \leq 195.6$ *MPa,* $45\% \leq RQD \leq 60\%$) and mudstone and shale (8.9 $MPa \leq UCS \leq 40.1$ *MPa,* $10\% \leq RQD \leq 40\%$).

From each investigation zone, rock samples were collected and values of *UCS*, Schmidt hammer rebound values (*SHRV*) were determined. The *SHRV* values were determined using an *L*-type hammer and the method suggested by Fowell and McFeat-Smith (1976). *UCS* values were measured using *ISRM* suggested standards (Ulusay and Hudson, 2007). Table 3-4 shows the descriptive statistics of the collected data.

3.1.2 Uskudar-Cekmekoy tunnel

The 50.286 *km* long Uskudar-Cekmekoy tunnel is located on the Asian side of Istanbul and stretches between the Uskudar and Cekmekoy districts. A 13.366 *km* section of the tunnel with a cross-sectional area of 75.6 m^2 (59.79 m^2 upper bench and 15.81 m^2 lower bench) was built using the *NATM*. Table 3-2 lists the average properties of the rock faced along the alignment of the tunnel.

A *Rammer BR* 2577 hydraulic hammer mounted on a *CAT* 323 *DL*2 carrier was used to excavate the tunnel (Figure 3-1). Table 3-3 lists the general specifications of the system used for the excavation.

Table 3-2: General characteristics of major rock types excavated along Uskudar-Cekmekoy metro tunnel

Geological Formation	Rock Type and its Percentage along the Tunnel Alignment	Unit Weight (kN/m^3)	Poisson's Ratio	Internal Friction Angle (*Degree*)	Cohesion (*MPa*)	Maximum Uniaxial Compressive Strength (*MPa*)	Elasticity Modulus (*GPa*)
Kartal	Shale, 29.9%	26.2	0.28	43.1	18.6	33.02	7.4
Kurtkoy	Sandstone and Conglomerate, 29.7%	26.9	0.29	43.1	19.5	53.33	10.31
Aydos	Quartzite-Andesite, 1.6%	26.1	0.28	54.2	-	73.03	12.64
Dolayoba	Limestone, 17.5%	27	0.3	49.4	10.6	42.96	15.82

Figure 3-1: System used to excavate Uskudar-Cekmekoy tunnel

Table 3-3: Technical features of excavation system used in construction of Uskudar-Cekmekoy tunnel

Specifications	Values
Operating weight (*kg*)	1600
Impact energy (*J*)	2500
Operating pressure (*bar*)	155
Maximum pressure for safety (*bar*)	175
Oil flow (*l*/*min*)	120–130
Back pressure (*bar*)	12
Hammer diameter (*mm*)	122
Oil temperature (°*C*)	-20 to +80
Accumulator pressure (*bar*)	40
Maximum blow frequency (*bpm*)	540–770
Machine's input power (*kW*)	48

The portion of the Uskudar-Cekmekoy tunnel that was excavated using a hydraulic hammer was divided into 25 sections. The performance of the machine for the upper bench excavation, was carefully recorded for each section, and the *RQD*, *SHRV*, and *UCS* value associated with the section were measured. *UCS* tests were conducted according to *ISRM* standards (Ulusay and Hudson, 2007). The *SHRV* values were determined using an *L*-type hammer and the method suggested by Fowell and McFeat-Smith (1976). The *RQD* values were determined based on the discontinuity spacing according to the method suggested by Brown (1981). After combining the collected data with the data from the Levent-Hisarustu tunneling project, a database consisting of 85 points was

Table 3-4: Descriptive statistics of data used in this study for development of a performance prediction model for impact hammer

	Measurements/Records	Number of Records	Minimum	Maximum	Mean	Std. Deviation
Levent-Hisarustu Metro Tunnel	*UCS*	60	8.90	195.60	69.04	44.46
	RQD	60	10.00	60.00	39.07	9.89
	SHRV	60	11	68	45.77	11.93
	P	60	22.38	22.38	22.38	0.00
	IBR	60	8.20	35.00	15.73	5.35
Uskudar-Cekmekoy Metro Tunnel	*UCS*	25	12.30	74.00	54.70	14.91
	RQD	25	25.00	65.00	41.74	10.83
	SHRV	25	37	68	54.08	9.28
	P	25	48.00	48.00	48.00	0.00
	IBR	25	7.97	29.90	16.89	5.96
Overall	*UCS*	85	8.90	195.60	64.37	38.85
	RQD	85	10.00	65.00	39.46	10.29
	SHRV	85	11	68	48.21	11.79
	P	85	22.38	48.00	29.91	11.74
	IBR	85	7.97	35	16.28	5.72

UCS: Uniaxial Compressive Strength (*MPa*); *RQD*: Rock Quality Designation; *SHRV*: Schmidt Hammer Rebound Value; *P*: Input Power of the Hydraulic Hammer (*kW*); *IBR*: Instantaneous Breaking Rate (m^3/h)

established. The data was used to find the relation between *IBR*, *UCS*, *SHRV*, *RQD*, and machine power. Table 3-4 lists the descriptive statistics of the established database. It should be mentioned that the *IBR* values were calculated based on the net breaking time only. In other words, the

IBR in Table 3-4 indicates the amount of rock broken by the machine (m^3) in 1 hour of machine utilization time, regardless of the time spent for support installation, muck removal, etc.

3.2 Specific energy required by point attack picks

Many researchers have shared the results of their experimental studies on specific energy (*SE*) required by point attack picks in relieved mode (see Figure 2-1 for the definition of relieved cutting mode) (Balci et al., 2004; Copur et al., 2003; Jeong, 2017; Park et al., 2018; Wang et al., 2018). However, in order to merge the data from different sources, their compatibility should be checked. According to Copur et al. (2017), the results of the full-scale experiment may be significantly affected by merely a small difference in factors such as cutting parameters, cutter geometry, cutting pattern, rock surface condition, lateral confinement, or moisture conditions. Therefore, after a detailed investigation on the test procedures used to generate each source of information, the data published by Jeong (2017) and Park et al. (2018) were selected to form the database used in the present study (Table 3-5).

Jeong (2017) and Park et al. (2018) conducted their tests using point attack picks and the same cutting pattern (single spiral) on dry samples with the same size, no lateral confinement, and with conditioned surface. Figure 3-2 shows schematic drawings of the cutting tools used by Jeong (2017) and Park et al. (2018).

Both Jeong (2017) and Park et al. (2018) used lab-scale linear cutting machine (*LSLCM*). Essentially, *LSLCM* is a scaled down version of the well-known full-scale linear cutting machine (*FSLCM*).

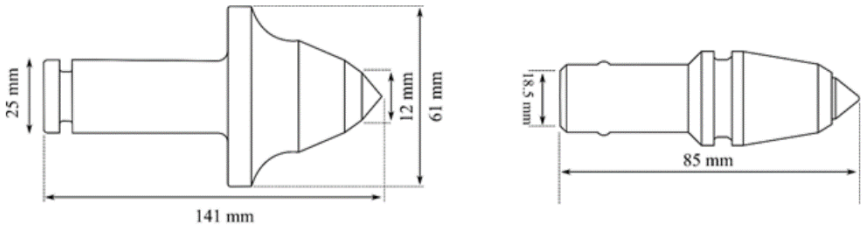

Park et. al. (2018) Jeong (2017)

Figure 3-2: Conical picks used by Park et al. (2018) (schematic drawing (a)) and Jeong (2017) (schematic drawing (b))

Table 3-5: Descriptive statistics for the data used in this study for development of a prediction model for specific energy required by point attack picks

Measurements	Number of Records	Minimum	Maximum	Mean	Std. Deviation
SE	186	12.42	106.80	38.60	17.61
UCS[*]	186	21.00	64.00	45.13	18.40
BTS[*]	186	1.80	4.70	3.76	1.25
d	186	4.00	11.00	6.33	2.15
s	186	4.00	44.00	18.55	8.02
s/*d*	186	1.00	7.00	2.97	1.01
θ_{tip}	186	70.00	75.00	72.50	2.51
θ_{attack}	186	45.00	60.00	47.42	5.31
θ_{skew}	186	-20.0	20.00	0.00	7.95

SE: Specific Energy (*MJ*/m^3); *UCS*: Uniaxial Compressive Strength (*MPa*); *BTS*: Brazilian Tensile Strength (*MPa*); *d*: Depth of Cut (*mm*); *s*: Cut Spacing (*mm*); θ_{tip}: Tip Angle (*Degree*); θ_{attack}: Attack Angle (*Degree*); θ_{skew}: Skew Angle (*Degree*)
[*] The tests were conducted based on *ISRM* standard testing methods (Ulusay and Hudson, 2007).

However, *LSLCM* is capable of applying the same range of force magnitude on a conical pick as *FSLCM* does (Kang et al., 2016). For more detailed information on *LSLCM*, please refer to Kang et al. (2016).

The specimens used by Jeong (2017) were made of Linyi sandstone (73 out of 102 tests) and concrete. The Linyi sandstone is originated from Shandong province in China. It is a homogeneous and fine grained rock with clastic structure and negligible anisotropy (Jeong, 2017; Yang and Jing, 2011). Table 3-6 shows the mechanical properties of the Linyi sandstone used by Jeong (2017) and cement mortar samples used by Park et al. (2018).

The established database was used to find the relation between *SE* and uniaxial compressive strength (*UCS*), Brazilian tensile strength (*BTS*), depth of cut (*d*), cut spacing (*s*), ratio of cut spacing to depth of cut (*s*/*d*), cutter tip angle (θ_{tip}), attack angle (θ_{attack}), and skew angle (θ_{skew}). *BTS* values for the data published by Park et al. (2018) were measured during the course of the present study using the same samples used by Park et al. (2018) (Table 3-7).

It should be added that Copur et al. (2003), Balci et al. (2004), Bilgin et al. (2006), Tumac et al. (2007), and Wang et al. (2018) have also generously shared the results of their full-scale linear cutting tests in relieved cutting mode. Since, according to Copur et al. (2017), surface conditioning can have a very important role in determination of *SE* using linear cutting test, those results could not be merged with the database used in this study as the data published in those sources are comprised of the tests conducted on unconditioned rock surface (H. Copur and X. Wang, by personal communication, 2019). The data published by Copur

et al. (2003), Balci et al. (2004), and Wang et al. (2018) was investigated by Hojjati et al. (2018). However, as the investigated data included only one value for each of θ_{tip}, θ_{attack}, and θ_{skew}, the study conducted by

Table 3-6: Mechanical properties of Linyi sandstone and Cement Mortar Samples (Jeong, 2017; Park et al., 2018)

Properties	Jeong (2017)		Park et al. (2018)		
	Linyi Sandstone	Concrete	Cement Mortar Sample I	Cement Mortar Sample II	Cement Mortar Sample III
Density (g/cm^3)	2.4	2.3	1.9	2.04	2.1
Porosity (%)	8.2	-	-	-	-
UCS (*MPa*)	64	21	21	41	57
BTS (*MPa*)	4.7	2.1	1.84	4.31	4.72
Young's Modulus (*GPa*)	10.2	21.9	-	-	-
Poisson's Ratio	0.2	0.17	-	-	-
Schmidt Hammer Rebound Hardness*	57.3	-	-	-	-
Shore Hardness*	43.5	-	-	-	-
P-Wave Velocity (*m*/*s*)	2317	-	-	-	-
S-Wave Velocity (*m*/*s*)	1531	-	-	-	-

UCS: Uniaxial Compressive Strength; *BTS*: Brazilian Tensile Strength.
*Schmidt hammer rebound and Shore hardness values were obtained by averaging the upper 10 values from 20 tests performed

Table 3-7: *BTS* values for the samples used by Park et al. (2018)

Sample	*UCS* (*MPa*)	*BTS* (*MPa*)
Low Strength	21.00	1.84
Moderate Strength	41.00	4.31
Medium Strength	57.00	4.72

UCS: Uniaxial Compressive Strength; *BTS*: Brazilian Tensile Strength

Hojjati et al. (2018) could not reflect the effect of variations of those angles on *SE*. The significant effect of θ_{tip}, θ_{attack}, and θ_{skew} on *SE* was previously shown in Figure 2-3.

3.3 Forces applied on point attack picks

The results of the same linear rock cutting tests, described in the previous section and conducted by Park et al. (2018) and Jeong (2017), were merged to establish the database. Overall, there are 195 sets of results. In each test, mean and peak values of cutting and normal force were reported. The mean and peak values of side force have been reported for 144 tests. Table 3-8 shows the descriptive statistics of the compiled database.

The established database was used in order to develop prediction models for average and maximum values of orthogonal forces acting on a point attack pick, defined by Figure 2-4, such that they can accommodate representative rock properties such as *UCS* or *BTS* as well as all of the machine-related parameters (i.e., d, s, θ_{tip}, θ_{attack}, and θ_{skew}) that have an impact on those forces.

Table 3-8: Descriptive statistics of the data used in this study for development of models for prediction of cutting, normal, and side force acting on a point attack pick

	Number of Records	Minimum	Maximum	Mean	Std. Deviation
UCS (*MPa*)	195	21.00	64.00	46.00	18.40
BTS (*MPa*)	195	1.84	4.72	3.80	1.24
d (*mm*)	195	4.00	11.00	6.31	2.11
s (*mm*)	195	4.00	44.00	18.44	8.01
s/*d*	195	1.00	7.00	2.96	1.02
θ_{tip} (*Degree*)	195	70.00	75.00	72.38	2.50
θ_{attack} (*Degree*)	195	35.00	60.00	46.85	5.80
θ_{skew} (*Degree*)	195	-20.00	20.00	0.00	7.77
Mean Side Force (*kN*)	144	0.12	6.58	1.23	1.03
Mean Cutting Force (*kN*)	195	0.45	18.38	4.35	3.67
Mean Normal Force (*kN*)	195	0.45	12.96	3.73	2.72
Peak Side Force (*kN*)	144	0.37	16.49	3.38	3.12
Peak Cutting Force (*kN*)	195	1.27	45.26	11.40	9.52
Peak Normal Force (*kN*)	195	0.58	27.90	8.87	7.55

UCS: Uniaxial Compressive Strength; *BTS*: Brazilian Tensile Strength; *d*: depth of penetration; *s*: cut spacing; θ_{tip}: Tip Angle; θ_{attack}: Attack Angle; θ_{skew}: Skew Angle

4. DATA ANALYSIS METHOD

As it was explained in Chapter 1, a supervised machine learning method had to be selected for analysis of statistical data. Artificial Neural Networks (*ANN*) and Symbolic Regression Methods (*SRMs*) are the two branches of machine learning methods that are capable of performing that task (Diveev and Shmalko, 2021; Mitchell, 1997). However, the fact that *ANN* does not reveal any information about the function or its properties made it a less desirable choice in comparison to *SRMs* (Diveev and Shmalko, 2021). In contrast to *ANN*, *SRM*s are machine learning techniques that are designed for generating mathematical functions and investigating the space of those equations with the objective of finding the function that fits best on the given data (Diveev and Shmalko, 2021).

Genetic Programming (*GP*), Gene Expression Programming (*GEP*), Grammatical Evolution, Analytic Programming, and Parse Matrix Evolution are instances of *SRM*s (Diveev and Shmalko, 2021; Ferreira, 2006). Customarily, symbolic regression models stem from *GP* and inherit its features to different extents. *GP* was originally created by Cramer (1985) and evolved by John R. Koza (1992). In brief, *GP* is an "evolutionary computation technique/evolutionary algorithm" that stochastically evolves a randomly generated population of "encoded individuals/computer programs/candidate solutions" through generations with the objective of improving their "fitness/prediction accuracy". Figure 4-1 shows the basic flow chart of *GP*.

As *GP* is an inherently random process, its results may not be guaranteed to be always fruitful. On the other hand, the very same attribute helps *GP* to avoid quagmires during its quest in the space of

candidate solutions. As a result, like the evolution process in nature, it has successfully generated fresh and amazing solutions to numerous problems in real world (Poli et al., 2008).

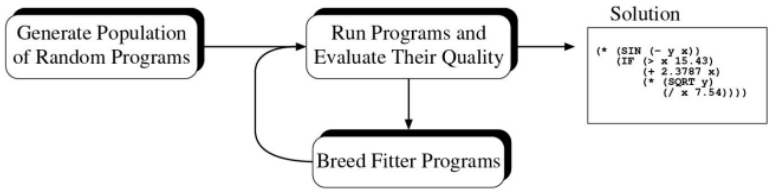

Figure 4-1: Basic flow chart of Genetic Programming (*GP*) (adapted from Poli et al. (2008))

In essence, other *SR* methods have been developed with the objective of dealing with shortcomings of *GP*. In the case of *GEP*, as it is not prone to generating syntactically incorrect genes, it benefits from more types of genetic operators compared to *GP* (see section 4.1.1, "Genetic Operators"). Thus, the "encoded individuals/computer programs/candidate solutions" generated by *GEP* can evolve in a more efficient way (Ferreira, 2006). Based on the mentioned grounds, *GEP* was selected for data analysis in this study. Section 4.1 provides a more comprehensive explanation of *GEP*.

The candidate solutions generated by *GEP* may contain numerical constants. The basic *GEP* algorithm can only adjust those constants randomly. In such a situation, use of an optimization algorithm may be helpful. Therefore, Particle Swarm Optimization (*PSO*) was used in

order to further optimize the numerical constants in the solutions generated by *GEP*. *PSO* is categorized as an evolutionary computation technique and is inspired by movements of swarms such as a flock of birds or a school of fish that are in search of food or getting away from a threat, etc. (Jones, 2007; J Kennedy and Eberhart, 1995). In this algorithm, a swarm of "particles/potential solutions" searches space of solutions in a guided manner. Section 4.2. provides a more detailed explanation of *PSO*.

4.1 Gene Expression Programming (*GEP*)

GEP is a "Individual/computer program/chromosomes" generating "evolutionary algorithm/evolutionary computation technique" that can generate a population of chromosomes/individuals which are interpreted to mathematical equations and are visually expressed as tree structures. Chromosomes/Individuals have the ability to evolve through generations such that the best fitness for each generation is at least as good as that of the previous generation. For a function fitting problem, the "fitness" can be defined as one, or a weighted combination of, mean squared error (*MSE*), root mean squared error (*RMSE*), correlation coefficient (*R*), determination coefficient (R^2), etc.

Each chromosome is consisted of a number of genes that are connected to each other by linking functions, which can be any mathematical operator such as addition, division, etc. Each gene has a head and a tail part. While the head can be constructed by a combination of members of functions set and terminals set, the tail part can only be consisted of terminals set subdivisions. The tail part, accompanied by the terminals in the head itself, feeds the functions in the head. Functions

and terminals sets are sets of mathematical operators, such as + or ×, and matrices of numerical values, respectively. The functions set may be chosen like the following:

Functions Set= {+, ×, -, ÷, Power, ln, Exp, Sin, Cos, Tan}

where "ln(x)" is the natural logarithm of the variable "x" and "Power" and "Exp" are defined as follows:

$$\text{Power}\ (x)=Ax^{B},\ A \text{ and } B \text{ are real numbers} \tag{4.1}$$

$$\text{Exp}(x)=Ce^{Dx},\ C \text{ and } D \text{ are real numbers} \tag{4.2}$$

The terminals set may be chosen like the following:

Terminals Set= {a, b, c, d, e, Random Numbers}

where a, b, c, d, and e are N × 1 matrices containing the values recorded/measured for parameters a, b, c, d, and e, respectively. Random Numbers is also an N × 1 matrix the elements of which are a repeated numerical value. Although *GEP* is theoretically capable of generating some random integers in the genes' outputs (please refer to Figure 4-3, Gene 1's output), Random Numbers may be added to the terminals set in order to provide the algorithm with more freedom for creating

models/genes with a wide range of numerical constants including integer and non-integer numbers.

The number of the units that form the tail part is determined based on the number of the units in the head, which is defined by the user. Figure 4-2 shows a chromosome with two genes. Figure 4-3 shows the expression tree for the chromosome's first gene, and its mathematical expression. In the expression tree, each circle is called a node.

Similar to what happens in the nature, each generation, except the first one, is created by the children of the individuals of the previous generation. The individuals forming the first generation are generated randomly. Within each generation, the individuals are given the opportunity of reproduction by means of genetic operators and with a chance proportional to their fitness.

4.1.1 Genetic Operators

The evolution procedure is carried out by means of genetic operator(s), which can be one, or a combination of, mutation, inversion, different types of transposition, and different types of recombination.

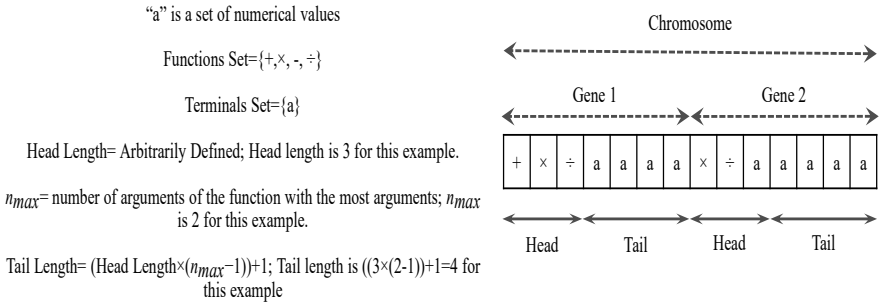

Figure 4-2: A schematic view of a chromosome with two genes

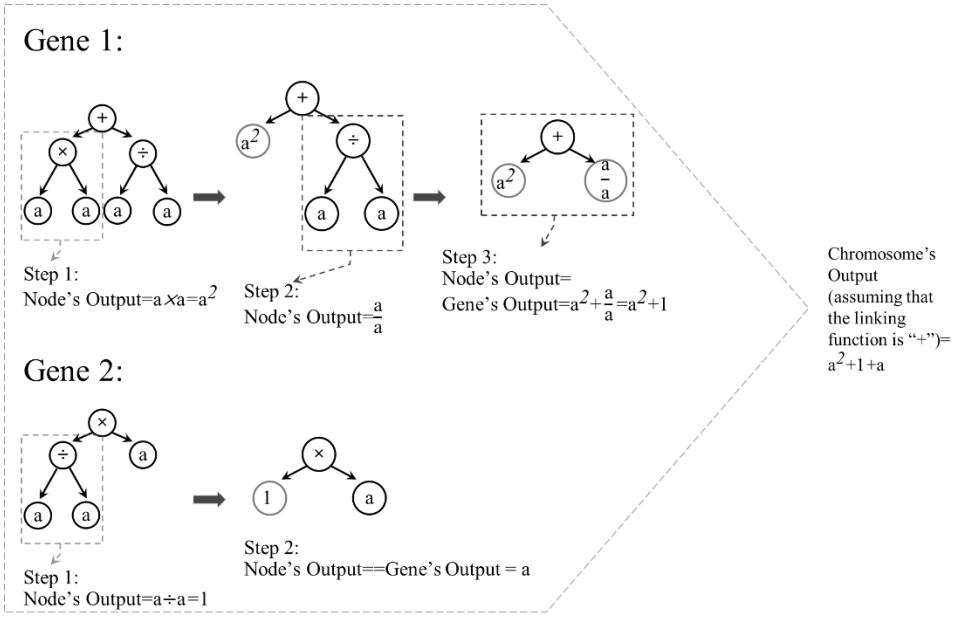

Figure 4-3: Expression trees and mathematical expressions of the genes shown in Figure 4-2; "a" is a numerical value.

Evolution continues for a certain number of generations or until the desired fitness is reached (Ferreira, 2006).

4.1.1.1 Mutation

Depending on the mutation rate defined by the user, mutations are free to happen at any randomly selected unit across a gene. The resulting gene's head can be consisted of functions and/or terminals while its tail is exclusively made of terminals, otherwise structurally incorrect chromosomes may be produced (Figure 4-4). Although it can take any value between zero to one, the mutation rate is usually set such that mutation happens for two units in each chromosome. It should be noted

that mutation occurs within all of the individuals in the new generation (Ferreira, 2006).

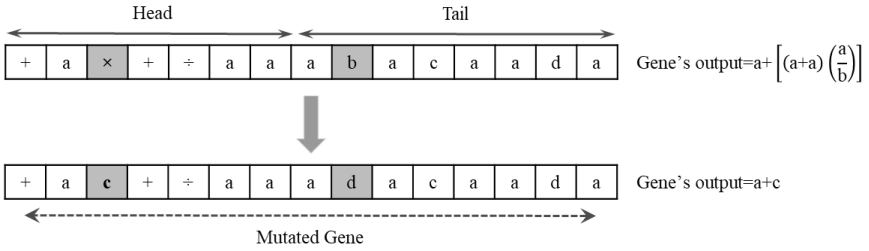

Figure 4-4: An example for mutation in a gene

4.1.1.2 Inversion

Through the inversion process, a randomly selected sequence from head of a randomly selected gene is inverted. It should be noticed that the start and end points of the sequence are randomly selected within gene's head Inversion is restricted to only the head part of the genes. Figure 4-5 shows an example of inversion operation in a gene.

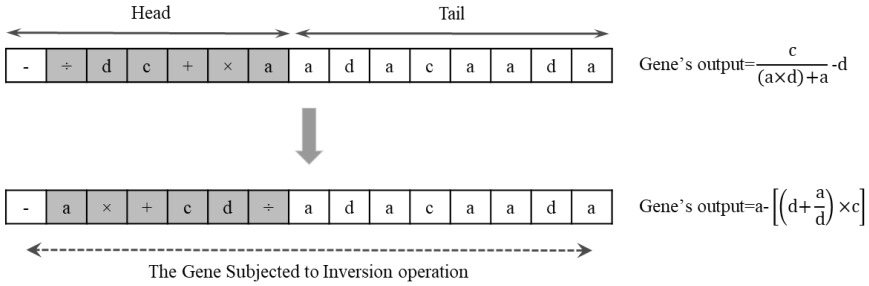

Figure 4-5: An example of inversion operation in a gene

This restriction helps the structural form of the chromosome to be maintained. In other words, by limiting inversion to the head, there will be no risk of having a function at the tail of a gene. Across each generation, the number of the chromosomes that undergo inversion depends on the arbitrarily defined inversion rate (Ferreira, 2006).

4.1.1.3 Transposition and Insertion Elements

Transposition operator, in simple words, randomly selects a piece of a gene and relocates it to a randomly selected place across the same chromosome. Three different types of transposable elements are defined in *GEP* algorithm, namely "Insertion Sequence (*IS*) elements", "Root Insertion Sequence (*RIS*) elements", and "Transposable Genes". The number of times that each of the different types of transposition are repeated in each iteration depends on the different types of transposition rates defined by the user (Ferreira, 2006).

Insertion Sequence (IS) elements

The first type is "*IS* elements". This type of transposition involves randomly selecting the start and ending positions (both positions can be either in head or tail of the gene) of a piece of a randomly selected gene and inserting that piece into the head of the same gene (except the first unit of the head or the root). Figure 4-6 shows an example for transposition of insertion sequence elements.

Root Insertion Sequence (RIS) elements

The second type, "*RIS* elements", is the same as the first with two differences. The selected piece of gene in *RIS* elements type, unlike in *IS*

elements, has to begin with a function and is inserted to the root of the same gene (Figure 4-7).

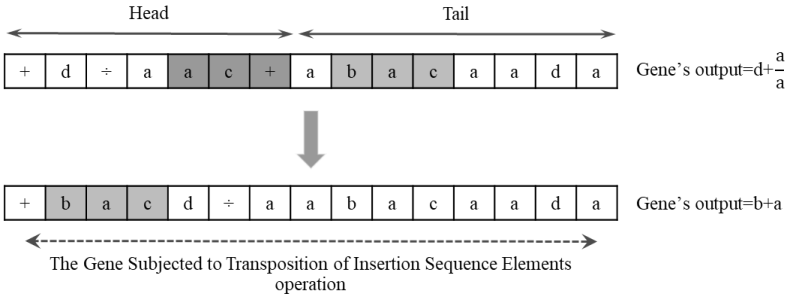

Figure 4-6: An example for transposition of insertion sequence elements. Please note that the part highlighted in light grey is the selected insertion sequence and the part highlighted in dark grey is removed at the end of the head.

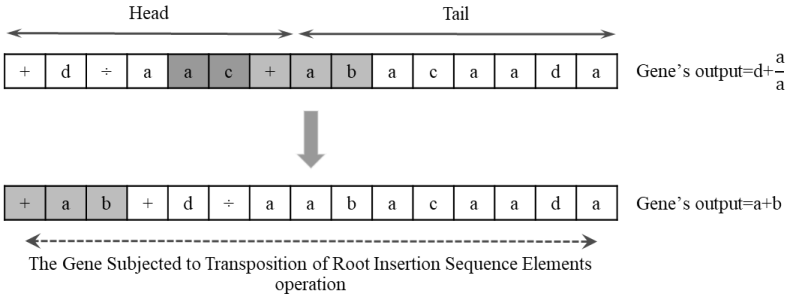

Figure 4-7: An example for transposition of root insertion sequence elements. Please note that the part highlighted in light grey is the selected sequence and the part highlighted in dark grey is removed at the end of the head.

Transposable Genes

The third type, gene transposition, works in a larger scale than the other types. Gene transposition randomly selects a gene in a randomly

selected chromosome and inserts it to the place of the first gene in that chromosome. Obviously, this operator makes a difference only for non-commutative linking functions. Figure 4-8 shows the effect of this operator on a chromosome with two genes and "subtraction" as the linking function.

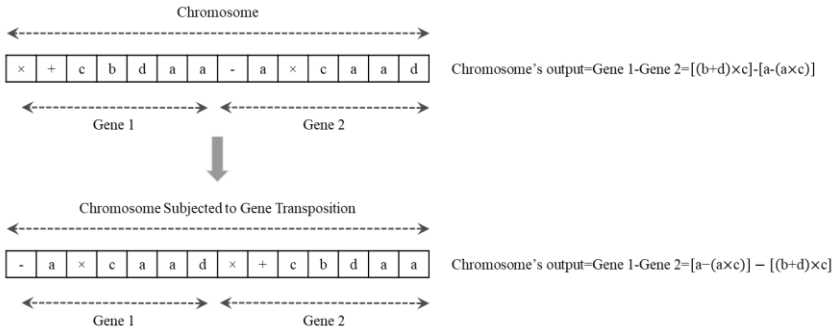

Figure 4-8: An example for gene transposition in a 2-gene chromosome with "subtraction" as the linking function.

4.1.1.4 Recombination

One-point, two-point, and gene recombination are the three different types of recombination that *GEP* algorithm uses as genetic operators. All of them involve randomly selecting two different chromosomes that are supposed to exchange some portions with each other. The number of times that each of the different types of recombination are repeated in each iteration depends on the different types of recombination rates defined by the user (Ferreira, 2006).

One-Point Recombination

One-point recombination is carried out by randomly selecting a position and exchanging the parts of two randomly selected chromosomes that start at that randomly selected position and end at the end of the selected chromosomes. In this operation, two chromosomes give birth to two children that usually are significantly different from each other and their parents. Figure 4-9 shows an example of one-point recombination.

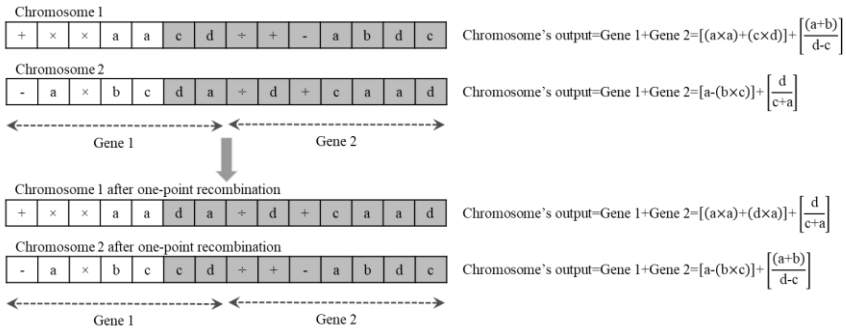

Figure 4-9: An example of one-point recombination. The parts highlighted in grey are exchanged between chromosomes.

Two-Point Recombination

In two-point recombination, two positions are randomly selected along two randomly selected chromosomes and the portions limited to those two points are exchanged (Figure 4-10). Usually, two-point recombination causes more dramatic changes in chromosomes than one-point recombination.

Gene Recombination

In gene recombination, whole randomly selected genes are exchanged between the two randomly selected chromosomes. The traded genes do not change their places in the chromosome. Figure 4-11 shows an example of gene recombination.

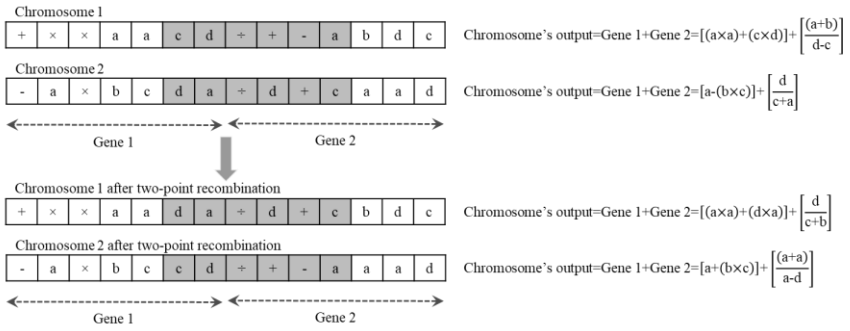

Figure 4-10: An example of two-point recombination. The parts highlighted in grey are exchanged between chromosomes.

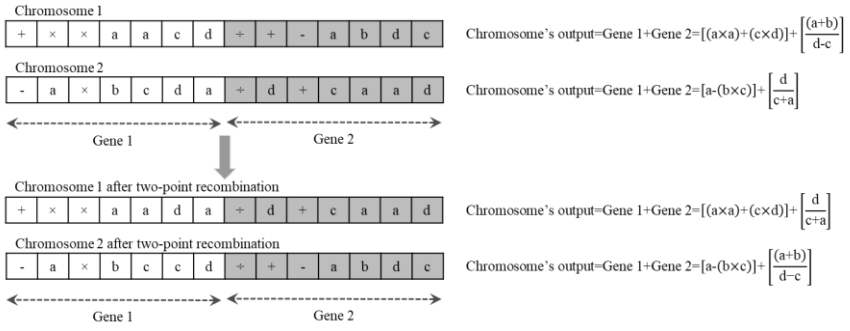

Figure 4-11: An example of gene recombination. The genes highlighted in grey are exchanged between chromosomes.

4.1.2 The Basic Flowchart of *GEP* algorithm

Figure 4-12 shows the basic flowchart for the basic *GEP* algorithm.

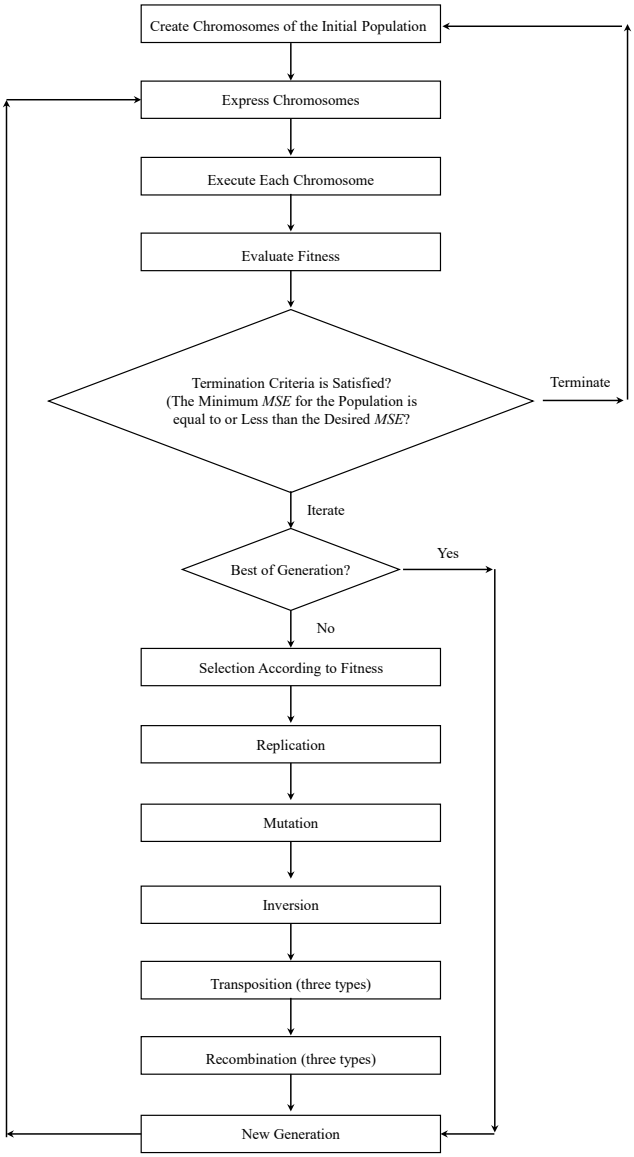

Figure 4-12: The standard flowchart of *GEP* algorithm (Ferreira, 2006)

4.2 Particle Swarm Optimization (*PSO*)

The presence of parameters such as A, B, C, D (Eqs. 4.1 and 4.2) and random numbers in genes creates an opportunity for application of an optimization method, which will lead to a more efficient evolution process for *GEP*. To take that opportunity, Particle Swarm Optimization (*PSO*) method was applied wherever those parameters appeared in a chromosome that had already reached an acceptable level of fitness using only *GEP*.

PSO is categorized as an evolutionary computation technique and is inspired by movements of swarms such as a flock of birds or a school of fish that are in search of food or getting away from a threat, etc. (Jones, 2007; J Kennedy and Eberhart, 1995). In this algorithm, a swarm of "particles/potential solutions" is randomly distributed over a search space with number of dimensions equal to the number of optimizable parameters, e.g. *A*-*B* plane in Figure 4-13 as the search space if the chromosome contains only one "Power" function (Eq. 4.1). Each member of the swarm is regarded as a candidate solution for the optimization problem at hand.

Then, an iteration process starts. Through the process, the particles move over the search space with velocities defined for each of them according to their fitness. The search space is explored until the satisfactory solution is found or the maximum number of iterations is reached. Depending on the user's preference, "fitness" can be defined as one, or a weighted combination of, *MSE*, *RMSE*, R, R^2, etc. associated with each swarm member. The velocity of each particle is updated with reference to its velocity in the previous iteration, the position of the best

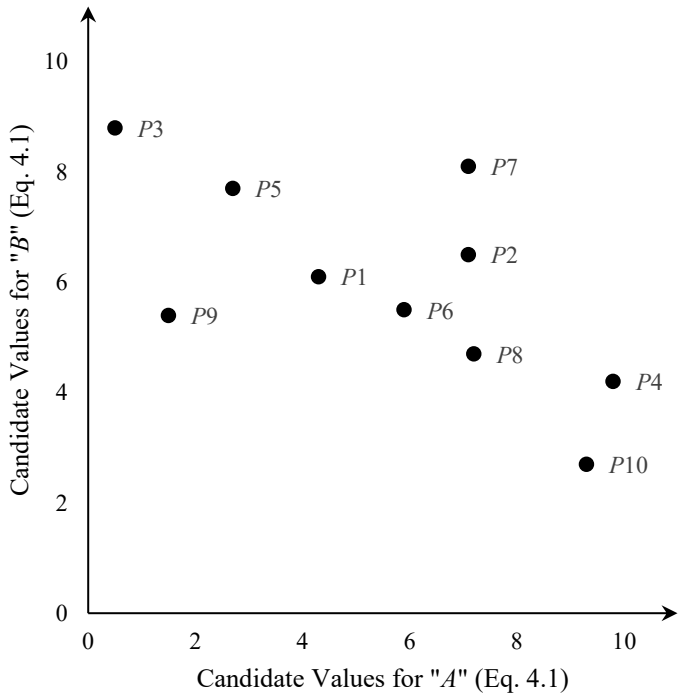

Figure 4-13: Random distribution of particles or candidate solutions (*P*1-*P*10) over *A*-*B* plane

particle in the population (the bird closest to the source of food or the particle with the highest fitness), and the particle's best position corresponding to its best fitness through iterations (the closest each bird has ever been to the source of food through its search for the food or the highest fitness the particle has ever experienced). In other words, in each iteration, a particle steers towards a direction that makes it closer to the best that it has ever experienced and the best particle across all iterations, which may be called the globally best particle. For particle P(x,y) on the x-y surface, the updated velocity is defined by Eq. 4.3:

$$V_{updated}=(\text{Inertia}\times V)+\left(\text{rand }()\times LRPI\times\left[P\left(x_{Particle's\ best},y_{Particle's\ best}\right)-P(x,y)\right]\right)+\left(\text{rand }()\times LRSI\times\left[P\left(x_{Globally\ Best\ Particle},y_{Globally\ Best\ Particle}\right)-P(x,y)\right]\right) \quad (4.3)$$

where $V_{updated}$ is the updated particle's velocity for the current iteration, V is the particle's velocity in the previous iteration, *Inertia* is a user-defined quantity that adjusts the extent of V's impact on $V_{updated}$ and is usually set to a number in the interval [0.9,1.2], *rand*() is a random number in the interval [0,1], *LRPI* is the Learning Rate for the Personal Impact and a quantitative parameter with a recommended value of 2, *LRSI* is the Learning Rate for Social Impact and is also a quantitative parameter with recommended value of 2 (James Kennedy and Eberhart, 1995; Shi and Eberhart, 1998). When the updated velocity for a particle is defined, its location in the search space will be updated according to the following equation:

$$P_{updated}=P+V_{updated} \quad (4.4)$$

where $P_{updated}$ is the updated position of the particle based on its previous position (P) and its updated velocity ($V_{updated}$).

The flowchart for *PSO* is presented in Figure 4-14.

4.3 *GEP-PSO* algorithm

In the current research, a customized combination of the *GEP* and *PSO* algorithms was used to solve problems in the field of mechanical

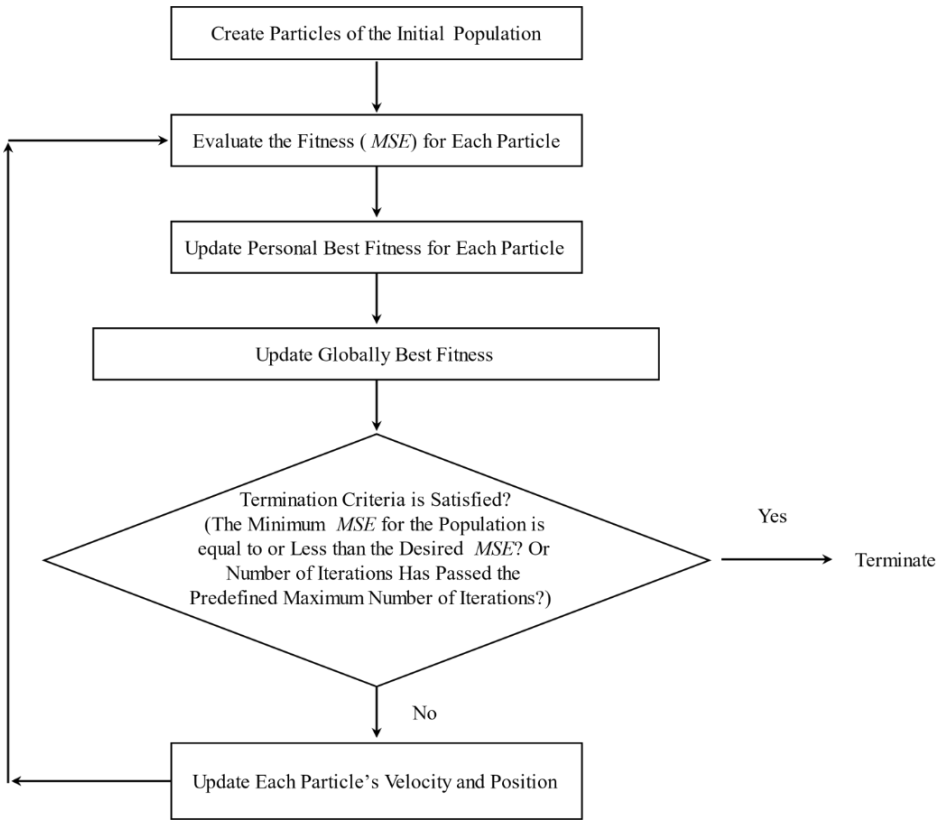

Figure 4-14: Standard flowchart for Particle Swarm Optimization (*PSO*) algorithm

excavation. The evolution of the *GEP* continued until it found at least one equation or chromosome with an acceptable *MSE* value, which was arbitrarily defined to be smaller than or equal to the *MSE* value associated with the equations generated by Multiple Linear Regression. At this stage, the values for *A*, *B*, *C*, and *D* (Eqs. 4.1 and 4.2), and "random numbers" were selected randomly for each iteration. When an acceptable *MSE* was reached, the chromosome(s) producing the acceptable results were subjected to *PSO* optimization to check whether the *MSE* could be further improved (Eqs 4.1 and 4.2).

Compared to the *GEP* algorithm, the *GEP–PSO* algorithm was presumably more efficient. The *GEP–PSO* had higher efficiency because instead of randomly selecting the values of A, B, C, D, along with random numbers in each iteration, to see how fit they were, the algorithm searched for their optimum values in a more supervised manner using the *PSO* algorithm. In other words, the structural evolution of the solution was carried out by the *GEP*, and *PSO* was used to assist in the numerical evolution of A, B, C, D, and the random numbers.

If the final goal was reached after the *PSO*, the algorithm stopped; otherwise, it started again by creating a new initial population for the *GEP*. Finally, when the algorithm stopped, *PSO* was used again to determine whether the output of the genes could be multiplied by certain coefficients to make the *MSE* even smaller. Figure 4-15 shows the flowchart for the *GEP-PSO* algorithm.

It should be added that there is a slight difference between the basic *GEP* algorithm and the *GEP* algorithm used in this study. In this research, unlike the basic *GEP* algorithm, in which all the genes are connected to each other by the same function, the *GEP-PSO* algorithm investigates all the different combinations of the genes and linking functions and selects the best rather than merely adding or multiplying the genes outputs to calculate the final chromosome output (see Figure 4-3).

The performance of the *GEP-PSO* algorithm was compared against that of *GEP* using a simple function fitting problem. Both algorithms were used to find a function that accurately fits over 25 (x,y) points generated using the following function.

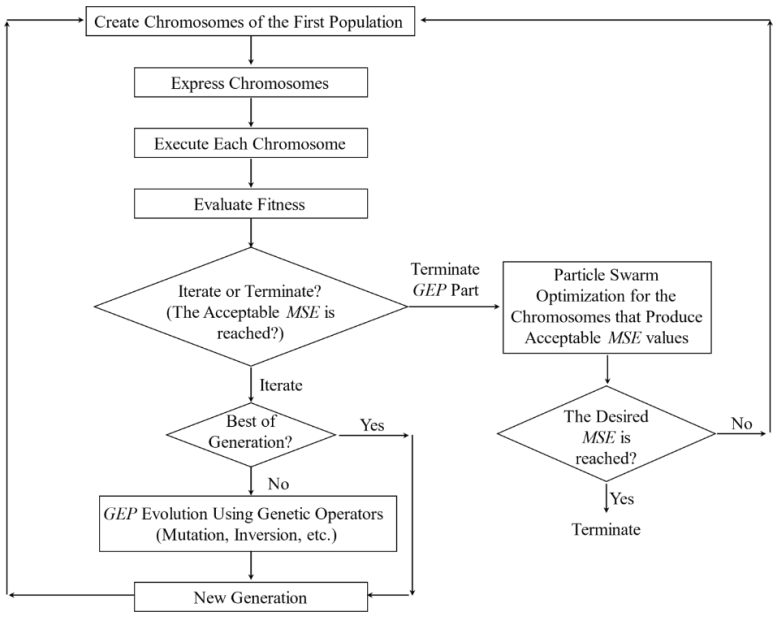

Figure 4-15: Flowchart for hybrid *GEP–PSO* algorithm used in this study

$y=\frac{x^2}{2.2}+3.33x+1.56$, where x is randomly selected from the range [-10,10]

The process was repeated for 100 times and for each time the best fitness value achieved by each algorithm and their associated computation time was recorded. Figure 4-16 shows the pseudocode of the algorithm used to draw a comparison between performance of *GEP* and *GEP-PSO*.

It should be mentioned that for the parts common between *GEP* and *GEP-PSO*, same settings have been used for both. In addition, the *GEP-PSO* algorithm was forced to reach at least the same level of accuracy as *GEP* did in each of the 100 times that the code was run (refer to the for-

```
for i=1:100
    Use the function f(x) and random x values in order to build a (x,y) database

    Run GEP in order to find the function that fits over the generated (x,y)
        points with "desired MSE" and record the run time for GEP and the
        achieved accuracy

    Run GEP-PSO in order to find the function that fits over the generated (x,y)
        points such that the MSE is equal to or less than the MSE generated by GEP
        and record the run time for GEP-PSO and the achieved accuracy
end
```

Figure 4-16: Pseudocode of the algorithm used in order to compare performance of *GEP* and *GEP-PSO*

loop in Figure 4-16). The fitness metric used to compare the accuracy of *GEP* and *GEP-PSO* is defined as:

$$\text{Fitness}=\sum_{i=1}^{n} \textit{Selection Range}-\left|y_i-\hat{y}_i\right|$$

Where "Selection Range" is an arbitrarily defined constant number (chosen as 100 here), y_i is the i^{th} y value generated by the function $y=\frac{x^2}{2.2}+3.33x+1.56$, $\hat{y}_i$ is the i^{th} predicted value, and n is the number of the (x,y) points. As n was set equal to 25, perfect fitness would be Selection range × number of fitness cases=100×25=2500.

Table 4-1 shows the results of the performance comparison. As the table shows, on average, *GEP-PSO* needed almost one third of the time required by *GEP* in order to solutions that are more accurate than the solutions generated by *GEP*.

Finally, it should be mentioned that, during the course of the present study, the fully automated *GEP-PSO* algorithm with dynamic linking

functions that takes advantage of all of the genetic variation sources such as mutation, inversion, one-point recombination, two-point recombination, gene recombination, and three types of transposition (insertion sequence elements, root insertion sequence elements, transposable genes) was used for the first time in order to develop prediction models for impact hammer performance, specific energy required by point attack picks, and forces acting on point attack picks.

Table 4-1: Results of the comparison between performance of *GEP* and that of *GEP-PSO*

Algorithm	Average Run Time (s)	Average Fitness
GEP	35.96	2460.49
GEP-PSO	11.75	2470.65

5. RESULTS AND DISCUSSION

In this chapter, results of the studies on the problems identified during the review of literature, in addition to their respective conclusions are provided.

The proposed *GEP–PSO* algorithm proved to be capable of finding reliable solutions for function-fitting problems, especially for those involving a large amount of data. Using this algorithm, precise models may be developed without making any prior judgment about their form. This advantage makes the *GEP–PSO* algorithm more attractive than function fitting methods such as multiple non-linear regression or other optimization techniques such as ant/bee colony optimization. In addition, the *GEP-PSO* algorithm has an advantage over artificial neural networks because it generates a mathematical equation rather than a network structure. The proposed *GEP–PSO* algorithm only showed one drawback in comparison to *MLR*. That is, as in all of the other iterative function fitting methods, the time required by *GEP–PSO* to find a good fit was not predetermined. However, this disadvantage may be outweighed by the high accuracy of *GEP–PSO* compared to that of *MLR*. As a result, this method of function fitting proved to be a very useful tool for engineering applications.

In statistical analysis, there is a strong warning against extrapolation beyond the range of the collected data (Montgomery and Runger, 2018). Therefore, the models suggested in this study should be used only within the range of their input variables, which may be found in Table 3-4, Table 3-5, and Table 3-8.

5.1 The suggested impact hammer performance prediction model

A stepwise multiple linear regression (*MLR*) analysis was conducted using SPSS (2017) to see if a linear equation could be used to satisfactorily describe the relationship between the *IBR*, as the dependent variable, and the rock properties and machine power, as independent variables (Table 3-4). The results revealed that the conventional *MLR* method was not capable of predicting the performance with a good fit (Eqs. 5.1 and 5.2):

$$IBR=(-0.035\times UCS)-(0.282\times RQD)-(0.171\times SHRV)+(0.121\times P)+34.356,\quad R^2=0.73,\ MSE=8.6 \tag{5.1}$$

$$MSE=\frac{\sum_{i=1}^{n}(y_i-\hat{y}_i)^2}{n} \tag{5.2}$$

where *UCS* is the uniaxial compressive strength in *MPa*, *RQD* is the rock quality designation in percent, *SHRV* is the Schmidt hammer rebound value, *P* is the input power of the machine in *kW*, y_i is the i^{th} measured value, $\hat{y}_i$ is the i^{th} predicted value, and *n* is the number of cases.

The *GEP–PSO* algorithm, developed in Matlab (2017), generated the following equations (Eqs. 5.6 to 5.7), which explain the variation in *IBR* in m^3/h based on variations in the *UCS* in *MPa*, rock quality designation (*RQD*) as a percentage, *SHRV*, and input *P* of the hydraulic hammer in *kW*. Table 5-1 shows the settings used in the *GEP-PSO* code.

$$Gene\ 1 = \frac{-606.84}{UCS \times RQD} \tag{5.3}$$

$$Gene\ 2 = \frac{UCS}{75.04} - (0.1 \times SHRV) \tag{5.4}$$

$$Gene\ 3 = 1.5 \times [(P\text{-}UCS + 1.5)]^{1/3} \tag{5.5}$$

$$Gene\ 4 = \frac{87.93}{RQD^{0.36}} \tag{5.6}$$

$$IBR = Gene1 + Gene2 + Gene3 + Gene4 \tag{5.7}$$

Only 80% of the collected data (68 points out of 85) was randomly selected to be used to train the *GEP–PSO* algorithm. The remaining 20% was reserved as test data to assess the ability of the *GEP–PSO* model. Table 5-2 lists the results of a comparison between the model generated using *GEP–PSO* algorithm (Eqs.5.3–5.7) and the model developed using *MLR* (Eq. 5.1). The R^2 values and mean squared error associated with each model show that the *GEP–PSO* model had a significantly higher accuracy (Table 5-2).

In order to learn more about the behavior of the suggested *GEP–PSO* function, three-dimensional surfaces were generated, each showing the changes in the *IBR* with respect to two out of the four input parameters (Figure 5-1–Figure 5-6). The data tips in Figure 5-1–Figure 5-6 show extremum values. In each case, two of the input parameters were held equal to their mean values, while the other two changed along their respective ranges (Table 3-4). In general, Figure 5-1–Figure 5-6 confirm that the *IBR* decreased as the rock became stronger. However, a closer look at Figure 5-1–Figure 5-3 reveals that within a range of small

Table 5-1: Settings used in *GEP–PSO* code for development of a performance prediction model for impact hammer

Gene Expression Programming (*GEP*)				Particle Swarm Optimization (*PSO*)	
Population Size (Number of Chromosomes)	1000	Insertion Sequence Transposition Rate	0.1	Number of Particles	350
Number of Genes Per Chromosome	4	Root Insertion Sequence Transposition Rate	0.1	Inertia	0.2
Head Length	5	Gene Transposition Rate	0.1	Learning Rate for Personal Influence	2
Tail Length	6	One-point Recombination Rate	0.4	Learning Rate for Social Influence	2
Functions Set	{+, ×, -, ÷, 2nd Root, 3rd Root, Power (Eq. 4.1), Exp (Eq. 4.2), Sin, Cos, Tan}	Two-point Recombination Rate	0.2	Maximum Number of Unsuccessful Iterations	40
Terminals Set	{*UCS*, *RQD*, *SHRV*, *P*, Random Number}	Gene Recombination Rate	0.1	Selection Range for *A* and *C* (Eqs. 4.1 and 4.2) and Random Numbers	[-1000,1000]
unctions Set used for Dynamic Linking Function Selection	{+, ×, -, ÷}	Fitness Function	Eq. 5.2	Selection Range for *B* and *D* (Eqs. 4.1 and 4.2)	[-10,10]
Mutation Rate	0.2	Ratio of the Training Data to the Whole Data	0.8	Selection Range for Random Numbers	[-15000,15000]
Inversion Rate	0.1	Ratio of the Test Data to the Whole Data	0.2	Fitness Function	Eq. 5.2

UCS: Uniaxial Compressive Strength (*MPa*); *RQD*: Rock Quality Designation (*%*); *SHRV*: Schmidt Hammer Rebound Value; *P*: Machines' Input Power (*kW*)

Table 5-2: Comparison of models developed using *MLR* and *GEP–PSO* algorithm for predicting performance of impact hammer

Statistical Model		R^2	Mean Squared Error (Eq. 5.2)
MLR (Eq. 5.1)	Whole Data	73.36%	8.62
GEP-PSO (Eqs.5.3 and 5.7)	Training Data	83.8%	5.48
	Test Data	83.88%	5.4
	Whole Data	83.17%	5.46

UCS values, the *IBR* is higher for greater *UCS* values. This was probably because rock somehow behaves similar to soil before it reaches a certain level of compressive strength. For a strength range smaller than a certain value, the excavation process is more like digging than breaking.

Figure 5-1–Figure 5-3 also show that there was a critical compressive strength value beyond which the *IBR* suddenly dropped. The critical value was dependent on the value of machine power and may be found using Eq. 5.8.

$$\frac{\partial IBR}{\partial P}=\frac{1}{2(P\text{-}UCS+1.5)^{\frac{2}{3}}}=-\infty \text{ or } 2(P\text{-}UCS+1.5)^{\frac{2}{3}}=0 \tag{5.8}$$

Figure 5-3 shows how for higher levels of machine power, the critical compressive strength value became greater. Therefore, it may be inferred that machines with higher input power can maintain a high level of *IBR* for a wider range of *UCS* values. This finding is of crucial

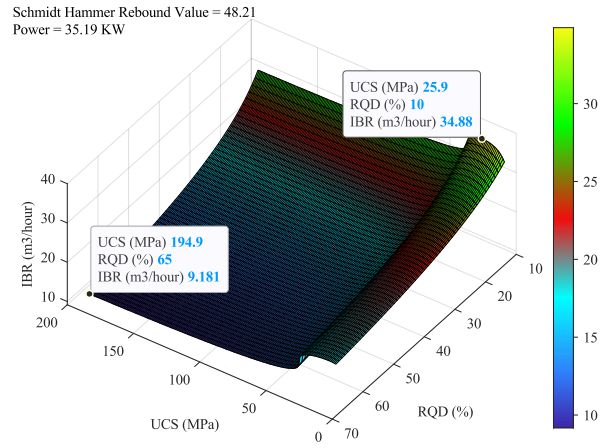

Figure 5-1: Changes of Predicted Instantaneous Breaking Rate (*IBR*) with respect to Uniaxial Compressive Strength (*UCS*) and Rock Quality Designation (*RQD*) while Power and Schmidt Hammer Rebound Values are held constant

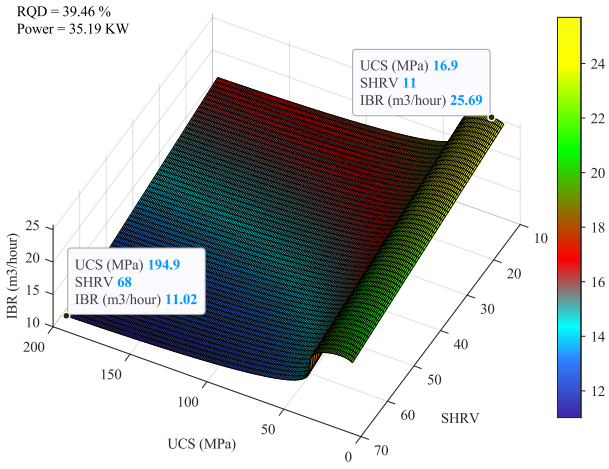

Figure 5-2: Changes of Predicted Instantaneous Breaking Rate (*IBR*) with respect to Uniaxial Compressive Strength (*UCS*) and Schmidt Hammer Rebound Values (*SHRV*) while Power and Rock Quality Designation (*RQD*) are held constant

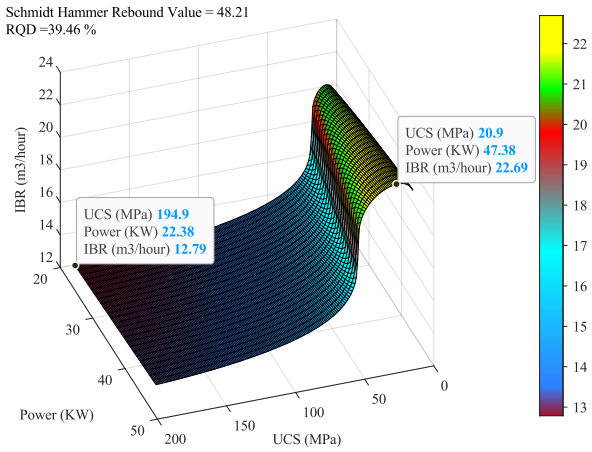

Figure 5-3: Changes of Predicted Instantaneous Breaking Rate (*IBR*) with respect to Uniaxial Compressive Strength (*UCS*) and Power while Schmidt Hammer Rebound Values (*SHRV*) and Rock Quality Designation (*RQD*) are held constant

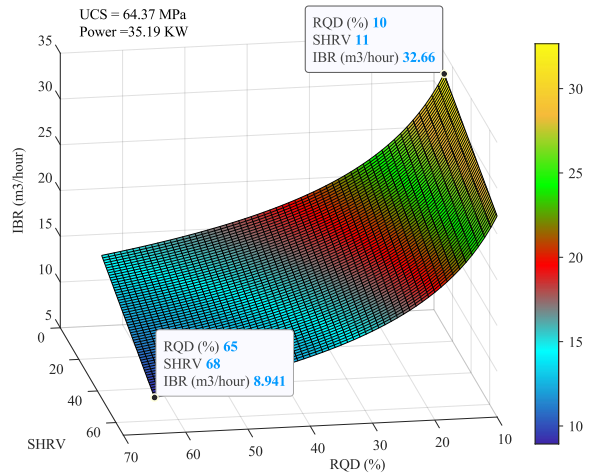

Figure 5-4: Changes of Predicted Instantaneous Breaking Rate (*IBR*) with respect to Rock Quality Designation (*RQD*) and Schmidt Hammer Rebound Values (*SHRV*) while Uniaxial Compressive Strength (*UCS*) and Power are held constant

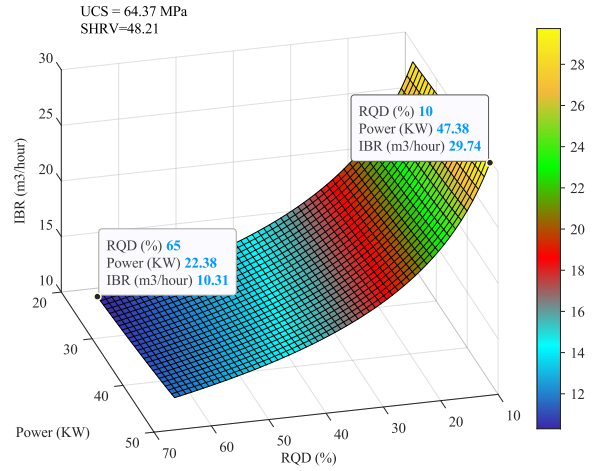

Figure 5-5: Changes of Predicted Instantaneous Breaking Rate (*IBR*) with respect to Rock Quality Designation (*RQD*) and Power while Uniaxial Compressive Strength (*UCS*) and Schmidt Hammer Rebound Values (*SHRV*) are held constant

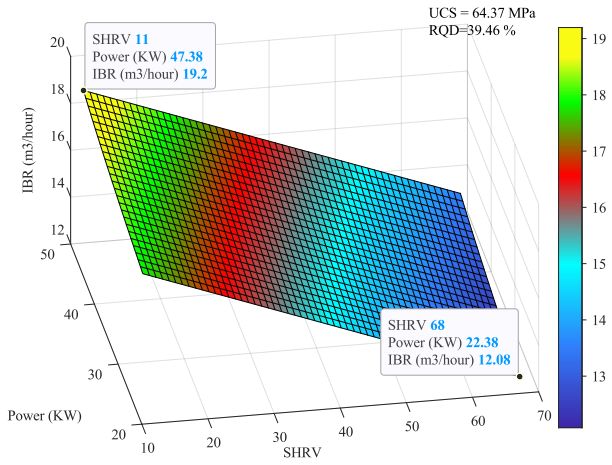

Figure 5-6: Changes of Predicted Instantaneous Breaking Rate (*IBR*) with respect to Schmidt Hammer Rebound Values (*SHRV*) and Power while Uniaxial Compressive Strength (*UCS*) and Rock Quality Designation (*RQD*) are held constant

importance for certain cases. For instance, for a hypothetical tunnel with randomly selected *UCS* values falling within the range of 22.9–47.9 *MPa* and *RQD* and *SHRV* values randomly selected from their respective ranges, as listed in Table 3-4 (10–65% and 11–68, respectively), the average breaking rate associated with a 48 *kW* machine was almost 1.4 times that of a 22.38 *kW* machine (Table 5-3).

To further assess the quality of the proposed *GEP–PSO* model, the performances of the previously published prediction models were compared to that of the model suggested in this study. There were three previously developed models for which the required input parameters were available. The models were proposed by Bilgin et al. (1996) (Eqs. 2.1 and 2.2), Bilgin et al. (2002) (Eq. 2.3), and Tumac and Hojjati (2016) (Eqs. 2.4–2.6). The application ranges for the model proposed by Bilgin et al. (1996) are 18% < *RQD* < 85% and 42 *MPa* < *UCS* < 125 *MPa*. The model proposed by Bilgin et al. (2002) is applicable for 41 < *SHRV* < 61 and 25% < *RQD* < 49%. Finally, the model suggested by Tumac and Hojjati (2016) is applicable for 10% < *RQD* < 60% and 8.9 *MPa* < *UCS* < 195.6 *MPa*. Points in the database that fell within the application ranges of each of the previously suggested models were used to compare it to the proposed *GEP–PSO* model. The results are presented in Table 5-4. As Table 5-4 shows, the proposed *GEP–PSO* model performed far better than the other prediction models under consideration.

As a result of the quantitative comparisons made between the proposed *GEP–PSO* model, the *MLR* model, and some of the previously published performance prediction models for impact hammers, it is safe to say that the *GEP–PSO* model may be used as a substantially more

Table 5-3: Performances of impact hammers with different power levels over same hypothetical tunnel

UCS (*MPa*)	*RQD* (%)	*SHRV*	*IBR* (m^3/h)			
			P=22.38 *kW*		*P*=48 *kW*	
27.93	32.26	49.63	17.52	Average *IBR*= 17.28 m^3/h	24.09	Average *IBR*= 24 m^3/h
41.4	60.54	60.22	10.46		17.37	
31.39	32.43	34.72	18.54		25.42	
28	34.75	16.51	20.21		26.78	
29.68	33.44	31.58	18.79		25.54	
37.8	45.71	38.98	14.86		21.87	
44.22	62.65	63.28	9.77		16.48	
38.19	57.55	15.14	15.52		22.53	
27.4	10.47	38.06	29.92		36.41	
37.64	55.35	29.44	14.4		21.42	
42.76	13.75	35.09	26.26		33.09	
26.09	41.54	57.01	15.12		21.37	
32.59	26.83	59.43	17.62		24.55	
28.67	52.1	16.44	16.99		23.65	
45.14	54.75	53.34	11.68		18.28	
32.43	42.28	67.45	13.02		19.95	
46.87	12.06	43.36	26.83		33.17	
32.05	41.35	19.59	18.01		24.93	
25.93	55.36	55.32	13.21		19.42	
42.51	41.6	23.46	16.88		23.72	

UCS: Uniaxial Compressive Strength; *RQD*: Rock Quality Designation; *SHRV*: Schmidt Hammer Rebound Values; *P*: Input Power; *IBR*: Instantaneous Breaking Rate

Table 5-4: Comparison between proposed *GEP–PSO* model and previously published performance prediction models for impact hammers

	No. of Points	R^2	Mean Squared Error (Eq. 5.2)
Bilgin et al. (1996) (Eqs. 2.1-2.2)	53	0.18	191.99
GEP-PSO Model		0.71	6.5
Bilgin et al. (2002) (Eq.2.3)	62	0.33	42.94
GEP-PSO Model		0.64	15.56
Tumac and Hojjati (2016) (Eqs. 2.4-2.6)	84	0.38	84.5
GEP-PSO Model		0.83	5.5

accurate performance estimation tool in the early phases of tunneling projects.

According to Copur et al. (2012), impact hammers may be used to excavate highly fractured rock with *UCS* values of less than 100 *MPa*. Therefore, according to Figure 5-7, it may be inferred that the suggested *GEP–PSO* model, which was developed using a database comprising *UCS* values of 8.9–195.6 *MPa* and *RQD* values of 10–65%, properly covers a wide range of applications for impact hammers. It should be noted that the proposed model is limited to machines with an input power of 22.38–48 *kW*.

A broader comparison to the existing performance prediction models revealed that the proposed model could be considered more advantageous because it either covers a wider range of applications, is more reliable because it was developed based on a well-distributed and

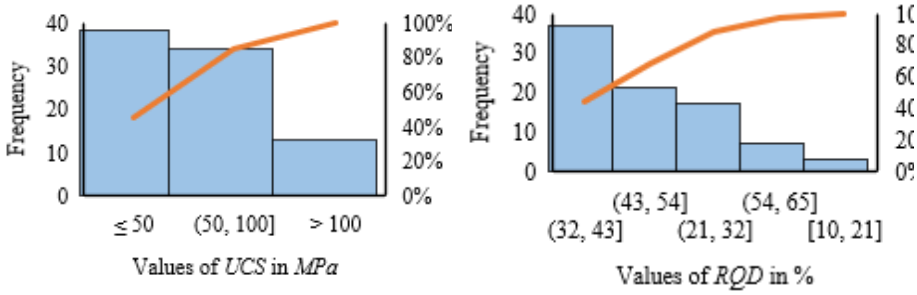

Figure 5-7: Distribution of the Uniaxial Compressive Strength (*UCS*) and Rock Quality Designation (*RQD*) values faced during excavation of Uskudar-Cekmekoy and Levent-Hisarustu tunnels

large number of data points, requires only a small number of easily obtainable input parameters, or can reach a significantly higher accuracy level. Finally, it should be added that, like any other statistical model, the model suggested in this study should be used only within the range of the data over which it has been fitted (Table 3-4).

5.2 The model suggested for prediction of specific energy required by point attack picks

In order to check whether a linear function fitting technique can sufficiently describe the data presented in Table 3-5, a stepwise *MLR* analysis was conducted using *SPSS* (2017). The results are presented in the following:

$$SE=(0.464\times UCS)-(5.313\times d)-(5.032\times \frac{s}{d})-(3.305\times \theta_{tip})-(0.499\times \theta_{attack})-(0.237\times \theta_{skew}) \quad (5.9)$$

where *SE* is the specific energy (*MJ*/m^3), *UCS* is the uniaxial compressive strength of rock (*MPa*), "*d"* is the depth of cut (*mm*), "*s*" is the cut spacing (*mm*), θ_{tip} is the tip angle (*degree*), θ_{attack} is the attack angle (*degree*), θ_{skew} is the skew angle (*degree*), R^2 is the coefficient of determination, *MSE* is the mean squared error calculated using Eq. 5.2.

Considering the low value of R^2 and the high value for *MSE* in comparison to the mean value of *SE* presented in Table 3-5, those results showed that *SE* may not be adequately expressed using a simple linear function. Therefore, more sophisticated methods of non-linear function fitting can be considered in order to find a function that can better describe the relation between *SE* and the input parameters collected in the database (*UCS*, *BTS*, *d*, *s*, *s*/*d*, θ_{tip}, θ_{attack}, and θ_{skew}).

Using the settings shown in

Table 5-5, *GEP-PSO* algorithm, written in Matlab (2017), generated the following equations (Eqs. 5.10 -5.14). They describe the change in *SE* in *MJ/m^3* based on changes of Brazilian Tensile Strength (*BTS*) in *MPa*, depth of cut (*d*) in *mm*, cut spacing (*s*) in *mm*, ratio of cut spacing to depth of cut (*s*/*d*), and tip angle (θ_{tip}), attack angle (θ_{attack}), and skew angle (θ_{skew}) in *degree*. 80% of the data was used for training and the remaining 20% were used to test the performance of the model. It should be noted that the trigonometric functions in Eqs. 5.10-5.14, treat their arguments as *radians*. For instance, *sin* (90) = 0.89 and *sin* (180) = -0.80.

$$Gene\ 1 = \ln\left[\frac{\left(\frac{\exp(0.66\times BTS)}{\theta_{attack}}\right)^{5.15}+0.08}{0.06}\right] \tag{5.10}$$

$$Gene\ 2=\left(\left(\frac{2.56}{s}\right)^{2}+\tan^{-1}\left(92.18-\theta_{skew}-\theta_{tip}\right)\right)^{1.48} \tag{5.11}$$

$$Gene\ 3=27.13\times\sin\left(\frac{\cot\left(\cos\left(\theta_{tip}\right)\right)+\left[0.35\times\exp\left(1.72\times\cos\left(\frac{s}{d}\right)\right)\right]}{1.37}\right) \tag{5.12}$$

$$Gene\ 4=\frac{0.86}{\cos^{-1}\left(\sin\left(d^{0.49}-2.71\right)\right)} \tag{5.13}$$

$$SE=\frac{Gene\ 1\times Gene\ 2\times Gene\ 3}{Gene\ 4} \tag{5.14}$$

Table 5-6 shows the comparison between the model above and the model developed using *MLR* (Eq. 5.9). The average percentage error in Table 5-6 is calculated using the following equation:

$$\text{Average Percentage Error}=\frac{\left|\hat{y}_i-y_i\right|}{y_i}\times 100 \tag{5.15}$$

where $\hat{y}_i$ and y_i are the value predicted by the *GEP-PSO* model for the *i*'th record and the target value for the *i*'th record, respectively.

The average error of the estimate is calculated using the following equation:

$$\text{Average Error of Estimate}=\frac{\sum_{i=1}^{186}\left(\hat{y}_i-y_i\right)}{186}=0.19\ MJ/m^3 \tag{5.16}$$

Table 5-5: Settings used in *GEP–PSO* code for development of a prediction model for specific energy required by point attack picks

Gene Expression Programming (*GEP*)				Particle Swarm Optimization (*PSO*)	
Population Size (Number of Chromosomes)	3000	Inversion Rate	0.1	Number of Particles	350
Number of Genes Per Chromosome	4	Insertion Sequence Transposition Rate	0.1	Inertia	0.2
Head Length	6	Root Insertion Sequence Transposition Rate	0.1	Learning Rate for Personal Influence	2
Tail Length	7	Gene Transposition Rate	0.1	Learning Rate for Social Influence	2
Function Set	{+, ×, -, ÷, Power (Eq. 4.1), ln, Exp (Eq. 4.2), Sin, Cos, Tan}	One-point Recombination Rate	0.4	Maximum Number of Iterations	40
Terminal Set	{*UCS*, *BTS*, *d*, *s*, *s*/*d*, θ_{tip}, θ_{attack}, θ_{skew}, Random Numbers}	Two-point Recombination Rate	0.2	Selection Range for *A* and *C* (Eqs. 4.1 and 4.2) and Random Numbers	[-1000,1000]
Function Set used for Dynamic Linking Function Selection	{+, ×, -, ÷}	Gene Recombination Rate	0.1	Selection Range for *B* and *D* (Eqs. 4.1 and 4.2)	[-10,10]
Mutation Rate	0.2	Fitness Function	Eq. 5.2	Fitness Function	Eq. 5.2

UCS: Uniaxial Compressive Strength (*MPa*); *BTS*: Brazilian Tensile Strength (*MPa*); *d*: Depth of Cut (*mm*); *s*: Cut Spacing (*mm*); θ_{tip}: Tip Angle (*degree*); θ_{attack}: Attack Angle (*degree*); θ_{skew}: Skew Angle (*degree*)

Table 5-6: Comparison of models developed using *MLR* and *GEP–PSO* algorithm for predicting specific energy required by point attack picks

Statistical Model		R^2	Mean Squared Error (Eq. 5.2)	Average Percentage Error (Eq. 5.15)
MLR (Eq. 5.9)	Whole Data	53.52%	143.42	25.19%
	Training Data	80.99%	58.76	16.49%
GEP-PSO (Eqs. 5.10-5.14)	Test Data	82.30%	56.49	12.86%
	Whole Data	81.17%	58.29	15.75%

where $\hat{y}_i$ and y_i are the value predicted by the *GEP-PSO* model for the *i*'th record and the target value for the *i*'th record, respectively and 186 is the number of data points.

As Eq. 5.16 shows, an average error of estimate equal to 0.19 across all of the 186 data points confirms the good distribution of the errors above and below 1:1 line in addition to the fact that the model tends to predict slightly higher, or conservative, *SE* values compared to the recorded/target values.

In order to demonstrate the physical implications of the suggested model, the following graphs are provided (Figure 5-8-Figure 5-13). Across each cluster only one of the parameters changes while the rest are held constant. The graphs use clusters of representative cases to show the effect of each input parameter on the predictions made by the model as well as the real test results. Figure 5-10, only shows the predicted values

as there were no cluster of tests results with the same other settings (*BTS*, d, s, θ_{attack}, θ_{skew}) and different tip angle values in the database.

In the past, researchers have endeavored to find models for predicting *SE* required by point attack picks (Table 5-7). However, the suggested prediction models are rather limited in terms of having a reasonably high accuracy, including the relevant input parameters, or the number of data used for statistical analysis. Among the models in Table 5-7, those suggested by Wang et al. (2018) use the highest number of data for statistical analysis (43 points). The prediction models suggested by Wang et al. (2018) for optimum *SE* are based on a model developed for prediction of *SE* in unrelieved cutting mode, which was fitted over 49 data points (Figure 2-1). The values of R^2 and average percentage error for the most accurate of those models are 79.1% and 32.72%, respectively. The models suggested by Wang et al. (2018) are the only prediction models for optimum *SE* that demonstrate the effect of a cutting parameter (d) in addition to the effect of rock properties (*UCS* or/and *BTS*). However, compared to the models suggested by Wang et al. (2018), the model suggested in this study is more beneficial as it can predict the value of *SE* by considering different settings of cutting conditions (i.e., depth of cut and cut spacing) and cutter related angles (θ_{tip}, θ_{attack} and θ_{skew}) that have a significant effect on *SE* (Figure 2-1 and Figure 2-3) (Roepke and Voltz, 1983; Park et al., 2018).

According to Copur et al. (2017), for hard rocks with *UCS* greater than 100 *MPa*, the cuts made using point attack picks and single, double, or triple spirals as cutting pattern require different values of optimum *SE*

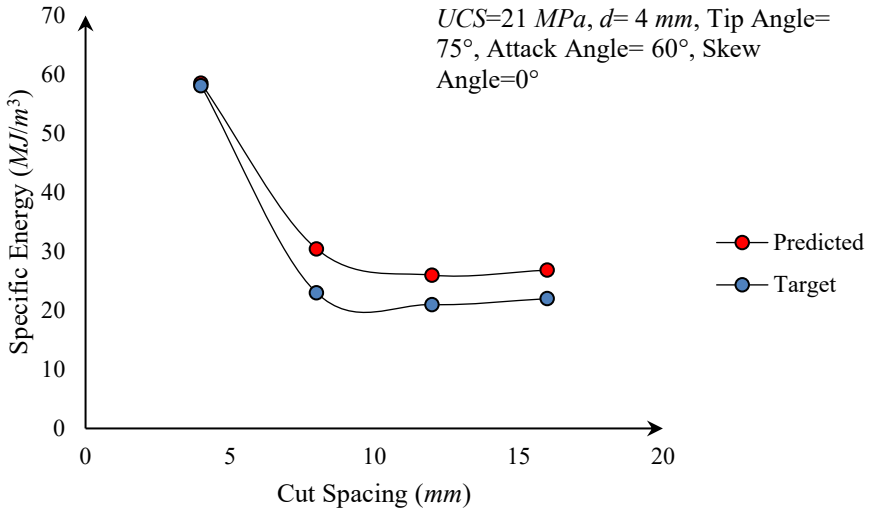

Figure 5-8: Representative cases showing the effect of cut spacing on specific energy

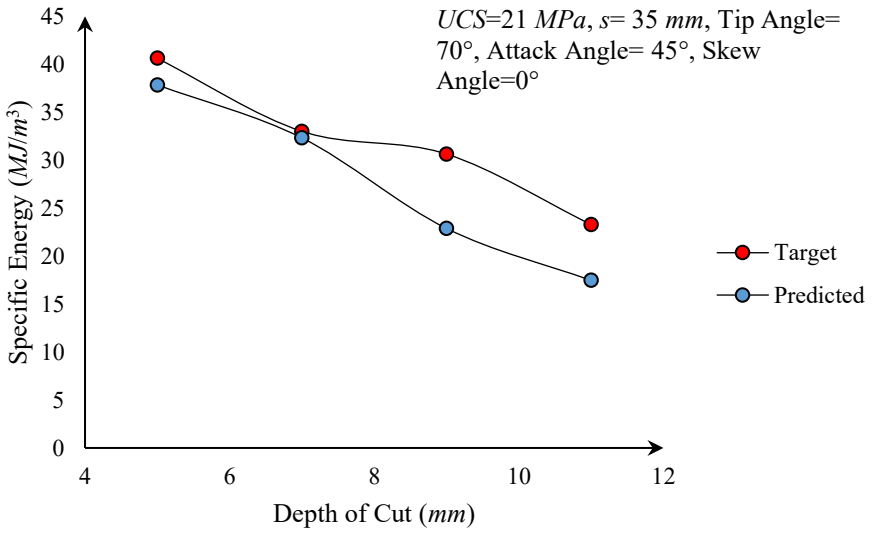

Figure 5-9: Representative cases showing the effect of depth of cut on specific energy

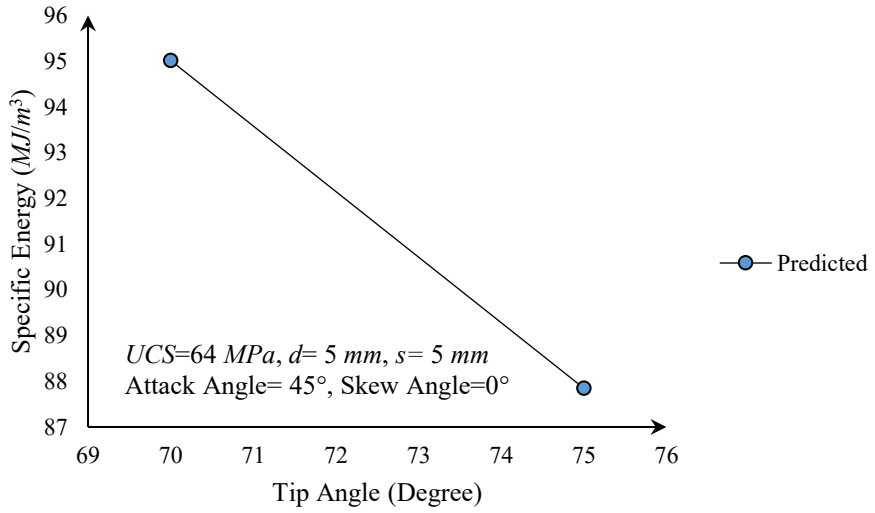

Figure 5-10: Representative cases showing the effect of tip angle on specific energy

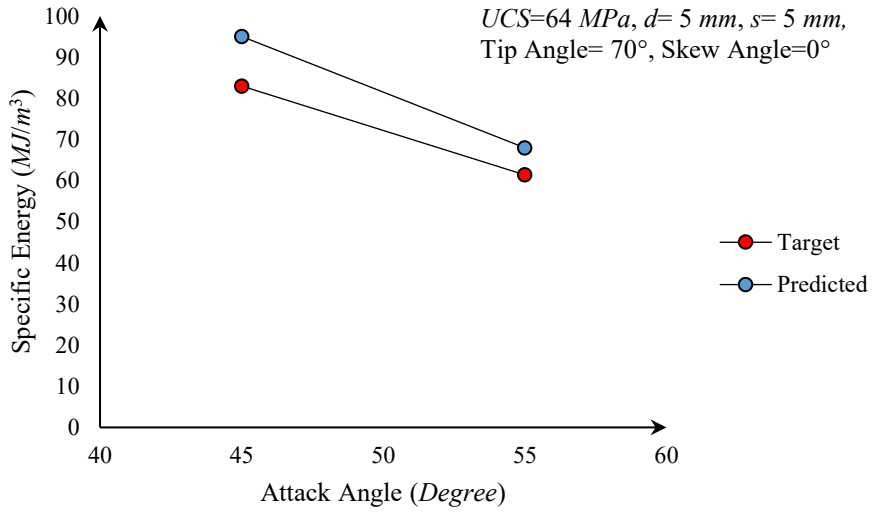

Figure 5-11: Representative cases showing the effect of attack angle on specific energy

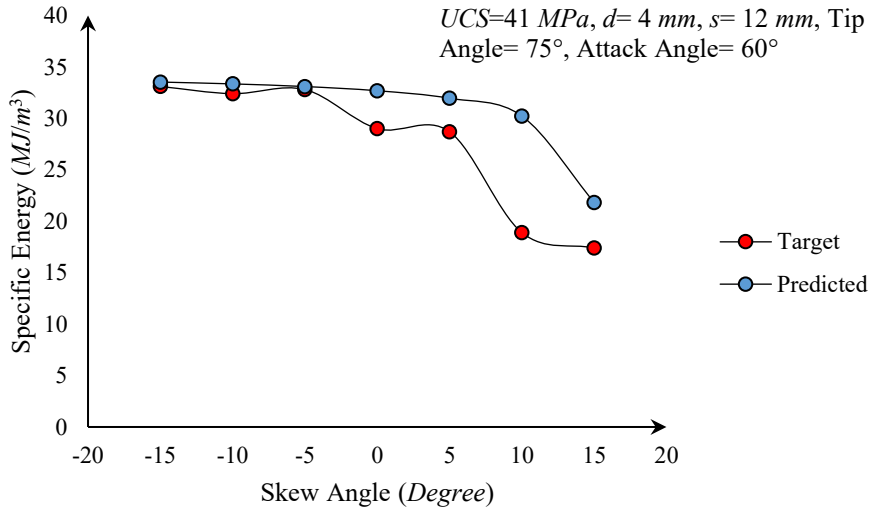

Figure 5-12: Representative cases showing the effect of skew angle on specific energy

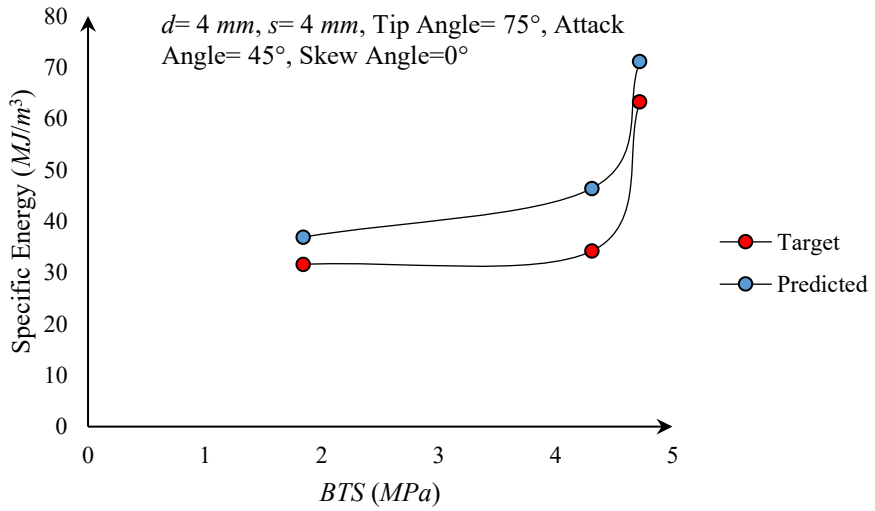

Figure 5-13: Representative cases showing the effect of Brazilian tensile strength on specific energy

Table 5-7:Existing prediction models for Specific Energy required by point attack picks

Statistical Models			Number of Data Points	R^{2*} (%)	Mean Squared Error (*MSE*)	Average Percentage Error** (%)
Copur et al. (2001):		$SE_{opt}=(0.027\times UCS\times BTS)+0.675$	10	86.85	0.66	8.38
Copur et al. (2003):		$SE_{opt}=0.728\times FT^{4.312}$	11	67.04	5.03	20.44
Balci et al. (2004):	*d*=5 *mm*	$SE_{opt}=0.37\times UCS^{0.86}$	13	86.85	3.44	21.01
		$SE_{opt}=3.36\times BTS^{0.72}$	13	99.22	42.89	106.79
		$SE_{opt}=3.55\times E_{sta}{}^{0.71}$	13	51.92	16.71	32.73
		$SE_{opt}=1.48\times E_{dyn}{}^{0.59}$	13	60.01	10.39	31.01
		$SE_{opt}=0.77\times e^{0.05SHRV}$	12	1.17	32.66	97.01
		$SE_{opt}=1.16\times(UCS\times BTS)^{0.4}$	13	88.83	2.96	19.28
	d=9 *mm*	$SE_{opt}=0.41\times UCS^{0.67}$	23	75.21	3.66	26.13
		$SE_{opt}=2.19\times BTS^{0.62}$	23	68.87	5.50	30.00
		$SE_{opt}=2.68\times E_{sta}{}^{0.40}$	17	58.98	7.12	34.91
		$SE_{opt}=1.15\times E_{dyn}{}^{0.50}$	19	46.51	8.67	35.99
		$SE_{opt}=0.46\times e^{0.06SHRV}$	16	78.72	4.50	30.00
		$SE_{opt}=0.92\times(UCS\times BTS)^{0.34}$	23	75.15	4.19	24.27
Bilgin et al. (2006):		$SE_{opt}=(0.083\times UCS)+1.424$	22	75.99	3.61	31.00
		$SE_{opt}=(1.259\times BTS)+0.142$	22	74.3	3.87	32.52
		$SE_{opt}=2.424\times E_{sta}{}^{0.414}$	18	55.82	7.68	37.67
		$SE_{opt}=0.984\times E_{dyn}{}^{0.542}$	19	47.51	8.90	37.37
		$SE_{opt}=0.3912\times e^{0.058SHRV}$	16	78.63	5.04	35.51
Tumac et al. (2007)		$SE_{opt}=(0.2316\times SH1)-2.0066$	16	78.20	3.92	43.89
		$SE_{opt}=(0.1705\times SH2)-3.9468$	16	43.94	10.08	69.4
		$SE_{opt}=243.01\times K^{-0.9171}$	16	70.53	5.72	35.82
Yilmaz et al. (2015)		$SE_{opt}=(0.2662\times HDH)+0.1975$	16	82.39	3.17	32.58

Table 5-7:(Continued) Existing prediction models for Specific Energy required by point attack picks

Statistical Models		Number of Data Points	R^{2*} (%)	Mean Squared Error (*MSE*)	Average Percentage Error** (%)
Copur et al. (2017)	$SE_{opt\text{-}single}=4.97\times BTS^{0.71}$	5	93	*NA****	*NA****
	$SE_{opt\text{-}double}=4.87\times BTS^{0.68}$	5	98	*NA****	*NA****
	$SE_{opt\text{-}single}=0.339\times E_{dyn}^{\ 0.97}$	5	98	*NA****	*NA****
	$SE_{opt\text{-}double}=0.461\times E_{dyn}^{\ 0.875}$	5	93	*NA****	*NA****
Wang et al. (2018)	$SE_{unrel}=1.448\times UCS^{0.876}\times d^{-0.817}$	49	76.1	68.95	37.63
	$SE_{unrel}=12.044\times BTS^{1.037}\times d^{-0.844}$	49	85.54	56.11	30.81
	$SE_{unrel}=([(0.3746\times UCS)+(6.005\times BTS)]\times d^{-0.76})-0.335$	49	82.54	60.23	33.62
	$SE_{opt}=0.672\times 1.448\times UCS^{0.876}\times d^{-0.817}$	43	75.19	5.19	32.23
	$SE_{opt}=0.672\times 12.044\times BTS^{1.037}\times d^{-0.844}$	43	77.8	4.25	34.13
	$SE_{opt}=0.672\times[([(0.3746\times UCS)+(6.005\times BTS)]\times d^{-0.76})-0.335]$	43	79.1	4.09	32.72

SE_{opt}: Required specific energy under optimum ratio of cut spacing to depth of cut for a conical cutter with tip angle, attack angle, and skew angle equal to 80, 55, and 0 *degree* in kWh/m^3 when the cuts are made using a single spiral pattern (relieved cutting mode); SE_{unrel}: Required specific energy for a conical cutter with tip angle, attack angle, and skew angle equal to 80, 55, and 0 *degree* in kWh/m^3 (unrelieved cutting mode); $SE_{opt\text{-}single}$: Optimum specific energy required for conical cutter in MJ/m^3 when the cut spacing is 25 *mm*, the cuts are made using a single spiral pattern, and tip angle, attack angle, and skew angle are 90, 45, and 0 *degree*, respectively; $SE_{opt\text{-}double}$: Optimum specific energy required for conical cutter in MJ/m^3 when the cut spacing is 25 *mm*, the cuts are made using a double spiral pattern, and tip angle, attack angle, and skew angle are 90, 45, and 0 *degree*, respectively; *UCS*: Uniaxial Compressive Strength (*MPa*); *BTS*: Brazilian Tensile Strength (*MPa*); *FI*: Force Index; *d*: Depth of Cut (*mm*); E_{sta}: Static Modulus of Elasticity (*GPa*); E_{dyn}: Dynamic Modulus of Elasticity (*GPa*); *SHRV*: Schmidt Hammer Rebound Value; *SH1* and *SH2*: Shore Hardness 1 and 2; *K*: Deformation Coefficient (%); *HDH*: Hybrid Dynamic Hardness;

* R^2 is the square of correlation coefficient between predicted and target values.
** Average percentage error is calculated using Eq.5.15.
*** The *MSE*, R^2, and Average Percentage Error for the models suggested by Copur et al. (2017) could not be calculated as they did not publish the values of target *SE* for their study.
The calculations for *MSE*, R^2, and Average Percentage Error are performed by the present authors using the data published by the researchers who developed the statistical models. There might be very small errors as the data published by those researchers may be the rounded version (fewer decimals) of the data they used in their calculations.

(Figure 5-14). Thus, as the excavation systems with point attack picks usually use double or more spiral cutting patterns, the results of full-scale rock cutting tests conducted using single spiral pattern on hard rock are not suitable to be used for design of cutter heads without appropriate calibration (Copur et al., 2017). For soft and medium strength rocks with maximum compressive strength of 100 *MPa*, however, such a problem

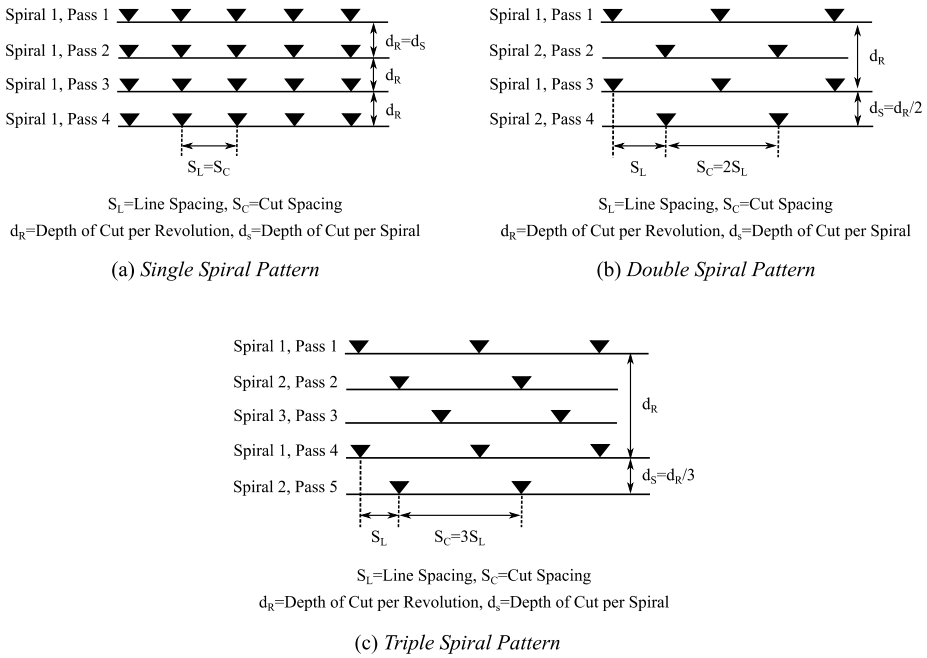

Figure 5-14: Definition of single, double, and triple spiral cutting patterns (adapted from Copur et al. (2017))

was not reported by Copur et al. (2017). Thus, the predictions made by Eqs. 5.10-5.14, which are the result of fitting a function on tests conducted using a single spiral pattern on rocks with maximum *UCS* of 64 *MPa*, may be safely used for predicting the performance of the machines using point attack picks.

According to the provided explanations, the *GEP-PSO* model may be suggested as a significantly more accurate prediction model for *SE* required by point attack picks in relieved cutting mode. The other advantage of the *GEP-PSO* model compared to the *MLR* model developed in this study, as well as the models in Table 5-7, is that it includes all of the important and adjustable cutting parameters. This

advantage makes the model particularly helpful in the design stage of the projects for comparing the advance rate associated with every combination of the available settings for cutting parameters and different types of rock. In addition, as the *GEP-PSO* model is capable of generating an estimate of *SE* for different settings of cutting parameters (d, s, θ_{tip}, θ_{attack}, and θ_{skew}) and for each type of rock, it may be used to reach a more optimized design of full-scale rock cutting experiments with fewer number of tests required to find the minimum *SE*.

Given the high capability of the *GEP-PSO* method used for function fitting in this study, it was intended to establish a database as large as possible by adding the data published by the other researchers to the database used in this study. Doing so could extend the range of application and improve the reliability of the resulting prediction model. However, it could not be done because of compatibility issues. While the data used in this study is the result of linear cutting tests conducted on a conditioned surface of rock, the rest of the data available in the literature is generated using tests conducted on a flat rock surface. Such a difference can drastically alter the results of the rock cutting tests. Thus, because of that critical difference in the process of testing, the merging was impossible. This situation can clearly demonstrate the need for a widely accepted standard procedure for conducting full-scale linear cutting tests in the future. Such a standard method of testing for the full-scale rock cutting test, will enable the researchers to combine the data from different sources and analyze them using the new and advanced methods of data analysis in order to find more accurate and reliable explanations for the rules that govern the process of rock cutting.

Finally, it should be added that, like any other statistical model, the model suggested in this study should be used only within the range of the data over which it has been fitted (Table 3-5). According to Copur et al. (2012), point attack picks may be used for excavation of rocks with *UCS* up to 100-120 *MPa*. In this regard, the *SE* prediction model covers around 40% of the range of application for point attack picks. While the application range for the suggested model is limited to *d* between 4-11 *mm* and *s* between 4-44 *mm*, the widest previously reported range for *d* and *s* is 3-12 *mm* and 9-45 *mm*, respectively. The values of θ_{tip}, θ_{attack}, and θ_{skew} reported in previous studies on relieved cutting mode are fixed at 80°, 55°, and 0°, respectively (Balci et al., 2004; Bilgin et al., 2006; Copur et al., 2003; Tumac et al., 2007). With regard to θ_{attack}, and θ_{skew} the application range for the current study covers the widest range reported up to date. According to Bilgin et al. (2013), θ_{tip} ranges from 60° to 90° with the range 75°-80° being the most commonly used range. The model suggested in this study may be applied for θ_{tip} values between 70°-75°.

5.3 The suggested models for prediction of forces acting on a point attack pick

A preliminary linear regression analysis was conducted on the established database in order to see if the relation between the forces and independent variables can be satisfactorily described in a linear form (Table 3-8). The analysis was conducted using stepwise *MLR* option in SPSS (2017):

$$F_{CM}=(0.125\times UCS)-(0.924\times BTS)+(0.172\times s)-\left(0.557\times\frac{s}{d}\right)-(0.331\times\theta_{tip})-(0.21\times\theta_{attack})+34.379 \quad (5.17)$$

$$F_{CP}=(0.101\times UCS)+(0.53\times s)-\left(1.69\times\frac{s}{d}\right)-(1.521\times\theta_{tip})-(0.417\times\theta_{attack})+131.575 \quad (5.18)$$

$$F_{NM}=(0.116\times UCS)-(0.839\times BTS)+(0.482\times d)+(0.094\times s)-(0.103\times\theta_{attack})-(0.035\times\theta_{skew})+1.6 \quad (5.19)$$

$$F_{NP}=(0.207\times UCS)-(1.354\times BTS)+(0.489\times s)+(0.561\times d)-\left(1.335\times\frac{s}{d}\right)-(0.625\times\theta_{tip})-(0.198\times\theta_{attack})-(0.089\times\theta_{skew})+51.507 \quad (5.20)$$

$$F_{SM}=(0.04\times s)-(0.11\times\theta_{tip})+8.308 \quad (5.21)$$

$$F_{SP}=(0.107\times s)-(0.333\times\theta_{tip})+24.974 \quad (5.22)$$

where F_{CM}, F_{CP}, F_{NM}, F_{NP}, F_{SM}, F_{SP}, R^2, and *MSE* are mean cutting force (*kN*), peak cutting force (*kN*), mean normal force (*kN*), peak normal force (*kN*), mean side force (*kN*), peak side force (*kN*), coefficient of determination and mean squared error, respectively. *MSE* is defined in Eq. 5.2.

Among the developed linear prediction models, Eq. 5.17-5.20 provide a relatively good level of accuracy. However, except for Eq. 5.20, at least one of the parameters that are important for determination of cutter forces is left out of each equation. As it was explained in Chapter 2, the developed prediction models are expected to include at least one of the rock related properties, i.e., *UCS* or *BTS*, as well as the important machine related parameters, i.e., s, d, θ_{tip}, θ_{attack}, and θ_{skew}. In addition, under certain circumstances, Eq. 5.17-5.20 are prone to predict negative values of forces within their application range. For each equation, range of application is defined as the minimum and maximum values of its respective input parameters (Table 3-8). For instance, according to Eq.

5.17-5.20, when UCS=21 MPa, BTS=1.84 MPa, p=4 mm, s=4 mm, θ_{tip} =75°, θ_{attack} =55°, and θ_{skew}=-15°, F_{CM}, F_{CP}, F_{NM}, and F_{NP} will be -0.94 MPa, -2.88 MPa, -0.34 MPa, and -0.20 MPa, respectively. As a result, it was decided to try a nonlinear function fitting technique in order to see if those shortcomings can be addressed.

The analysis conducted using the *GEP-PSO* code, set as shown in Table 5-8, yielded the following equations:

$$F_{CM}=0.25\left[\exp\left(\frac{\frac{s}{d}-\theta_{attack}+UCS}{2.59}\right)\right]^{0.32}+\frac{ds^{0.27}-\cot^{-1}(\theta_{skew})}{4.14}+0.5\left(BTS-UCS-\theta_{tip}+89.23\right)^{0.2}, \quad (5.23)$$

R^2=0.90, MSE=1.31

$$F_{CP}=\frac{\left(BTS+{}^{s}/_{d}\right)\times 0.25BTS}{528.74+2\theta_{skew}}+\frac{1}{4}\left[\frac{UCS+{}^{s}/_{d}}{\theta_{attack}-8.43}\right]^{5}+\frac{d\sqrt{s}}{\theta_{tip}-67.23}, \quad (5.24)$$

R^2=0.90, MSE=9.52

$$F_{NM}=\frac{d}{2.11}+0.52\left[\left(\frac{UCS+d}{1.94}+s-\theta_{skew}^{\frac{1}{3}}-\theta_{attack}-5.57\right)\times\theta_{tip}\right]^{1/5}+1.48, \quad (5.25)$$

R^2=0.85, MSE=1.07

$$F_{NP}=\frac{(\theta_{skew}-UCS)\times(\theta_{attack}-66.53)}{190.92}+\left[\frac{\frac{s}{d}+d-\theta_{tip}+67.9}{2\sqrt{2}}\right]^{2}, \quad (5.26)$$

R^2=0.91, MSE=4.78

$$F_{SM}=0.25s^{\frac{76.22-\theta_{tip}}{13.4}}+73.43(\theta_{attack}-d)^{\frac{\theta_{skew}-31.12}{12.18}}+0.32UCS^{\frac{-\theta_{skew}-9.55}{17.44}}, \quad (5.27)$$

R^2=0.80, MSE=0.21

$$F_{SP}=\frac{1}{4}\left[\frac{BTS-\theta_{attack}+\theta_{skew}{}^{2}}{4(\theta_{attack}-2BTS)}+\frac{-1.03^{\theta_{tip}/3}}{2}\right]^{3}+\left[\frac{1}{2}\times\left(\frac{s}{d}\right)^{1/3}\right]+\frac{d}{4}, \quad (5.28)$$

R^2=0.86, MSE=1.32

As Figure 5-15 and Figure 5-16 show, in comparison to Eq. 5.17-

Table 5-8: Settings used in *GEP–PSO* code for development prediction models for cutting, normal, and side force acting on a point attack pick

Gene Expression Programming (*GEP*)				Particle Swarm Optimization (*PSO*)	
Population Size (Number of Chromosomes)	3000	Inversion Rate	0.1	Number of Particles	350
Number of Genes Per Chromosome	4	Insertion Sequence Transposition Rate	0.1	Inertia	0.2
Head Length	6	Root Insertion Sequence Transposition Rate	0.1	Learning Rate for Personal Influence	2
Tail Length	7	Gene Transposition Rate	0.1	Learning Rate for Social Influence	2
Function Set	{+, ×, -, ÷, Power (Eq. 4.1), ln, Exp (Eq. 4.2), Sin, Cos, Tan}	One-point Recombination Rate	0.4	Maximum Number of Iterations	40
Terminal Set	{*UCS*, *BTS*, *d*, *s*, *s*/*d*, θ_{tip}, θ_{attack}, θ_{skew}, Random Numbers}	Two-point Recombination Rate	0.2	Selection Range for *A* and *C* (Eqs. 4.1 and 4.2) and Random Numbers	[-1000,1000]
Function Set used for Dynamic Linking Function Selection	{+, ×, -, ÷}	Gene Recombination Rate	0.1	Selection Range for *B* and *D* (Eqs. 4.1 and 4.2)	[-10,10]
Mutation Rate	0.2	Fitness Function	Eq. 5.2	Fitness Function	Eq. 5.2

UCS: Uniaxial Compressive Strength (*MPa*); *BTS*: Brazilian Tensile Strength (*MPa*); *d*: Depth of Cut (*mm*); *s*: Cut Spacing (*mm*); θ_{tip}: Tip Angle (*degree*); θ_{attack}: Attack Angle (*degree*); θ_{skew}: Skew Angle (*degree*)

5.22, Eq. 5.23-5.28 provide higher values of R^2 and lower values of *MSE*. For mean and peak values of cutting and side force, equations developed using the *GEP-PSO* algorithm achieve significantly higher accuracy in terms of R^2 and *MSE* values. Table 5-9 shows the accuracy of the developed models over training and test data. It should be added that only 80% of the available data was used to generate *GEP-PSO* models. The remaining 20% was reserved and used for validation.

In order to demonstrate the physical implications of the suggested

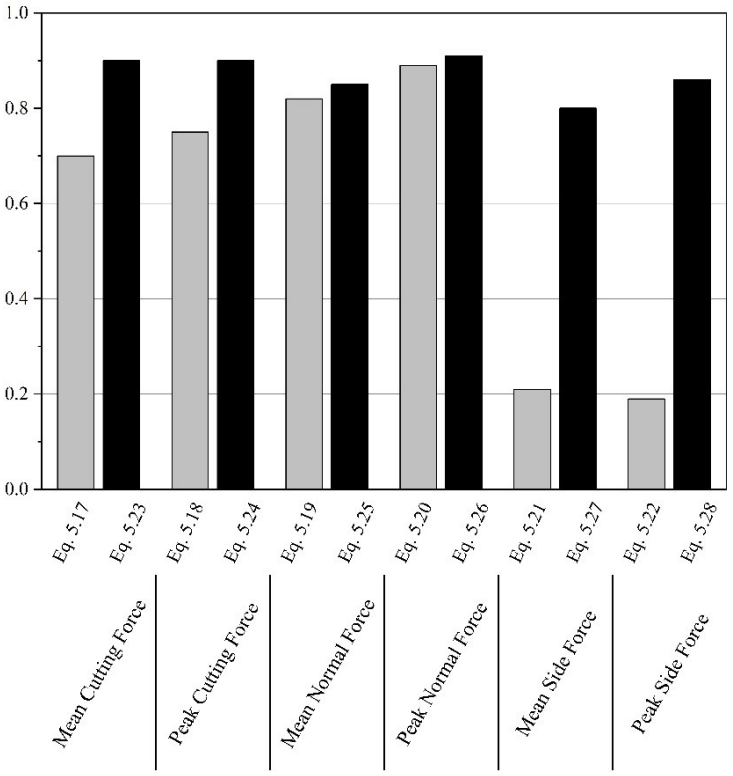

Figure 5-15: R^2 values associated with the equations developed using *MLR* and *GEP-PSO* for prediction of cutting, normal, and side force acting on a point attack pick

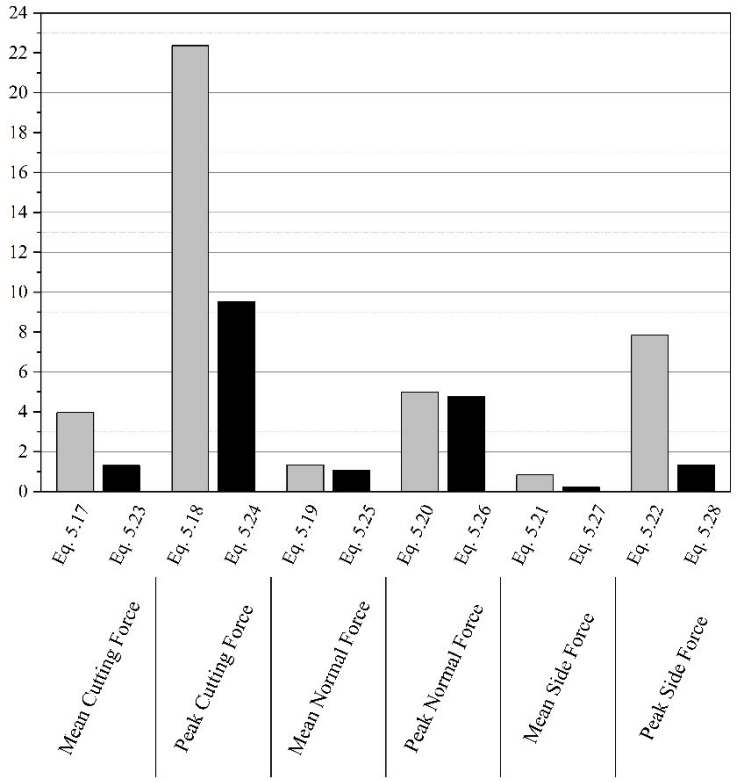

Figure 5-16: Mean squared error values associated with the equations developed using *MLR* and *GEP-PSO* for prediction of cutting, normal, and side force acting on a point attack pick

model, 38 graphs are provided in Appendix A. The graphs use clusters of representative cases to show the effect of each input parameter on the predictions made by the model as well as the real rest results. Across each cluster only one of the parameters changes while the rest are held constant. Based on the generated graphs, the equations developed for prediction of peak cutting force and peak and mean side force (Eq. 2.24, Eq. 5.27 and Eq. 5.28) show negligible sensitivity to some of their respective input parameters across the clusters of data that were available to generate them (Figure A-12, Figure A-28, Figure A-30, Figure A-36,

Figure A-38 in Appendix A). As a result, although those equations may be considered significant improvements over the linear equations (Eq. 2.18, Eq. 5.21 and Eq. 5.22), their limitations should be considered when one chooses to use them.

For mean and peak values of normal force, although equations developed using *GEP-PSO* algorithm are associated with higher values of R^2 and lower values of *MSE*, the difference is not so great. Moreover, Eq. 5.23-5.26 take account of both of the important rock and machine properties, whereas the linear equations fail in doing so. For instance, please note the fact that Eq. 5.17 and 5.18 are not sensitive to changes in rock strength (*UCS* or *BTS*), d, θ_{attack}, and θ_{skew}. It should be added that, Eq. 5.23-5.28 were all checked to make sure that, unlike Eq. 5.17-5.20, they are not prone to producing unrealistic negative values for tool forces within their range of application.

It should be added that, like any other statistical model, the model suggested in this study should be used only within the range of the data over which it has been fitted (Table 3-8). According to Copur et al. (2012), point attack picks may be used for excavation of rocks with UCS up to 100-120 MPa. In this regard, the suggested prediction models cover around 40% of the range of application for point attack picks. While the application range for the suggested model is limited to d between 4-11 *mm* and s between 4-44 *mm*, the widest previously reported range for d and s is 3-12 *mm* and 9-45 *mm*, respectively. The values of θ_{tip}, θ_{attack}, and θ_{skew} reported in previous studies on relieved cutting mode are fixed at 80°, 55°, and 0°, respectively (Balci et al., 2004; Bilgin et al., 2006; Copur et al., 2003; Tumac et al., 2007). With regard to θ_{attack}, and θ_{skew}

Table 5-9: Comparison of models developed using *MLR* and *GEP–PSO* algorithm for predicting forces acting on a point attack pick

Statistical Model			R^2	Mean Squared Error (Eq. 5.2)
Mean Cutting Force (F_{CM})	*MLR* (Eq. 5.17)	Whole Data	70.44%	3.96
	GEP-PSO (Eq. 5.23)	Training Data	90.00%	1.33
		Test Data	91.07%	1.25
		Whole Data	90.21%	1.31
Peak Cutting Force (F_{CP})	*MLR* (Eq. 5.17)	Whole Data	75.22%	22.36
	GEP-PSO (Eq. 5.23)	Training Data	89.54%	9.57
		Test Data	90.57%	9.35
		Whole Data	89.64%	9.52
Mean Normal Force (F_{NM})	*MLR* (Eq. 5.19)	Whole Data	81.98%	1.33
	GEP-PSO (Eq. 5.25)	Training Data	85.86%	1.09
		Test Data	85.02%	1.02
		Whole Data	85.44%	1.07
Peak Normal Force (F_{NP})	*MLR* (Eq. 5.19)	Whole Data	90.43%	5
	GEP-PSO (Eq. 5.25)	Training Data	91.32%	4.77
		Test Data	88.63%	4.80
		Whole Data	90.86%	4.78
Mean Side Force (F_{SM})	*MLR* (Eq. 5.17)	Whole Data	21.14%	0.84
	GEP-PSO (Eq. 5.28)	Training Data	80.58	0.21
		Test Data	79.86%	0.20
		Whole Data	80.31%	0.21
Peak Side Force (F_{SP})	*MLR* (Eq. 5.22)	Whole Data	18.67%	7.85
	GEP-PSO (Eq. 5.28)	Training Data	86.57%	1.33
		Test Data	85.05%	1.26
		Whole Data	86.34%	1.32

the application range for the current study covers the widest range reported up to date. According to Bilgin et al. (2013), θ_{tip} ranges from 60° to 90° with the range 75°-80° being the most commonly used range. The models suggested in this study may be applied for θ_{tip} values between 70°-75°.

6. CONCLUSIONS

Each of the following sections provide the conclusions associated with one of the objectives that were pursued over the course of this study.

6.1 Performance prediction model for impact hammer

A relatively large database with 85 points that each contained records of machine power, Uniaxial Compressive Strength (*UCS*), Rock Quality Designation, Schmidt Hammer Rebound Values, and Instantaneous Breaking Rate (*IBR*) was established. The data were collected during the construction of two tunneling projects in Istanbul. Based on Gene Expression Programming (*GEP*) and Particle Swarm Optimization (*PSO*), a hybrid evolutionary algorithm was generated to analyze the data. The result yielded an accurate performance prediction model for an impact hammer. The accuracy of the new model was compared to that generated by Multiple Linear Regression (*MLR*) analysis as well as some of the models that were already available in the literature. The results showed that the suggested model was more reliable and accurate, with a broader range of application, while it required only four easy-to-obtain input parameters. Compared to the *MLR* model, the values of R^2 and *MSE* were improved by around 10% and 35%, respectively.

The behavior of the proposed model was examined under different conditions. The results showed that for any value of machine power, there was a critical *UCS* value beyond which the performance of the machine dramatically decreased. The critical value of *UCS* could be

calculated using the proposed *GEP–PSO* model. In addition, the model showed that the performance of the machine decreased for very low values of *UCS*. It was speculated that for those *UCS* values, the excavation process is more comparable to digging than breaking.

The proposed *GEP–PSO* algorithm proved to be capable of finding reliable solutions for function-fitting problems, especially for those involving a large amount of data. Using this algorithm, precise models may be developed without making any prior judgment about their form. This advantage makes the *GEP–PSO* algorithm more attractive than function fitting methods such as multiple non-linear regression or other optimization techniques such as ant/bee colony optimization. In addition, the *GEP-PSO* algorithm has an advantage over artificial neural networks because it generates a mathematical equation rather than a network structure. The proposed *GEP–PSO* algorithm only showed one drawback in comparison to *MLR*. That is, as in all of the other iterative function fitting methods, the time required by *GEP–PSO* to find a good fit was not predetermined. However, this disadvantage may be outweighed by the high accuracy of *GEP–PSO* compared to that of *MLR*. As a result, this method of function fitting may be a very useful tool for engineering applications.

It is recommended that researchers who are interested in working on the subject of this paper should collect databases that include a larger number of different values for machine power and rock properties, which are properly distributed over a wide range. Given the high capabilities of the new data analysis techniques for handling large amounts of

information, analyzing such databases using these methods may lead to a better understanding of excavation using an impact hammer.

6.2 Prediction model for specific energy required by point attack picks

Review of the literature on the prediction models for specific energy (*SE*) required by point attack picks showed that there are various statistically developed equations that can predict the optimum *SE* within certain limits. However, those models did not include variations of some significantly important parameters that have an effect on *SE*; mostly because of a limited number of statistical data, which itself is a result of the fact that conducting full-scale linear rock cutting (*FSLC*) test is not an easy task. It should be added that it is impossible to collect that information from real excavation projects over the diverse items and range of variables.

In order to overcome the limitations of the previous studies, a database of 186 points containing the results of lab-scale linear cutting test was established. First, the statistical analysis was conducted using *MLR* to see if a simple linear function can describe the relation between *SE* and the other parameters in the database. The results of *MLR* analysis did not yield reasonably accurate results (Eq. 5.9). Thus, the *GEP-PSO* algorithm was used for non-linear function fitting.

The statistical analysis using the *GEP-PSO* algorithm yielded a considerably more accurate prediction model than the one generated by *MLR* (Eqs. 5.10-5.14). The prediction model developed using the *GEP-PSO* algorithm also included all of the significantly important cutting parameters (cut spacing (s), depth of cut (d), s/d, tip angle (θ_{tip}), attack

angle (θ_{attack}), and skew angle (θ_{skew})) as well as a representative property of rock (Brazilian Tensile Strength (*BTS*)).

The equations developed by *GEP-PSO* algorithm (Eqs. 5.10-5.14) are suggested to be used as a prediction model for the *SE* required by point attack picks in relieved cutting mode within the limits of the database used in this study (Table 3-5). The model may be very useful in the early stages of a project as it can be used to predict the advance rate of the mechanical miners with point attack picks or to reduce the number of full-scale linear cutting tests required to determine the optimum *SE*.

Finally, although the database used for analysis in this study may be considered to be large, it could be improved if more variations of rock properties and cutting parameters were included.

6.3 Models for prediction of cutting, normal, and side force acting on a point attack pick

The aim of this part of the present research was to suggest models that can predict cutting and normal force acting on a point attack pick in relieved cutting mode. The suggested models were supposed to be accurate, generate only non-negative values for forces over their range of application, and be sensitive to rock properties, i.e. *UCS* or *BTS*, in addition to *s*, *d*, θ_{tip}, θ_{attack}, and θ_{skew}. Using the suggested models, the torque and the trust required by the machine for excavation of different rock types using different *s*, p, θ_{tip}, θ_{attack}, and θ_{skew} settings may be determined.

Although the presented non-linear models proved to be more useful compared to the other available prediction models, there is still room for improvement. According to some of the previously developed prediction

models for cutting and normal force, friction between rock and cutter can be an important factor in determination of those forces. However, due to the understandably reluctant approach of cutter producers to providing cutter tip material and its specifications, friction coefficient between cutter and rock could not be determined during the course of the present study. On the positive side, however, excluding such a hard-to-determine parameter from the models contributes to their ease of use. Finally, the data used in order to develop the present prediction models includes two different values for θ_{tip}. Combining the data used in the present research with more data points that are, preferably, results of tests that cover a broader variety of θ_{tip} values can significantly increase the reliability of the outcomes of the future research on empirical force prediction models.

REFERENCES

Abu Bakar, M.Z., Gertsch, L.S., 2013. Evaluation of saturation effects on drag pick cutting of a brittle sandstone from full scale linear cutting tests. Tunn. Undergr. Sp. Technol. 34, 124–134. https://doi.org/10.1016/j.tust.2012.11.009

Abu Bakar, M.Z., Gertsch, L.S., Rostami, J., 2014. Evaluation of fragments from disc cutting of dry and saturated sandstone. Rock Mech. Rock Eng. 47, 1891–1903. https://doi.org/10.1007/s00603-013-0482-8

Acaroglu, O., Ozdemir, L., Asbury, B., 2008. A fuzzy logic model to predict specific energy requirement for TBM performance prediction. Tunn. Undergr. Sp. Technol. 23, 600–608. https://doi.org/10.1016/j.tust.2007.11.003

Aksoy, C.O., 2009. Performance prediction of impact hammers by block punch index for weak rock masses. Int. J. Rock Mech. Min. Sci. 8, 1383–1388.

Aksoy, C.O., Ozacar, V., Demirel, N., Ozer, S.C., Safak, S., 2011. Determination of instantaneous breaking rate by geological strength index, block punch index and power of impact hammer for various rock mass conditions. Tunn. Undergr. Sp. Technol. 26, 534–540. https://doi.org/10.1016/j.tust.2011.02.005

Aksoy, C.O., Ozacar, V., Safak, S., 2013. An updated formula and method to predict the performance of impact hammers. Int. J. Rock Mech. Min. Sci. 61, 289–295. https://doi.org/10.1016/j.ijrmms.2013.02.008

Anagnostou, G., Ehrbar, H., 2013. Underground. The Way to the Future. CRC Press.

Balci, C., 2009. Correlation of rock cutting tests with field performance of a TBM in a highly fractured rock formation: A case study in Kozyatagi-Kadikoy metro tunnel, Turkey. Tunn. Undergr. Sp. Technol. 24, 423–435. https://doi.org/10.1016/j.tust.2008.12.001

Balci, C., Bilgin, N., 2007. Correlative study of linear small and full-scale rock cutting tests to select mechanized excavation machines. Int. J. Rock Mech. Min. Sci. 44, 468–476. https://doi.org/10.1016/j.ijrmms.2006.09.001

Balci, C., Demircin, M. a., Copur, H., Tuncdemir, H., 2004. Estimation of optimum specific energy based on rock properties for assessment of roadheader performance. J. South African Inst. Min. Metall. 104, 633–641.

Bilgin, N., 1977. Investigations into the mechanical cutting characteristics of some medium and high strength rocks.

Bilgin, N., Copur, H., Balci, C., 2013. Mechanical Excavation in Mining and Civil Industries, Mechanical Excavation in Mining and Civil Industries. CRC Press. https://doi.org/10.1201/b16083

Bilgin, N., Demircin, M.A., Copur, H., Balci, C., Tuncdemir, H., Akcin, N., 2006. Dominant rock properties affecting the performance of conical picks and the comparison of some experimental and theoretical results. Int. J. Rock Mech. Min. Sci. 43, 139–156. https://doi.org/10.1016/j.ijrmms.2005.04.009

Bilgin, N., Dincer, T., Copur, H., 2002. The performance prediction of impact hammers from Schmidt hammer rebound values in Istanbul metro tunnel drivages. Tunn. Undergr. Sp. Technol. 17, 237–247. https://doi.org/10.1016/S0886-7798(02)00009-3

Bilgin, N., Tumac, D., Feridunoglu, C., Karakas, A.R., Akgul, M., 2005. The performance of a roadheader in high strength rock formations in Küçüksu tunnel. Undergr. Sp. Use Anal. Past Lessons Futur. - Proc. 31st ITA-AITES World Tunn. Congr. 2, 815–820.

Bilgin, N., Yazici, S., Eskikaya, S., 1996. A Model to Predict the Performance of Roadheaders And Impact Hammers In Tunnel Drivages. Eurock 96 715–721.

Brown, E.T., 1981. Rock characterization testing and monitoring. Pergamon press.

Chang, S.-H., Choi, S.-W., Bae, G.-J., Jeon, S., 2006. Performance prediction of TBM disc cutting on granitic rock by the linear cutting test. Tunn. Undergr. Sp. Technol. 21, 271.

Cho, J.W., Jeon, S., Jeong, H.Y., Chang, S.H., 2013. Evaluation of cutting efficiency during TBM disc cutter excavation within a Korean granitic rock using linear-cutting-machine testing and photogrammetric measurement. Tunn. Undergr. Sp. Technol. 35, 37–54. https://doi.org/10.1016/j.tust.2012.08.006

Comakli, R., 2019. Performance of roadheaders in low strength pyroclastic rocks, a case study of cold storage caverns in Cappadocia. Tunn. Undergr. Sp. Technol. 89, 179–188. https://doi.org/10.1016/j.tust.2019.04.007

Comakli, R., Kahraman, S., Balci, C., 2014. Performance prediction of roadheaders in metallic ore excavation. Tunn. Undergr. Sp. Technol. 40, 38–45. https://doi.org/10.1016/j.tust.2013.09.009

Copur, H., 2010. Linear stone cutting tests with chisel tools for identification of cutting principles and predicting performance of chain saw machines. Int. J. Rock Mech. Min. Sci. 47, 104–120. https://doi.org/10.1016/j.ijrmms.2009.09.006

Copur, H., Balci, C., Bilgin, N., Tumac, D., Avunduk, E., 2012. Predicting cutting performance of chisel tools by using physical and mechanical properties of natural stones, in: ISRM International Symposium-EUROCK 2012. International Society for Rock Mechanics, Stockholm, Sweden.

Copur, H., Balci, C., Tumac, D., Bilgin, N., 2011. Field and laboratory studies on natural stones leading to empirical performance prediction of chain saw machines. Int. J. Rock Mech. Min. Sci. 48, 269–282. https://doi.org/10.1016/j.ijrmms.2010.11.011

Copur, H., Bilgin, N., Balci, C., Tumac, D., Avunduk, E., 2017. Effects of Different Cutting Patterns and Experimental Conditions on the Performance of a Conical Drag Tool. Rock Mech. Rock Eng. 50, 1585–1609. https://doi.org/10.1007/s00603-017-1172-8

Copur, H., Bilgin, N., Balci, C., Tumac, D., Avunduk, E., Mamaghani, A.S., 2016. Full-scale linear cutting experiments with a conical cutter for simulating different cutting patterns. Rock Mech. Rock Eng. From Past to Futur. 153.

Copur, H., Bilgin, N., Tuncdemir, H., Balci, C., 2003. A set of indices based on indentation tests for assessment of rock cutting performance and rock properties. J. South African Inst. Min. Metall. 103, 589–599.

Copur, H., Tuncdemir, H., Bilgin, N., Dincer, T., 2001. Specific energy as a criterion for the use of rapid excavation systems in Turkish mines. Inst. Min. Metall. Trans. Sect. A Min. Technol. 110, 149–157. https://doi.org/10.1179/mnt.2001.110.3.149

Cramer, N.L., 1985. A representation for the adaptive generation of simple sequential programs, in: Proceedings of an International Conference on Genetic Algorithms and the Applications. pp. 183–187.

Diveev, A., Shmalko, E., 2021. Machine Learning Control by Symbolic Regression. Springer.

Dogruoz, C., Bolukbasi, N., 2014. Effect of cutting tool blunting on the performances of various mechanical excavators used in low- and medium-strength rocks. Bull. Eng. Geol. Environ. 73, 781–789. https://doi.org/10.1007/s10064-013-0551-y

Dogruoz, C., Bolukbasi, N., Rostami, J., Acar, C., 2016. An Experimental Study of Cutting Performances of Worn Picks. Rock Mech. Rock Eng. 49, 213–224. https://doi.org/10.1007/s00603-015-0734-x

Dursun, A.E., Gokay, M.K., Kemal, M., Gokay, M.K., 2016. Cuttability Assessment of Selected Rocks Through Different Brittleness Values. Rock Mech. Rock Eng. 49, 1173–1190. https://doi.org/10.1007/s00603-015-0810-2

Dursun, A.E., Kemal, M., 2016. Cuttability Assessment of Selected Rocks Through Different Brittleness Values 1173–1190. https://doi.org/10.1007/s00603-015-0810-2

Entacher, M., Lorenz, S., Galler, R., 2014. Tunnel boring machine performance prediction with scaled rock cutting tests. Int. J. Rock Mech. Min. Sci. 70, 450–459. https://doi.org/10.1016/j.ijrmms.2014.04.021

Evans, I., 1984. A theory of the cutting force for point-attack picks. Int. J. Min. Eng. 2, 63–71. https://doi.org/10.1007/BF00880858

Ferreira, C., 2006. Gene expression programming: mathematical modeling by an artificial intelligence. Springer.

Fowell, R.J., McFeat-Smith, I., 1976. Factors influencing the cutting performance of a selective tunnelling machine, in: Int. Tunnelling'76 Symp. pp. 301–318.

Gertsch, R., Gertsch, L., Rostami, J., 2007. Disc cutting tests in Colorado Red Granite: Implications for TBM performance prediction. Int. J. rock Mech. Min. Sci. 44, 238–246. https://doi.org/10.1016/j.ijrmms.2006.07.007

Göktan, R.M., 1990. Effect of cutter pick rake angle on the failure pattern of high-strength rocks. Min. Sci. Technol. 11, 281–285. https://doi.org/10.1016/0167-9031(90)90981-W

Goktan, R.M., Gunes, N., 2005. A semi-empirical approach to cutting force prediction for point-attack picks. J. South African Inst. Min. Metall. 105, 257–263.

Hojjati, S., Jeong, H., Jeon, S., 2018. Prediction model for specific cutting energy of pick cutters based on gene expression programming and particle swarm optimization. Tunn. Undergr. Sp. 28, 651–669.

Iphar, M., 2012. ANN and ANFIS performance prediction models for hydraulic impact hammers. Tunn. Undergr. Sp. Technol. 27, 23–29. https://doi.org/10.1016/j.tust.2011.06.004

Jeong, H., Choi, S., Jeon, S., 2020. Effect of skew angle on the cutting performance and cutting stability of point-attack type picks. Tunn. Undergr. Sp. Technol. 103, 103507.

Jeong, H.Y., 2017. Assessment of rock cutting efficiency of pick cutters for the optimal design of a mechanical excavator. Seoul National University.

Jones, M.T., 2007. Artificial Intelligence: A Systems Approach, 1st ed. Infinity Science Press.

Kang, H., Cho, J.W., Park, J.Y., Jang, J.S., Kim, J.H., Kim, K.W., Rostami, J., Lee, J.W., 2016. A new linear cutting machine for assessing the rock-cutting performance of a pick cutter. Int. J. Rock Mech. Min. Sci. 88, 129–136. https://doi.org/10.1016/j.ijrmms.2016.07.021

Kel, K., 2003. Investigation of the cuttability of coal measure rocks in Zonguldak coal basin.

Kennedy, J, Eberhart, R., 1995. Particle swarm optimization, in: Proceedings of ICNN'95 - International Conference on Neural Networks. pp. 1942–1948 vol.4. https://doi.org/10.1109/ICNN.1995.488968

Kennedy, James, Eberhart, R., 1995. Particle swarm optimization, in: Proceedings of ICNN'95 - International Conference on Neural Networks. pp. 1942–1948 vol.4. https://doi.org/10.1109/ICNN.1995.488968

Khademi Hamidi, J., Shahriar, K., Rezai, B., Rostami, J., 2010. Performance prediction of hard rock TBM using Rock Mass Rating (RMR) system. Tunn. Undergr. Sp. Technol. 25, 333–345. https://doi.org/10.1016/j.tust.2010.01.008

Koza, J.R., 1992. Genetic Programming: On the Programming of Computers by Means of Natural Selection. MIT Press, Cambridge, MA, USA.

Kucuk, K., Aksoy, C.O., Basarir, H., Onargan, T., Genis, M., Ozacar, V., 2011. Prediction of the performance of impact hammer by adaptive neuro-fuzzy inference system modelling. Tunn. Undergr. Sp. Technol. 26, 38–45. https://doi.org/10.1016/j.tust.2010.06.011

Ma, H., Gong, Q., Wang, J., Yin, L., Zhao, X., 2015. Study on the influence of confining stress on TBM performance in granite rock by linear cutting test. Tunn. Undergr. Sp. Technol. 57, 145–150. https://doi.org/10.1016/j.tust.2016.02.020

Matlab, 2017. Version R2017b. The MathWorks, Inc.,Natick, Massachusetts, United States. www.mathworks.com.

Mitchell, T.M., 1997. Machine Learning, 1st ed. McGraw-Hill, Inc., USA.

Montgomery, D.C., Runger, G.C., 2018. Applied statistics and probability for engineers. Wiley Hoboken, NJ.

Nisbet, R., Elder, J., Miner, G.D., 2018. Handbook of statistical analysis and data mining applications, Second. ed. Academic press.

Ozdemir, L., 1998. Mechanical hard rock mining: Present and future. Min. Eng. 50, 36–37.

Ozdemir, L., 1992. Mechanical excavation-today and tomorrow, in: International GeoEngineering Conference, Torino, Italy.

Ozdemir, L., 1990. Recent developments in hard rock mechanical mining technologies, in: 4th Canadian Symposium on Mine Automation, Saskatoon, Canada.

Ozfirat, K.M., Malli, T., Ozfirat, P.M., Kahraman, B., 2017. The performance prediction of roadheaders with response surface analysis for underground metal mine. Kuwait J. Sci. 44.

Pan, Y., Liu, Quansheng, Liu, J., Liu, Qi, Kong, X., 2018. Full-scale linear cutting tests in Chongqing Sandstone to study the in fl uence of con fi ning stress on rock cutting e ffi ciency by TBM disc cutter. Tunn. Undergr. Sp. Technol. 80, 197–210. https://doi.org/10.1016/j.tust.2018.06.013

Pang, P.L.R., 2015. Developments in tunnelling practice in Hong Kong, in: International Conference & Exhibition on Tunnelling & Underground Space (ICETUS2015). Kuala Lumpur, Malaysia.

Park, J.Y., Kang, H., Lee, J.W., Kim, J.H., Oh, J.Y., Cho, J.W., Rostami, J., Kim, H.D., 2018. A study on rock cutting efficiency and structural stability of a point attack pick cutter by lab-scale linear cutting machine testing and finite element analysis. Int. J. Rock Mech. Min. Sci. 103, 215–229. https://doi.org/10.1016/j.ijrmms.2018.01.034

Poli, R., Langdon, W.B., McPhee, N.F., 2008. A Field Guide to Genetic Programming. Lulu Enterprises, UK Ltd.

Pomeroy, C.D., 1963. The breakage of coal by wedge action: factors influencing breakage by any given shape of tools. Colliery Guard. 672–677.

Poole, R.W., Farmer, I.W., 1980. Consistency and repeatability of Schmidt hammer rebound data during field testing. Int. J. Rock Mech. Min. Sci. 17.

Ritchie, H., 2019. India's population growth will come to an end: the number of children has already peaked [WWW Document]. OurWorldInData.org. URL https://ourworldindata.org/indias-population-growth-will-come-to-an-end

Roepke, W.W., Voltz, J.I., 1983. Coal cutting forces and primary dust generation using radial gage cutters. US Department of the Interior, Bureau of Mines.

Rostami, J., 2011. Mechanical Rock Breaking, in: SME Mining Engineering Handbook, Third Edition. p. 417.

Rostami, J., Ozdemir, L., Neil, D.M., 1994. Performance prediction: a key issue in mechanical hard rock mining. Min. Eng. 46, 1263–1267.

Roxborough, F.F., 1973. Cutting rock with picks. Min. Eng. 132, 445–454.

Roxborough, F.F., Liu, Z.C., 1995. Theoretical considerations on pick shape in rock and coal cutting, in: Proceedings of the Sixth Underground Operator's Conference, Kalgoorlie. pp. 189–193.

Russell, S., Norvig, P., 2020. Artificial intelligence: a modern approach, Fourth. ed. Pearson, Boston.

Shi, Y., Eberhart, R., 1998. A modified particle swarm optimizer, in: 1998 IEEE International Conference on Evolutionary Computation Proceedings. IEEE World Congress on Computational Intelligence (Cat. No.98TH8360). pp. 69–73. https://doi.org/10.1109/ICEC.1998.699146

SPSS, 2017. IBM SPSS statistics for Windows. New York IBM Corp.

Terezopoulos, N.G., 1987. Influence of geotechnical environments on mine tunnel drivage performance, in: Advances in Mining Science and Technology. Elsevier, pp. 139–156.

Tiryaki, B., Boland, J.N., Li, X.S., 2010. Empirical models to predict mean cutting forces on point-attack pick cutters. Int. J. Rock Mech. Min. Sci. 47, 858–864. https://doi.org/10.1016/j.ijrmms.2010.04.012

Tiryaki, B., Dikmen, A.C., 2006. Effects of rock properties on specific cutting energy in linear cutting of sandstones by picks. Rock Mech. Rock Eng. 39, 89–120. https://doi.org/10.1007/s00603-005-0062-7

Tumac, D., 2014. Predicting the Performance of Chain Saw Machines Based on Shore Scleroscope Hardness. Rock Mech. Rock Eng. 47, 703–715. https://doi.org/10.1007/s00603-013-0416-5

Tumac, D., Bilgin, N., Feridunoglu, C., Ergin, H., 2007. Estimation of Rock Cuttability from Shore Hardness and Compressive Strength Properties. Rock Mech. Rock Eng. 40, 477–490. https://doi.org/10.1007/s00603-006-0108-5

Tumac, D., Hojjati, S., 2016. Predicting performance of impact hammers from rock quality designation and compressive strength properties in various rock masses. Tunn. Undergr. Sp. Technol. 59, 38–47. https://doi.org/https://doi.org/10.1016/j.tust.2016.06.008

Tuncdemir, H., 2008. Impact hammer applications in Istanbul metro tunnels. Tunn. Undergr. Sp. Technol. 23, 264–272.

Tuncdemir, H., 2002. Investigation into application of boom type machines for mineral excavation.

Ulusay, R., Hudson, J.A. (Eds.), 2007. The Complete ISRM Suggested Methods for Rock Characterization, Testing and Monitoring:1974-2006.

Wallace, M.I., Ng, K.C., 2016. Development and application of underground space use in Hong Kong. Tunn. Undergr. Sp. Technol. 55, 257–279.

Wang, X., Liang, Y., Wang, Q., Zhang, Z., 2017a. Empirical models for tool forces prediction of drag-typed picks based on principal component regression and ridge regression methods. Tunn. Undergr. Sp. Technol. 62, 75–95. https://doi.org/10.1016/j.tust.2016.11.006

Wang, X., Su, O., Wang, Q.-F.F., Liang, Y.-P.P., 2017b. Effect of cutting depth and line spacing on the cuttability behavior of sandstones by conical picks. Arab. J. Geosci. 10, 525. https://doi.org/10.1007/s12517-017-3307-3

Wang, X., Wang, Q.-F., Liang, Y.-P., Su, O., Yang, L., 2018. Dominant Cutting Parameters Affecting the Specific Energy of Selected Sandstones when Using Conical Picks and the Development of Empirical Prediction Models. Rock Mech. Rock Eng. 51, 3111–3128. https://doi.org/10.1007/s00603-018-1522-1

Xue, Y. dong, Zhao, F., Zhao, H. xiang, Li, X., Diao, Z. xing, 2018. A new method for selecting hard rock TBM tunnelling parameters using optimum energy: A case study. Tunn. Undergr. Sp. Technol. 78, 64–75. https://doi.org/10.1016/j.tust.2018.03.030

Yang, S.-Q., Jing, H.-W., 2011. Strength failure and crack coalescence behavior of brittle sandstone samples containing a single fissure under uniaxial compression. Int. J. Fract. 168, 227–250.

Yao, Q.Y.Y., Mostafavi, S.S.S., Bao, R.B.B., Zhang, L.C.C., Lunn, J., Melmeth, C., 2011. Pick profile effect on linear cutting of sandstone. 45th US Rock Mech. / Geomech. Symp. 1–5.

Yasar, S., 2020. A General Semi-Theoretical Model for Conical Picks. Rock Mech. Rock Eng. https://doi.org/10.1007/s00603-020-02078-3

Yasar, S., Capik, M., Yilmaz, A.O., 2015. Cuttability assessment using the Drilling Rate Index (DRI). Bull. Eng. Geol. Environ. 74, 1349–1361. https://doi.org/10.1007/s10064-014-0715-4

Yetkin, M.E., Özfırat, M.K., Yenice, H., Şimşir, F., Kahraman, B., 2016. Examining the relation between rock mass cuttability index and rock drilling properties. J. African Earth Sci. 124, 151–158.

Yilmaz, N. Gunes, Tumac, D., Goktan, R.M., 2015. Rock cuttability assessment using the concept of hybrid dynamic hardness (HDH). Bull. Eng. Geol. Environ. 74, 1363–1374. https://doi.org/10.1007/s10064-014-0692-7

Yilmaz, N Gunes, Tumac, D., Goktan, R.M., 2015. Rock cuttability assessment using the concept of hybrid dynamic hardness (HDH). Bull. Eng. Geol. Environ. 74, 1363–1374. https://doi.org/10.1007/s10064-014-0692-7

Zielesny, A., 2016. From curve fitting to machine learning, Second. ed. Springer. https://doi.org/10.1007/978-3-319-32545-3

초 록

암반 기계 굴착 기술의 발전으로 기존의 발파 공법이 아닌 기계 굴착을 사용하여 지하 공간을 건설하는 사례가 증가하고 있다. 기계식 암석 굴착 분야에는 다양한 변수 간의 관계에 대한 상당한 수의 결정론적 해법이 있지만, 많은 경우 변수 간의 결정적 관계를 설정하는 것은 극히 어렵다. 그 결과 많은 연구자들이 회귀 분석을 사용하여 이러한 관계를 설명하려고 한다. 암석 파쇄 현상의 복잡하고 비선형적인 특성으로 인해 기존의 함수 피팅 기법에서 요구하는 통계 데이터에 부합하는 비선형 함수의 형태를 합리적으로 결정하기가 쉽지 않다. 따라서 본 연구에서는 기계 굴착 분야의 문제점을 해결하기 위해 유전자 발현 프로그래밍(GEP)과 입자 군집 최적화 (PSO)의 조합을 데이터 분석에 사용하였다. GEP 및 PSO는 진화적 계산 기술이며 GEP-PSO 알고리즘을 통해 데이터 세트에 맞는 비선형 함수의 형식과 상수를 자동으로 찾을 수 있다. 본 연구에서는 임팩트 해머에 대한 성능 예측 모델, 픽커터에 필요한 비에너지 예측 모델, 픽커터에 작용하는 절삭력, 수직력, 횡방향력 예측 모델을 개발하기 위해 알고리즘을 사용하였다. 모든 경우에 GEP-PSO 알고리즘을 사용하여 생성된 결과는 다중 선형 회귀에 의해 생성된 결과와 비교하여 상당히 높은 예측 정확도를 생성함을 확인하였다. 가능한 경우 GEP-PSO 알고리즘에 의해 생성된 결과와 다른 연구자가 개발한 예측 모델을 비교하여 현재 연구 과정에서 개발된 모델의 장점을 보여 줄 것으로 보인다. 높은 수준의 정확도 외에도 GEP-PSO 알고리즘을 사용하여 개발된 모델은 기존 예측

모델의 단점을 상당 부분 극복할 수 있다. 개발된 모델은 얻기 쉬운 입력 매개변수를 거의 요구하지 않으면서 더 많은 신뢰성 및 정확도를 제공하거나 기존 예측 모델에서 무시되었던 중요한 입력 매개변수를 포함하므로 더 유리하다고 볼 수 있다.

주요어: 인공지능, 예측모델, 임팩트 해머, 픽커터, 비에너지, 커터작용력

학번: 2017-34695

APPENDIX A

In order to demonstrate the physical implications of the suggested model for prediction of the forces acting on a point attack pick, the following graphs are provided. The graphs use clusters of representative cases to show the effect of each input parameter on the predictions made by the model as well as the real rest results. Across each cluster only one of the parameters changes while the rest are held constant. Figure A-3, Figure A-10, Figure A-17, Figure A-23, Figure A-29, and Figure A-35 only show the predicted values as there were no cluster of test results with the same other settings (*UCS*, *BTS*, *d*, *s*, θ_{attack}, θ_{skew}) and different tip angle values in the database.

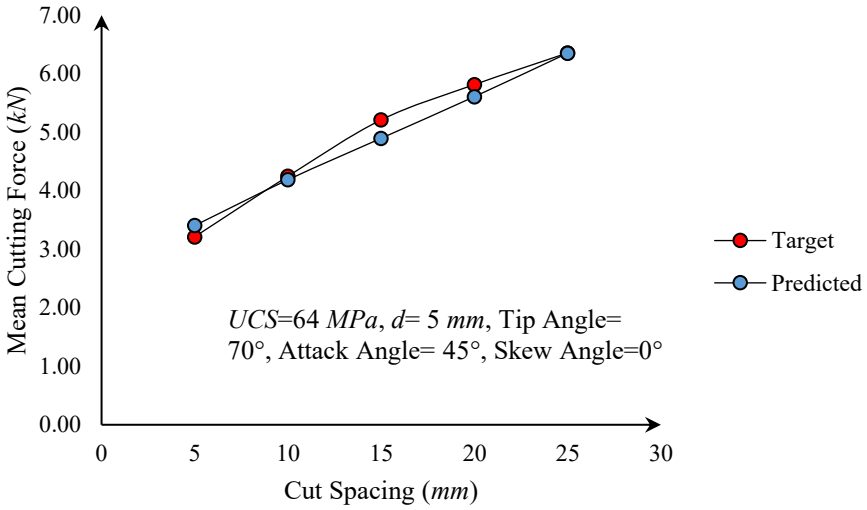

Figure A-1: Representative cases showing the effect of cut spacing on mean cutting force

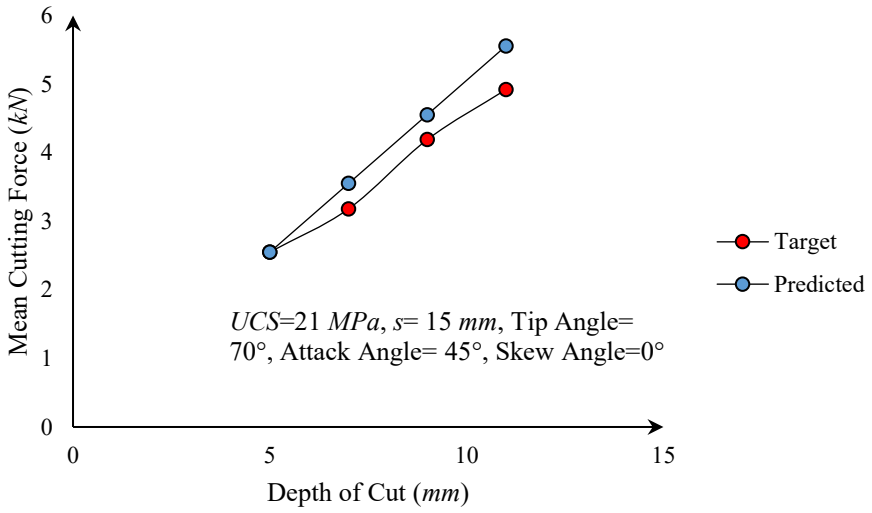

Figure A-2: Representative cases showing the effect of depth of cut on mean cutting force

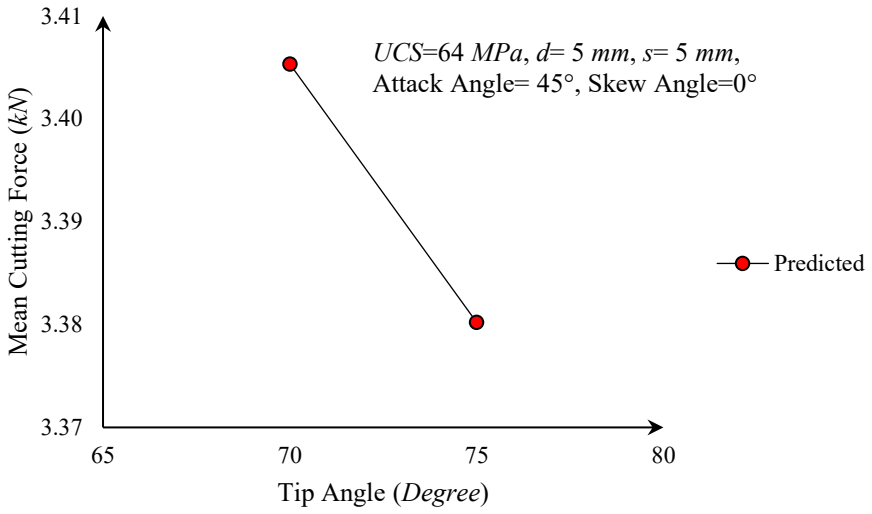

Figure A-3: Representative cases showing the effect of tip angle on mean cutting force

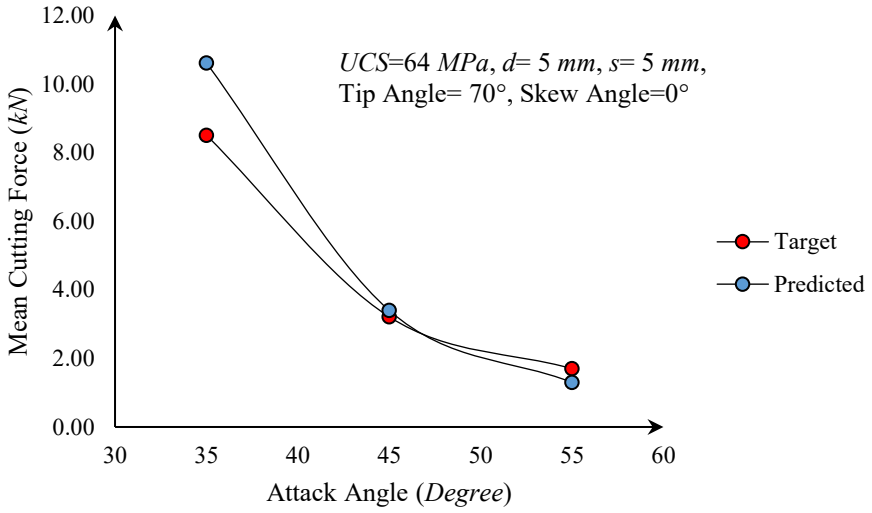

Figure A-4: Representative cases showing the effect of attack angle on mean cutting force

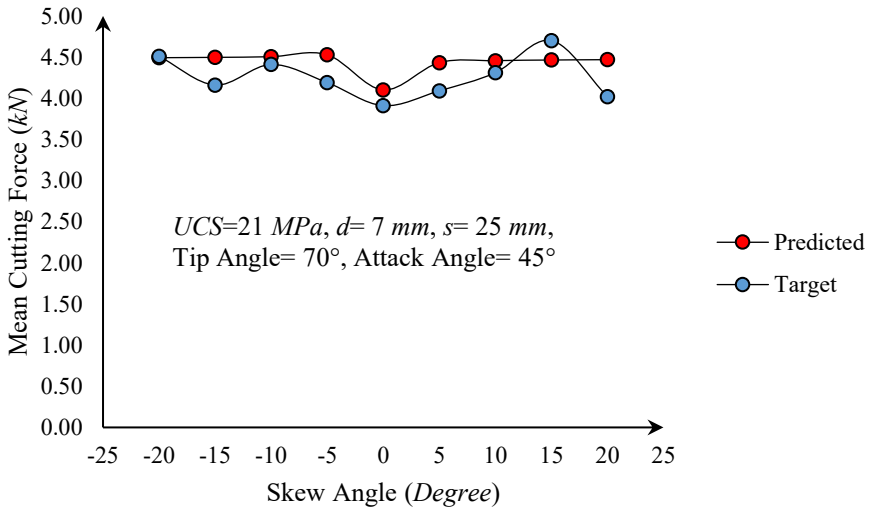

Figure A-5: Representative cases showing the effect of skew angle on mean cutting force

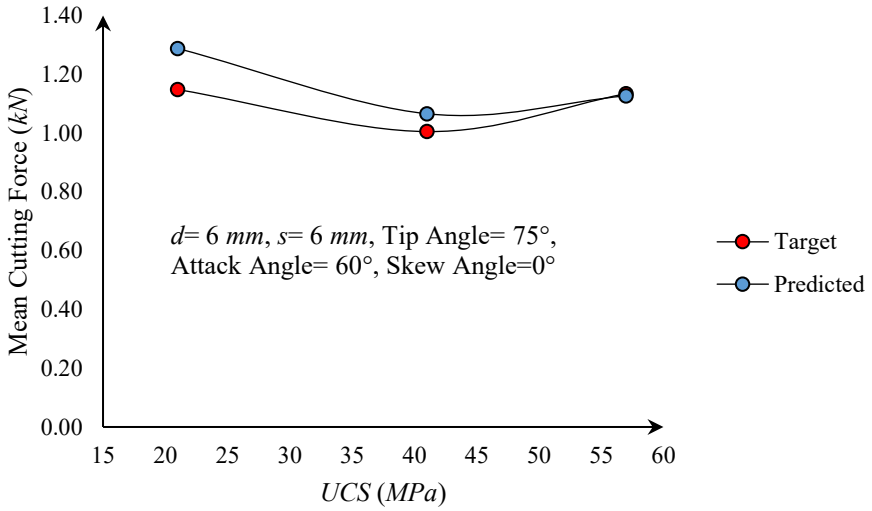

Figure A-6: Representative cases showing the effect of uniaxial compressive strength on mean cutting force

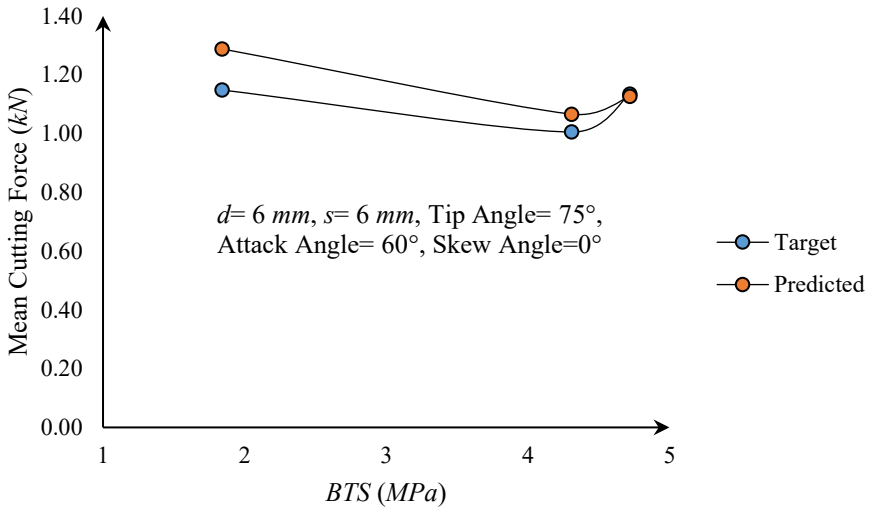

Figure A-7: Representative cases showing the effect of Brazilian tensile strength on mean cutting force

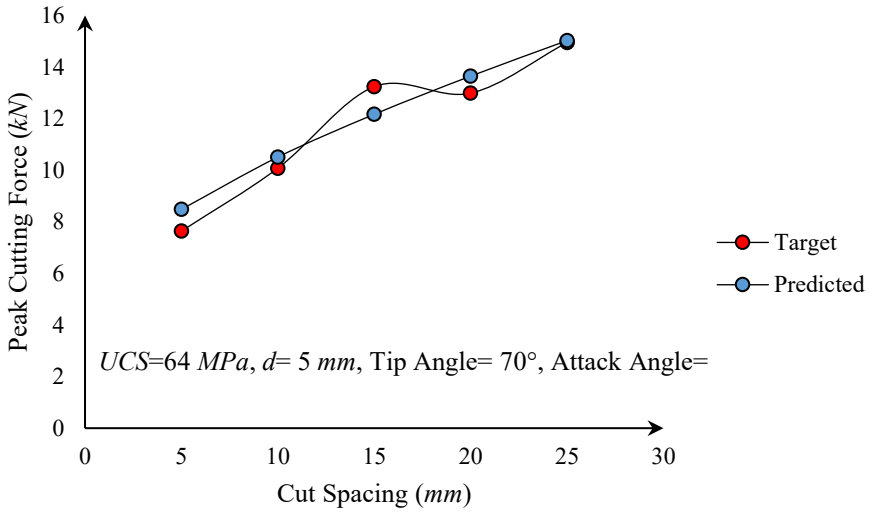

Figure A-8: Representative cases showing the effect of cut spacing on peak cutting force

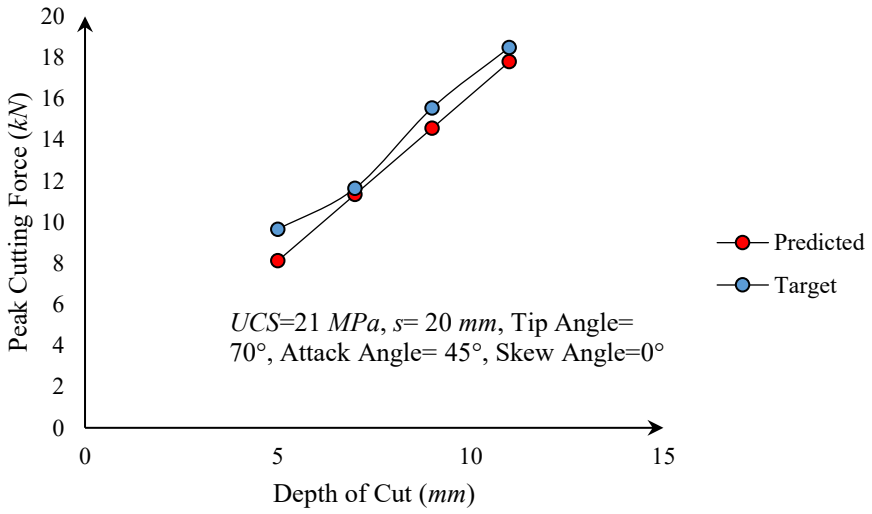

Figure A-9: Representative cases showing the effect of depth of cut on peak cutting force

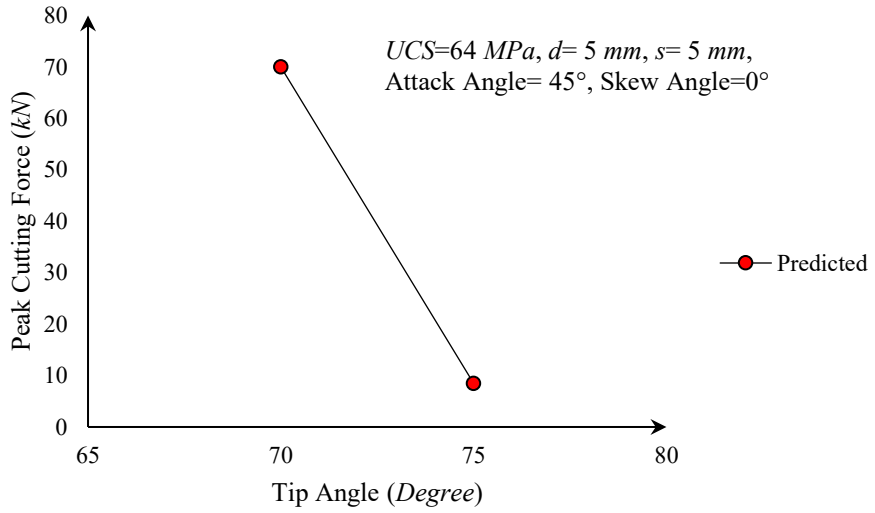

Figure A-10: Representative cases showing the effect of tip angle on peak cutting force

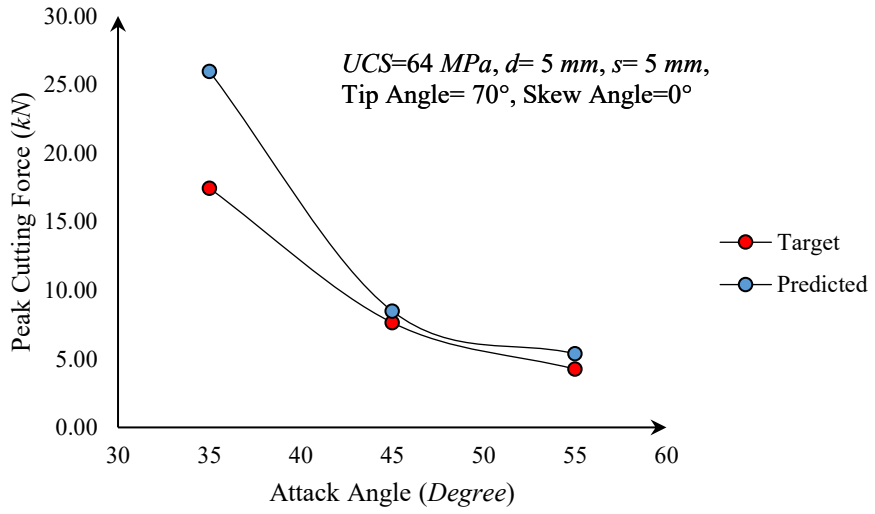

Figure A-11: Representative cases showing the effect of attack angle on peak cutting force

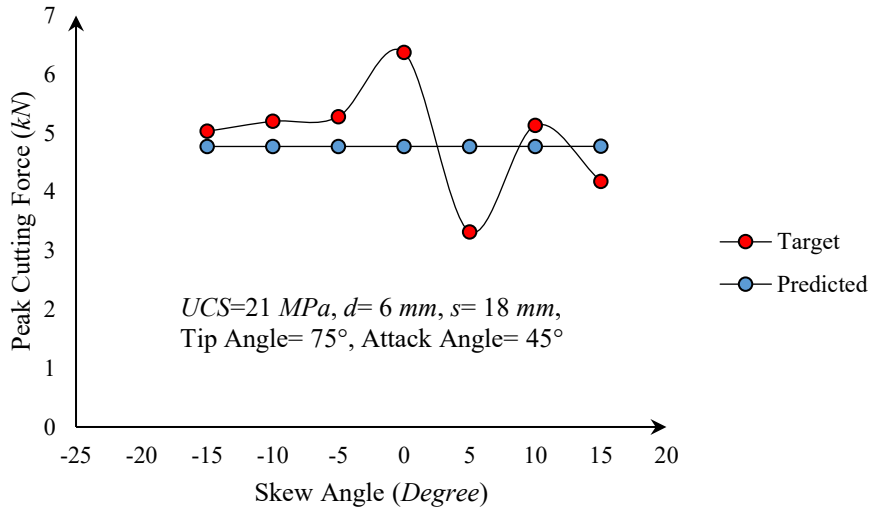

Figure A-12: Representative cases showing the effect of skew angle on peak cutting force

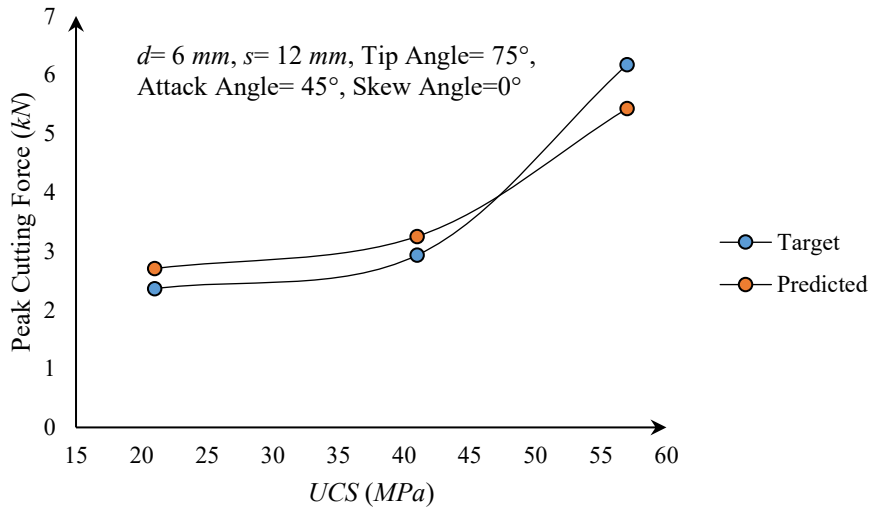

Figure A-13: Representative cases showing the effect of uniaxial compressive strength on peak cutting force

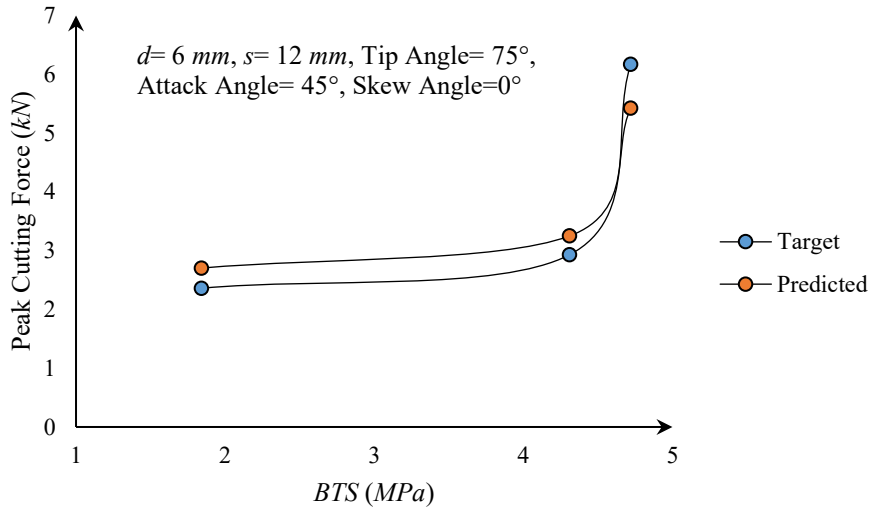

Figure A-14: Representative cases showing the effect of Brazilian tensile strength on peak cutting force

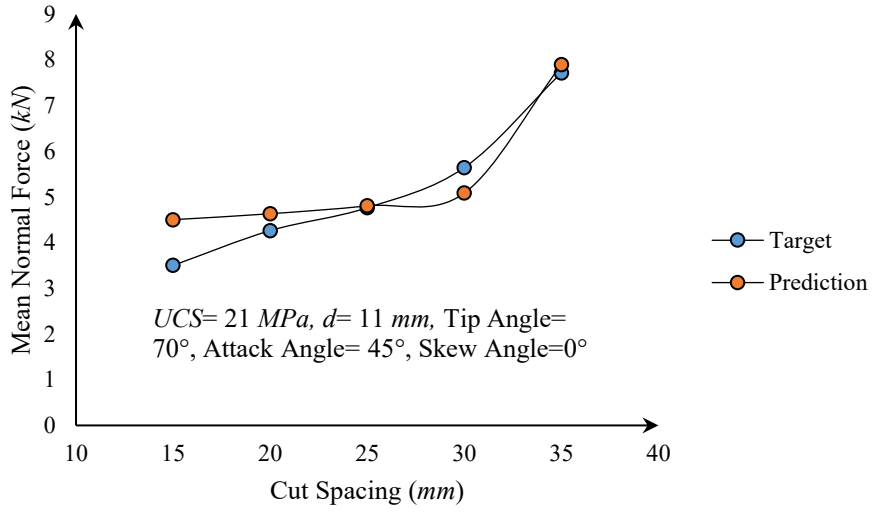

Figure A-15: Representative cases showing the effect of cut spacing on mean normal force

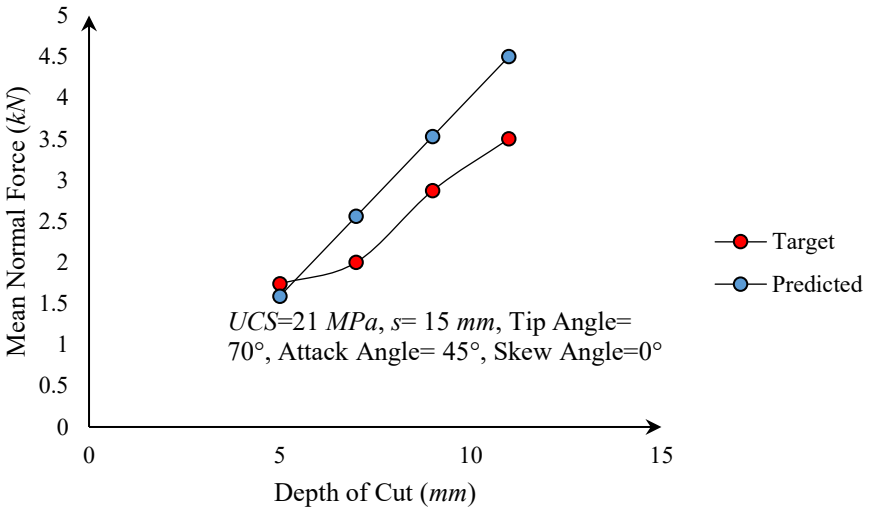

Figure A-16: Representative cases showing the effect of depth of cut on mean normal force

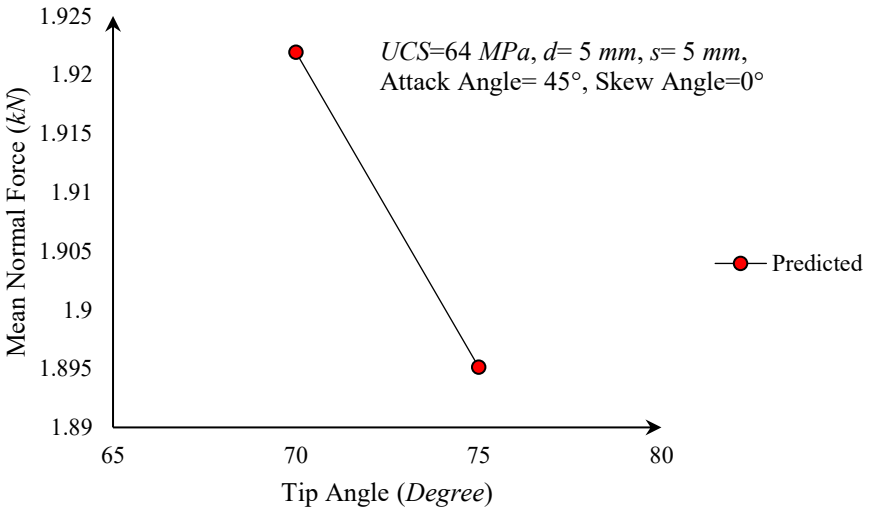

Figure A-17: Representative cases showing the effect of tip angle on mean normal force

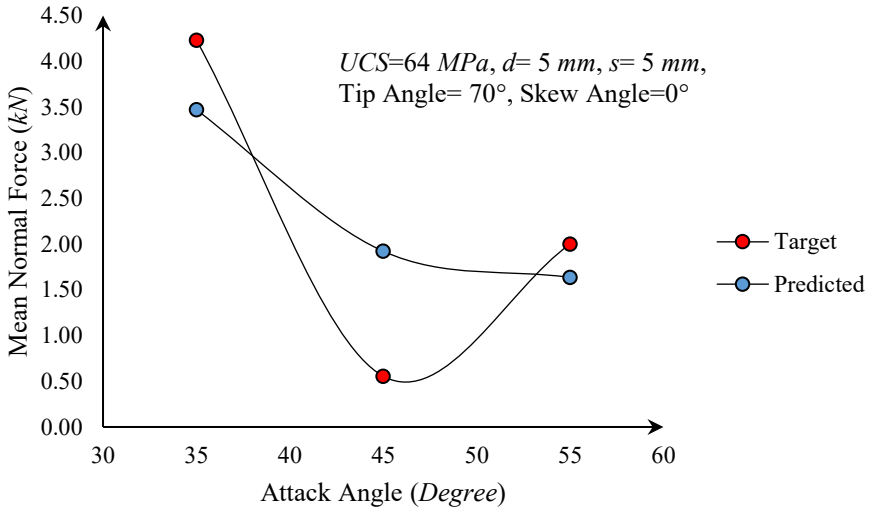

Figure A-18: Representative cases showing the effect of attack angle on mean normal force

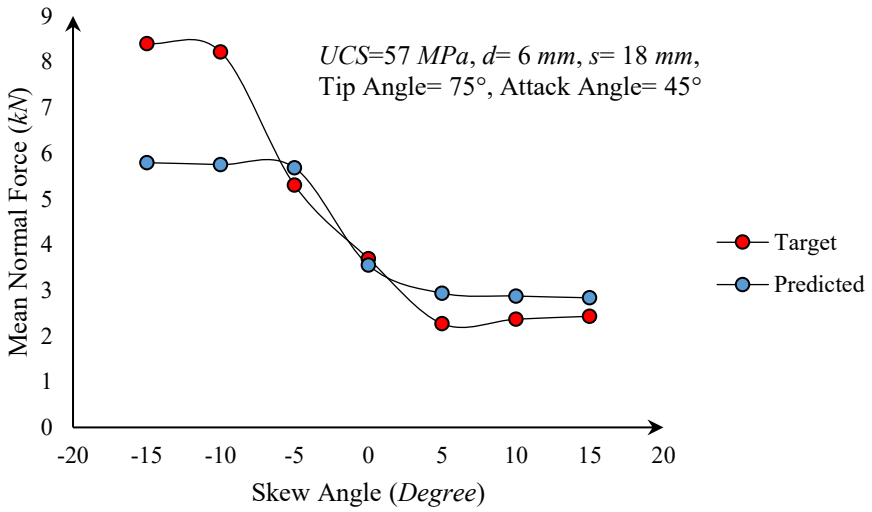

Figure A-19: Representative cases showing the effect of skew angle on mean normal force

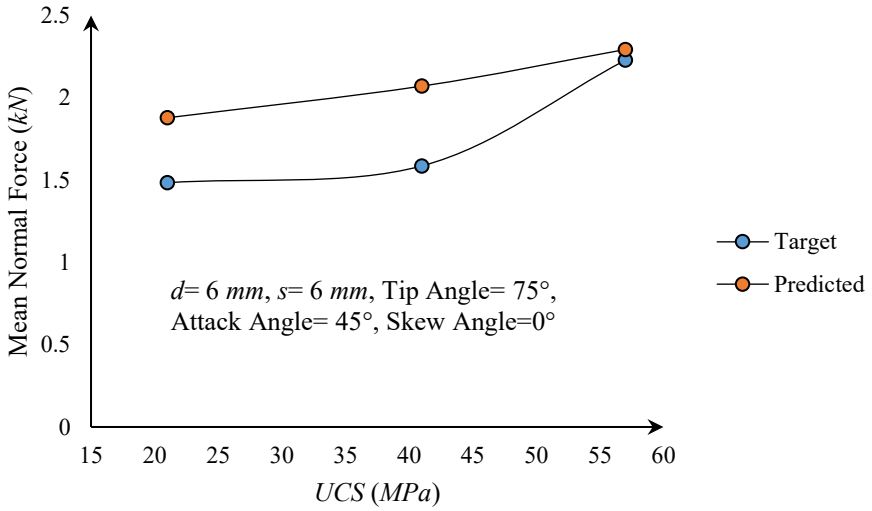

Figure A-20: Representative cases showing the effect of uniaxial compressive strength on mean normal force

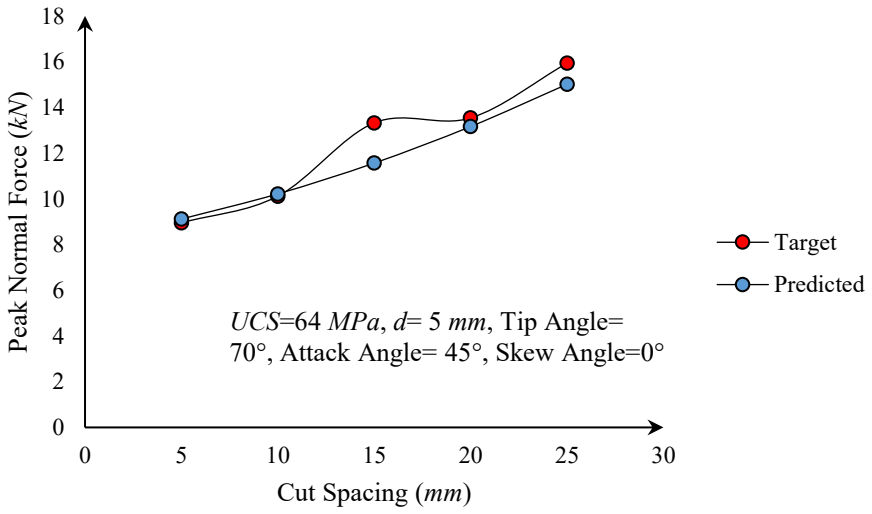

Figure A-21: Representative cases showing the effect of cut spacing on peak normal force

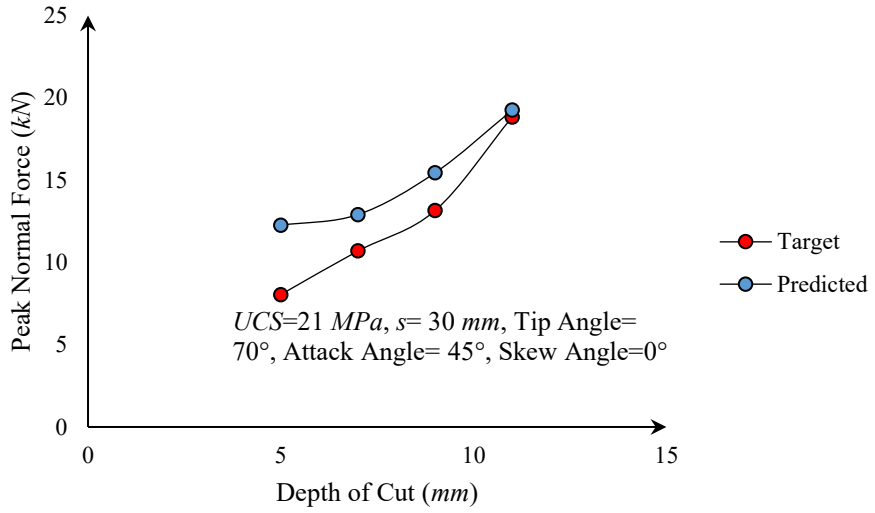

Figure A-22: Representative cases showing the effect of depth of cut on peak normal force

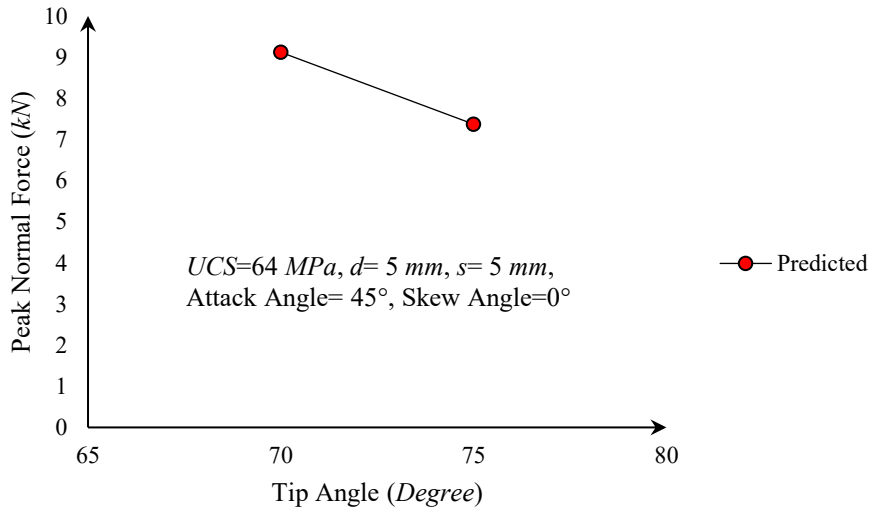

Figure A-23: Representative cases showing the effect of tip angle on peak normal force

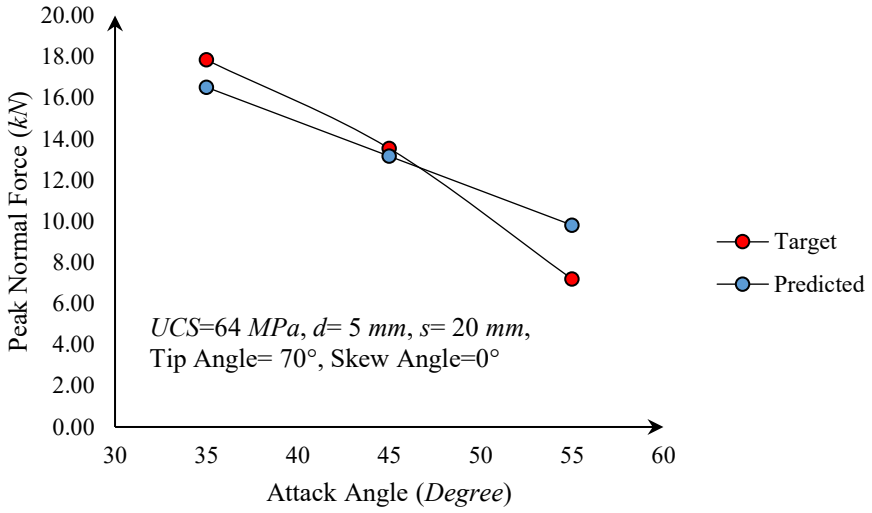

Figure A-24: Representative cases showing the effect of attack angle on peak normal force

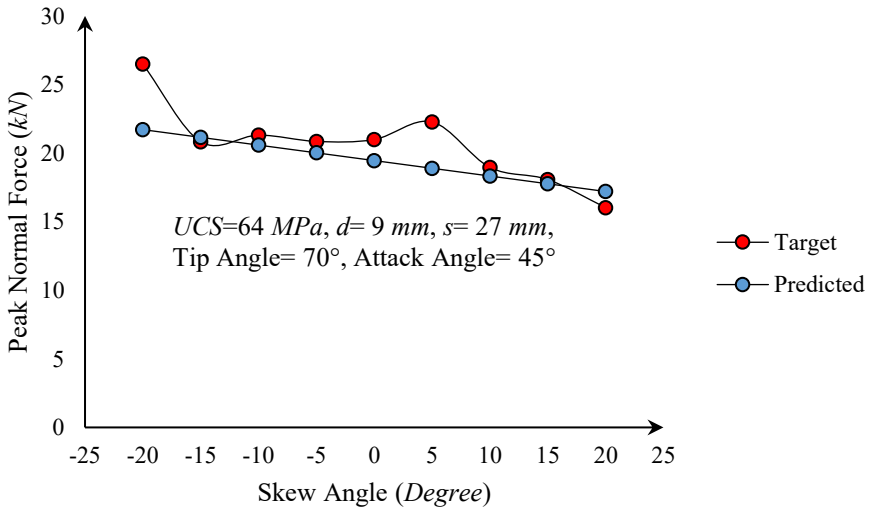

Figure A-25: Representative cases showing the effect of skew angle on peak normal force

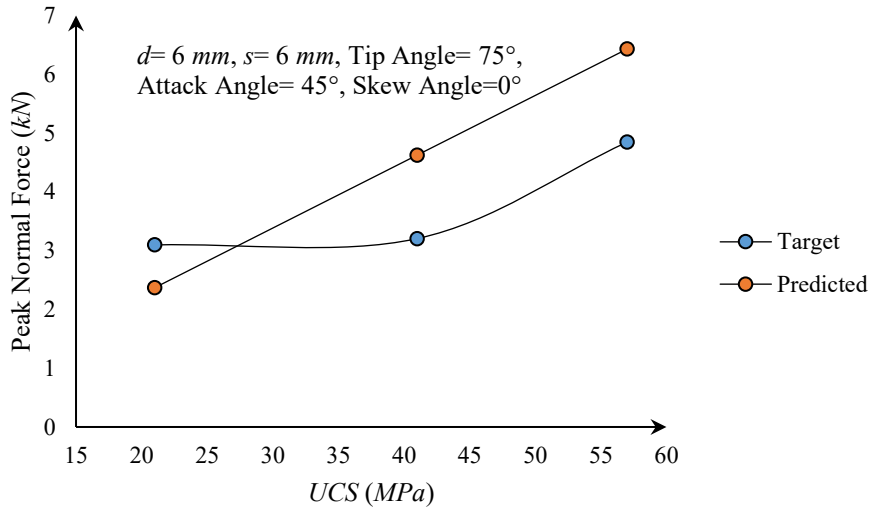

Figure A-26: Representative cases showing the effect of uniaxial compressive strength on peak normal force

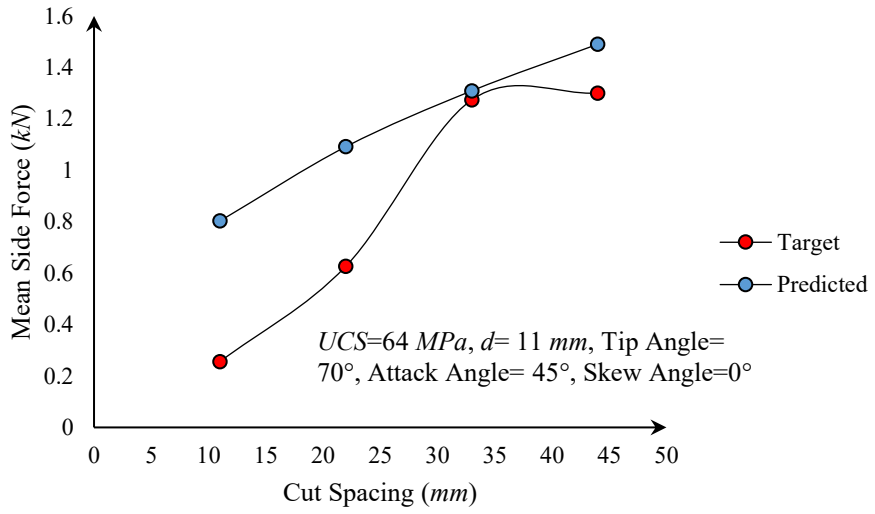

Figure A-27: Representative cases showing the effect of cut spacing on mean side force

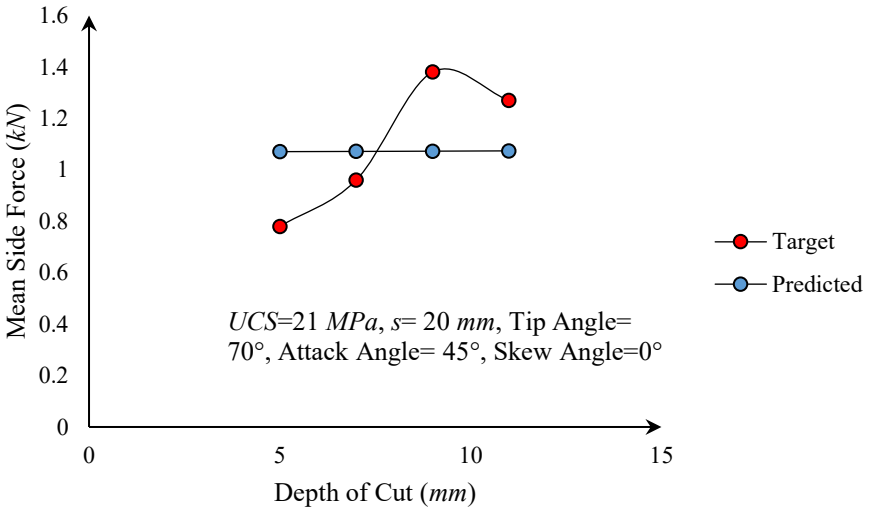

Figure A-28: Representative cases showing the effect of depth of cut on mean side force

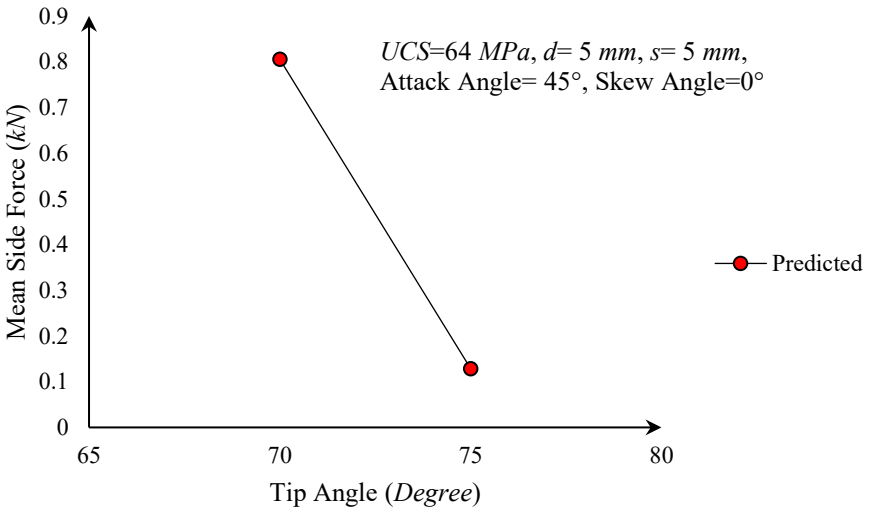

Figure A-29: Representative cases showing the effect of tip angle on mean side force

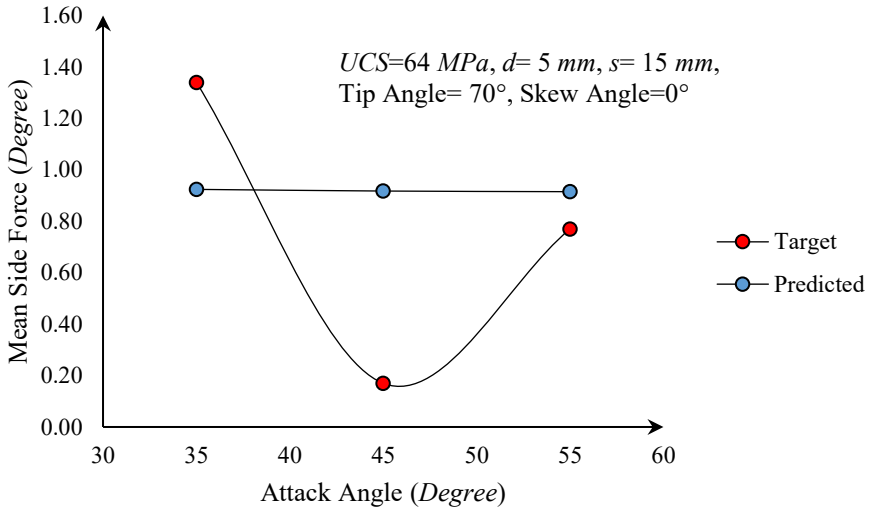

Figure A-30: Representative cases showing the effect of attack angle on mean side force

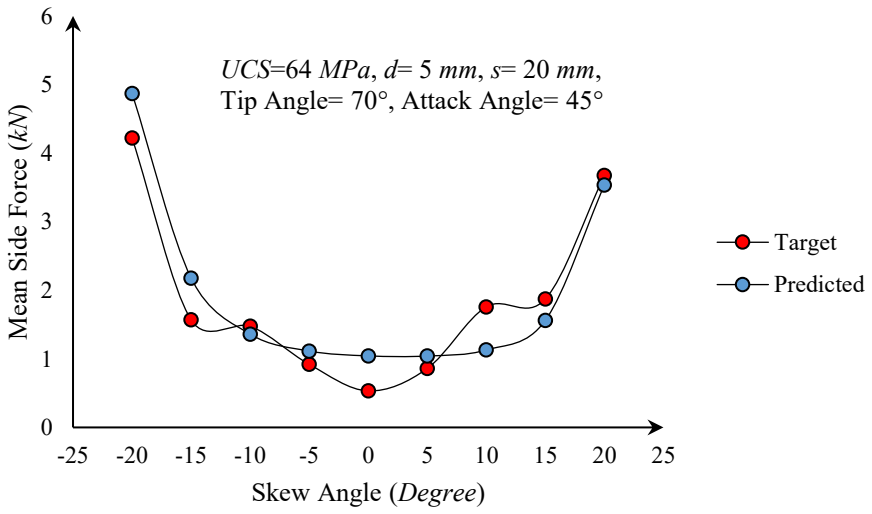

Figure A-31: Representative cases showing the effect of skew angle on mean side force

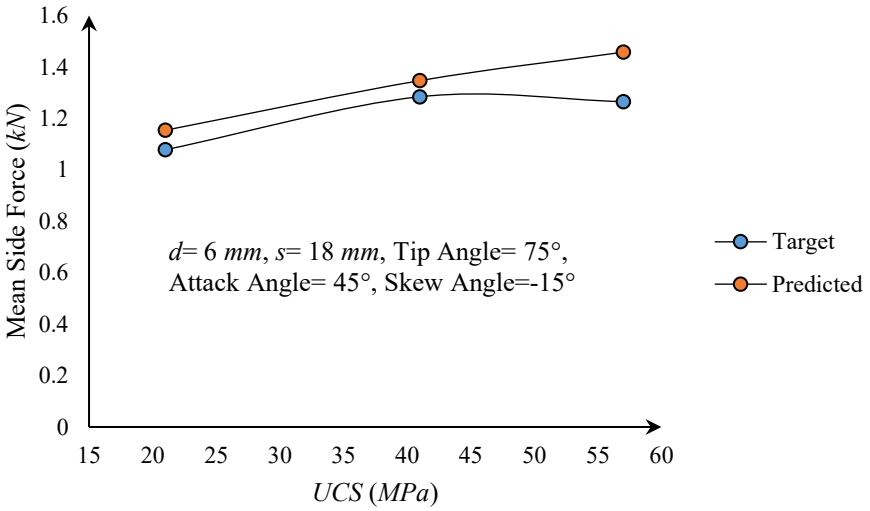

Figure A-32: Representative cases showing the effect of uniaxial compressive strength on mean side force

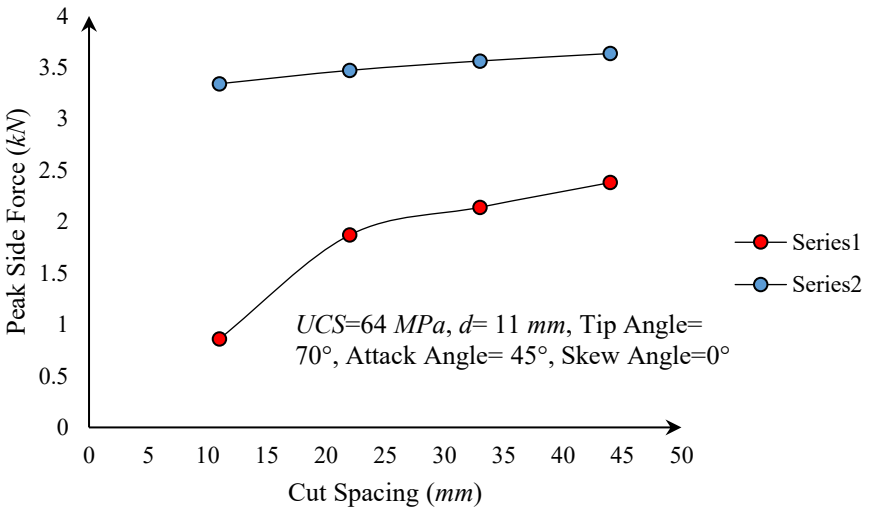

Figure A-33: Representative cases showing the effect of cut spacing on peak side force

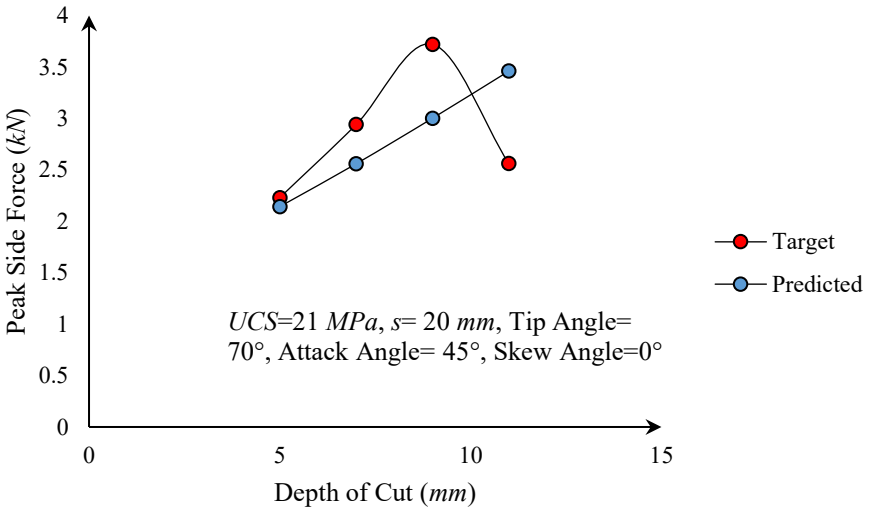

Figure A-34: Representative cases showing the effect of depth of cut on peak side force

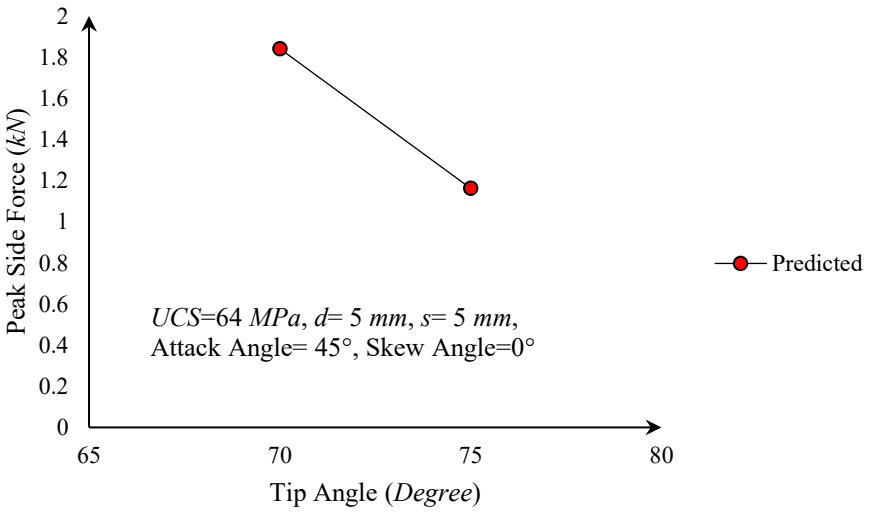

Figure A-35: Representative cases showing the effect of tip angle on peak side force

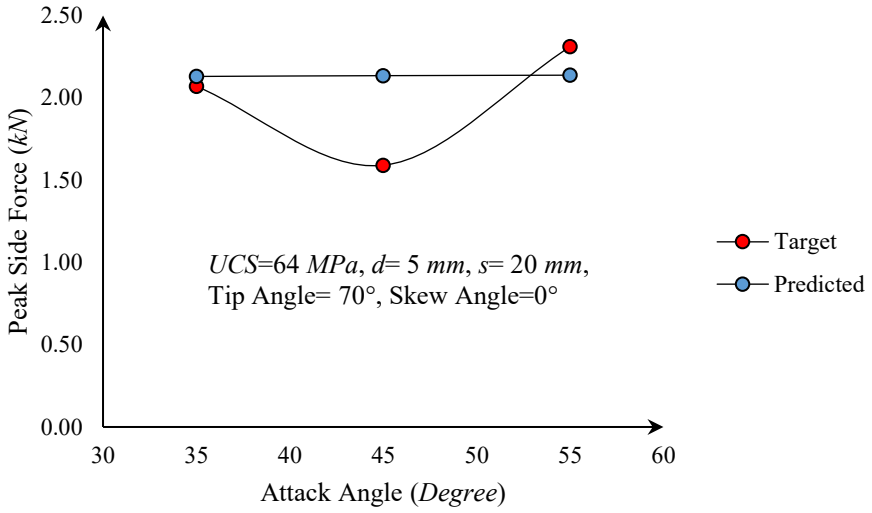

Figure A-36: Representative cases showing the effect of attack angle on peak side force

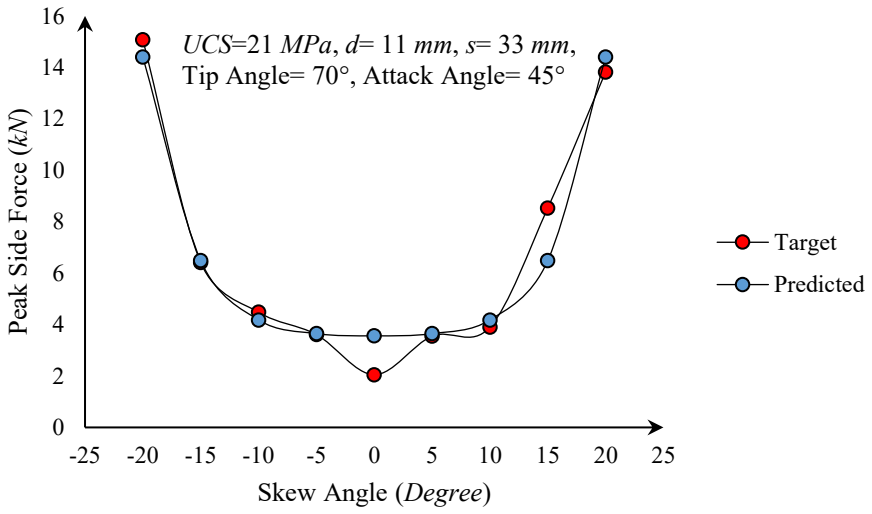

Figure A-37: Representative cases showing the effect of skew angle on peak side force

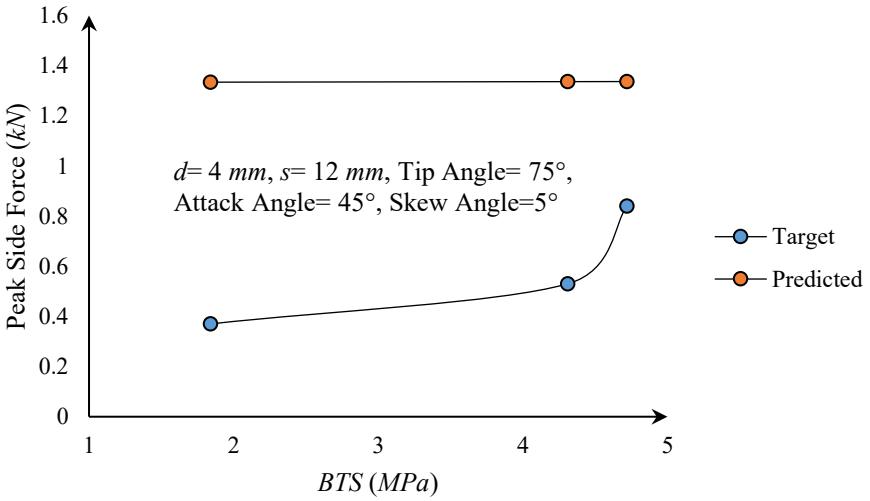

Figure A-38: Representative cases showing the effect of Brazilian tensile strength on peak side force

ACKNOWLEDGEMENT

I would like to express my appreciation to those who helped me during the course of this study. First of all, I would like to thank my advisor, Prof. Seokwon Jeon, for letting me join his lab and for creating a mentorship space where I could learn and grow. During all these years, I have been confident that I have his support whenever/wherever it was needed, even beyond the calls of his duty. Through numerous personal discussions, critical comments, and constructive recommendations, Prof. Jeon generously shared his gift of wisdom, kept me in the right track, and helped me to greatly improve the quality of my research. I would also like to thank him for the generous financial support throughout my Ph.D. studies. I consider myself very lucky for having had the great chance of working under his supervision.

I would also like to express my sincere thanks to Prof. Deniz Tumac, my M.Sc. advisor, who has been an irreplaceable source of guidance and encouragement for me from the first day that I met him. I could not even imagine such a high level of commitment and support years after I finished my Master's studies under his supervision. Prof. Tumac is specially thanked for agreeing to be on my dissertation committee in spite of the fact that he was extremely occupied during my dissertation defense period.

Prof. Jae-Joon Song, Prof. Ki-Bok Min, and Dr. Dong-Woo Ryu are thanked for the insightful feedbacks and constructive comments as my dissertation committee members. I feel so blessed to have had such an outstanding and patient committee as their contributions helped me to significantly improve the quality of my dissertation.

I would also thank my fellow graduate students in Seoul National University for their help and support during the course of this study. During this whole time, I have enjoyed their kindness and friendship. First, I extend my special thanks to all of the Prof. Jeon's lab members who have helped me more closely during the past five years. Dr. Yudhidya Wicaksana is deeply thanked for his wide range of support, from helping me adjust myself to daily life in beautiful Seoul to scientific discussions about my research. Prof. Ho-Young Jeong is sincerely thanked for sharing the results of his work and his expertise in linear rock cutting experiments. Wonhee Lee is thanked for helping me collect rock samples, helping me handle any situation where a Korean speaking friend's help was needed, and for all of the handy tips on Korean food and culture. Yeongmin Yoon is thanked for all of his critical help for handling many aspects of my life in Korea. His support ranged from helping me buy a sim card during the first days of my arrival to helping me prepare the forms and documents related to my salary and the official documents required for my graduation. Seungwon Lee is sincerely thanked for his congenial assistance for preparing the official documents required for graduation. I would also like to express my deep appreciation to Dr. Byungkyu Jeon, Dr. Nan Zhang, Dr. Su-Deuk Lee, and Moonjoo Kim for being such attentive friends during the past years.

I wish to express my appreciation for Dr. Juhyi Yim's helping hand at some integral steps during my graduation process. Dr. Linmao Xie, Dr. Chae-Soon Choi, Dr. Sayedalireza Fereshtenejad, Dr. Yong-Ki Lee, Dong-Ho Yoon, Dr. Sehyeok Park, Dr. Kwang-Il Kim, Dr. Saeha Kwon, Il-Seok Kang, Hoon Byun, Hwa-Jung Yoo, Ali Mehrabifard, Seungki Lee, Jinoen Kim, Suyeon Hong, Sejin Kim, and Donyoung Yoon are

appreciated for their considerate and caring approach during my studies at Seoul National University. Jiwon Choi is specially thanked for her critical help in setting up the presentation room.

Prof. Emeritus Chung-In Lee is cordially thanked for being such a great source of inspiration. I would also like to express my deep gratitude for Prof. Emeritus Nuh Bilgin and Prof. Hanifi Copur for generously sharing their knowledge and expertise whenever I asked them for help. I am also grateful to Prof. R. Mete Goktan and Dr. Jung-Woo Cho for warmly sharing the details of their research work in response to my inquiries. My sincere thanks are extended to Prof. Ardeshir Hezarkhani, my undergraduate advisor, for encouraging me to pursue my graduate studies and for the life/scientific lessons he taught me during my work under his supervision.

Finally, I am extremely grateful for my family's love and patience during my graduate studies. I could not even imagine doing this without them.